Biophysical Responses of Plankton to Natural and Human-Driven Environmental Variability in the California Current

By

HELEN JULIA KILLEEN
DISSERTATION

Submitted in partial satisfaction of the requirements for the degree of

DORTOR OF PHILOSOPHY

in

Ecology

in the

OFFICE OF GRADUATE STUDIES

of the

UNIVERSITY OF CALIFORNIA

DAVIS

Approved:

_____
Steven Morgan, Chair

_____
John Largier

_____
Jeffrey Dorman

Committee in Charge

2022

ACKNOWLEDGEMENTS

What an adventure! No amount of writing or any number of figures and tables could convey the amazing experiences and friendships that these last six years have held. Seeing the glow of phytoplankton in the wake of the R/V Mussel Point at the end of a night's work offshore, exploring beaches and tidepools with students, hearing the stories of fishers and boaters, kayaking from island to island in the Gulf of California, celebrating research milestones with friends and colleagues, and so much more – all are experiences that I feel so privileged to have had and will treasure. I am grateful to Dr. Steven Morgan, my graduate advisor, for taking me on as a student and affording me these opportunities. Steven's support and patient guidance have enabled me to become a better scientist while making my own mistakes and continuing to do the things that I love. His former students and I wish him all the best in his retirement!

I am also thankful for the mentorship and support of my other committee members, Drs. John Largier and Jeff Dorman whose feedback and kindness were instrumental in completing this dissertation. Drs. Jim Sanchirico, Bill Sydeman, David Gold, and faculty at Bodega Marine Lab and UC Davis provided additional guidance, helping me to expand my skillset as a scientist and thinker. I am also grateful for the time and expertise of NMFS staff at the Southwest Fisheries Science Center, who were particularly helpful in the completion of chapter one of this dissertation.

Chapters two and three of my dissertation required an enormous about of boat-based fieldwork that would have been impossible without the patient training and assistance I had from James Fitzgerald (UC Davis Boating Safety), Steve Neil, David Dann, Grant Susner, and Alex Spooner (Bodega Marine Lab Marine Operations). I'm so thankful for the sleep they sacrificed to help on overnight offshore plankton surveys and for the countless times they saved our

research from unanticipated obstacles like hidden crab pots, nets full of jellies, and the vicissitudes of computers. A complete list of those who assisted with field and lab work is given at the end of this section. I'm also grateful for the support of all the other staff at BML and at UC Davis in the Ecology, Department of Environmental Science and Policy, and Coastal and Marine Sciences Institute offices. Their daily kindnesses and generosity helped me navigate the University and life as a graduate student while feeling part of a broader community.

When research felt draining, Steven supported me in engaging in all sorts of other teaching, mentorship, outreach and service activities. I'm especially thankful to Dr. Ellie Fairbairn for taking me on as a co-teacher in her summer Marine Science Pre-College program, which was such a joy to be a part of and fed the K-12 teacher in me. I was also privileged to work with artists Andrea Murchie and Zoe Farmer to showcase *Hidden Journeys*, our exhibition on the life of California's larval marine fishes that drew families from all over the Bay Area.

The work described in the chapters that follow was completed during a tumultuous time. Repeated wildfires in Northern California and the COVID-19 pandemic interrupted research and altered collaborations. These changes were intensely frustrating, but they also forced my colleagues and I to adapt to new realities, embrace flexibility, and truly relish the opportunities we have to work together. I'm thankful for the friendship of other Ecology and BML students and staff who helped create a supportive network in happy and challenging times, especially Ellie Bolas, Ann Holmes, Kristen Elsmore, Hannah Palmer, Alisha Saley, and my labmates Connor Dibble, Sam Bashevkin, Sadie Small, Marian Parker, Erin Satterthwaite and Sarah Hameed.

Finally, I am infinitely grateful for the example, inspiration, and love of my friends and family, especially my husband, Kevin, my parents, Roberta and Tim, my siblings, Phil, Cormac and Elaina. Our shared love of the natural world and hope for a better future have shaped my work and are values that Kevin and I look forward to sharing with our son, Wesley Luka Killeen Davis, born on January 30th this year.

FOR HELP IN THE FIELD AND LAB THANKS ALSO TO,

Gynelle Mendoca
Alma Groehnert
Robin Roettger
Brittany Jellison
Chloe Parish
Niko Schoffer
Ava Smith
Eda Spaletta
Rafael Stankiewicz
Claire Sydeman
Jeffrey You
Katherine Fierro
Mrudula Chodavarapu
Armand McFarland
Alma Mechler
Benjamin Rubinoff
Patrick Zeigler
Jordan Hollarsmith
Sean Luis
Vanessa Lo
Malina Loeher
Sarah Erickson
Stephanie Tsui
Ian Brown
Roshni Mangar
Katie Weaver
Rebecca Fanning
Isaiah Bluestein
John Liu
Melissa Crews
Allen Huynh
Haley Hudson
Joscelyn de la Torre
Laura Vary
Anya Stajner
Margaret Johnson
Marissa Levinson
Gabe Ng
Aaron Ninokawa
Eduardo Hernandez
Giovanna Poulos
Andy Lee
Matthew Meram

THIS WORK WAS FUNDED BY

American Philosophical Society
Bilinski Educational Foundation
California Sea Grant
Farallon Institute
National Science Foundation
National Science Policy Network
University of California Natural Reserve System
University of California, Davis, Genomics Center
University of California, Davis, Graduate Group in Ecology

DEDICATION

This dissertation is dedicated to my mom, Roberta Marie Johnson Killeen, and my grandmothers Marie Yvonne Sage Marshall and Nora Christine Curran Killeen. All three women loved learning. Nora received her doctor of medicine degree in 1946, and was one of the first women in Wales to do so. Marie completed a doctorate in Psychology in 1981 while raising two small children. Roberta received her Ph.D. in Geophysics and Space Physics in 1987 and made enormous contributions to earth and space science education and outreach throughout her career. I am immensely privileged to have had the example and love of these three women.

Drs. Roberta Johnson Killeen (left) and Marie Sage Marshall

Nora Curran Killeen, MD

ABSTRACT

Plankton play an essential role in marine ecology as the base of ocean food webs and, in the case of marine larvae, as the next generation of marine populations. Consequently, understanding how oceanography and environmental conditions impact the distribution, abundance, and condition of plankton is fundamental to both community ecology and population dynamics. However, the miniscule size of plankton relative to the scale of their pelagic environment makes it uniquely difficult to examine biophysical processes of plankton in the field. In this dissertation, I present three studies documenting the findings from field-based investigations of plankton biophysics across scales in the California Current Ecosystem on the North American West Coast. In chapter one, I examine the influence of the 2014-2016 marine heatwave and El Niño event on the body size of krill off the coast of California and show that the length of two temperate krill species declined during the heatwave, while the size of a third subtropical species increased. In chapter two, I document, for many species for the first time, the existence of discrete depth preference behaviors among larval fishes that mediate dispersal trajectories across and along the continental shelf of northern California. In chapter 3, I test the hypothesis that small-scale, ephemeral, and topographically generated fronts forming on the poleward side of a small headland during relaxation flows create spatial heterogeneity in nearshore plankton assemblages. Although the front surveyed proved to be transient and weak, it did appear to act as a barrier segregating offshore and onshore plankton communities. Together, these studies offer portraits of how biophysical interactions in the plankton may impact ecological processes from local to ecosystem scales and highlight their importance for management and conservation of marine systems in an era of climate change.

INTRODUCTION

The vast majority of marine organisms spend all or part of their lives as plankton. This means that, unlike most terrestrial species, most marine species experience a period during which they are very small, possess limited motility, and are more or less subject to transport by ocean currents. Consequently, planktonic dispersal and thus population connectivity in the sea are strongly influenced by physical oceanography and the response of planktonic organisms to their surroundings. Other aspects of the physical environment can shape the condition of planktonic organisms. For example, metabolism and growth rates of ecotothermic plankton are constrained by seawater temperature and the physiology of particular taxa. Thus, population demography in the sea is also linked to biophysical dynamics of plankton.

Though the population dynamics of many marine species are tied to interactions between organisms and their environments taking place in the plankton, characterization of these interactions is an ongoing endeavor in marine ecology. Tracking individual marine plankton in a dynamic ocean is infeasible, so field-based observations of biophysical dynamics in the plankton largely rely on net-based or acoustic surveys that aim to capture plankton over various spatiotemporal scales. The cost and logistical challenges associated with conducting such surveys and enumerating plankton in a laboratory setting are significant obstacles to understanding planktonic processes. However, field-based hypothesis testing is an essential step in understanding the differences between expected and realized population dynamics. This knowledge is all the more critical as oceanographic patterns shift as the result of global and regional climate change. To help fill this gap, I present three investigations into various aspects of plankton biophysics at the ecosystem, regional, and local scales within the California Current upwelling Ecosystem on the West Coast of North America.

In chapter one, I test the hypothesis that the body size of three numerically abundant krill species, *Euphausia pacifica*, *Thysanoessa spinifera*, and *Nematoscelis difficilis*, declined during the 2014-2016 marine heatwave and El Niño event in the Western Pacific. I identified krill species and sexes from samples collected by the National Marine Fisheries Service Rockfish Recruitment and Ecosystem Assessment Survey from across the California continental shelf between 2011 and 2018, before, during, and after the heatwave. Hierarchical mixed effects modeling of krill lengths with random effects for sampling location revealed that body size of the two temperate species did indeed decline, but the size of subtropical *Nematoscelis difficilis* increased during the heatwave. I also present results from analyses to determine environmental drivers of changes in body size and regional variation in length response to environmental change.

While marine larvae have the potential to disperse over very large distances, particularly for species that spend months as pelagic larvae prior to settlement, it has become increasingly clear that many larvae are more limited in their dispersal range than was previously thought. There is now ample evidence that many larvae possess traits that mitigate long distance dispersal, such as vertical and horizontal swimming behaviors. However, the prevalence of these behaviors among larval fishes is not well understood. In chapter two, I investigate how the behaviors of larval fishes structure biophysical dispersal dynamics and mediate transport trajectories over and along the California continental shelf. Extensive cross-shelf, depth segregated surveying of the full ichthyoplankton assemblage show that vertical depth preferences are likely common among larval fishes with varying outcomes for dispersal trajectories, recruitment, and local retention.

Finally, in chapter three, I test the hypotheses that (1) small-scale, ephemeral, and topographically generated fronts form on the poleward side of Bodega Head, a small headland north of San Francisco, during relaxation flows and (2) that these secondary flow features create spatial heterogeneity in nearshore plankton assemblages by interactions between swimming plankton and frontal hydrodynamics. I show that the headland front is indeed associated with a gradient in assemblage composition that may be attributable to the species-specific effects of the front on cross-shore movement; and that these characteristics arise despite the ephemeral nature of fronts that form on the poleward side of headlands. As small headlands like Bodega Head are prevalent all along the West Coast of North America, these dynamics may play an important role in structuring coastal plankton assemblages and benthic communities.

TABLE OF CONTENTS

CHAPTER 1

Effects of a marine heatwave on adult body length of three numerically dominant krill species in the California Current Ecosystem[1]

ABSTRACT

Krill are an abundant and globally distributed forage taxon in marine ecosystems, including the California Current Ecosystem (CCE). The role of krill in trophodynamics depends on both abundance and size (biomass), but the impact of extreme climate events on krill body size is poorly understood. Using samples collected from 2011-2018, we tested the hypotheses that adult body length of three krill species (*Euphausia pacifica*, *Thysanoessa spinifera*, and *Nematoscelis difficilis*) declined during the 2014-2016 Northeast Pacific marine heatwave/El Niño event due to elevated seawater temperatures, reduced upwelling, and low primary productivity. Hierarchical mixed-effects modelling showed that mean length of adult *E. pacifica* and *T. spinifera* declined and *N. difficilis* length increased during 2015. These trends differed by sex and reverted to a pre-heatwave state in 2016. Temperature, upwelling, and food availability (chlorophyll-*a* content) did not explain decreased length in 2015, but environmental drivers of length varied regionally and by sex across all years. This study documents the impact of a major marine heatwave on adult krill length in one of the world's major upwelling systems and indicates how pelagic ecosystems may respond to increasingly frequent marine heatwaves.

[1] This chapter is a reproduction of an article by the same name originally published in *ICES*

Helen Killeen, Jeffrey Dorman, William Sydeman, Connor Dibble, Steven Morgan, Effects of a marine heatwave on adult body length of three numerically dominant krill species in the California Current Ecosystem, *ICES Journal of Marine Science*, Volume 79, Issue 3, April 2022, Pages 761–774, https://doi.org/10.1093/icesjms/fsab215

INTRODUCTION

Krill are an abundant and globally distributed taxon within marine ecosystems. They are opportunistic and omnivorous filter feeders that consume phytoplankton, microzooplankton, and detritus (Dilling *et al*., 1998; Nakagawa *et al*., 2004; Pinchuk & Hopcraft, 2007) and are in turn preyed upon by a wide variety of ecologically and economically important taxa, including fish (Field & Francis, 2006; Thayer *et al*., 2014), seabirds (Hipfner, 2009), mammals (Nickels, *et al.*, 2018; Barlow, *et al*, 2020), and invertebrates (Trathan & Hill, 2016). In the California Current Ecosystem (CCE), a highly productive upwelling region extending from British Columbia to Baja California peninsula, krill comprise a substantial portion of the prey biomass and support productive, economically valuable fisheries (Field *et al*., 2006; see update by Koehn *et al*., 2016). Three species are particularly abundant in this region and occupy different cross-shelf and latitudinal habitats: *Euphausia pacifica* is found in greatest densities on the outer continental shelf (Brinton, 1962), *Thysanoessa spinifera* is mostly limited to the inner continental shelf north of 34.5°N (Brinton, 1962), and *Nematoscelis difficilis* is abundant throughout the Southern California Bight and is more oceanic in distribution north of 34.5°N (Brinton, 1960). All three are crucial to CCE foodwebs. Thus, understanding variation in their biomass is valuable for interpreting ecosystem-wide phenomena, predicting fisheries yields (Wells *et al*., 2016), and evaluating changes and die-offs of seabirds and other marine predators (e.g., Sydeman *et al*., 2015; Jones *et al*., 2018)

Biomass is the product of abundance (ind. m^{-3}) and body size (mg $ind.^{-1}$). Extensive observational and laboratory research has identified drivers of changes in krill abundance and body size (growth) in the CCE. For instance, both krill abundance and growth have been positively linked to coastal upwelling (Shaw *et al.*, 2010; García-Reyes *et al*., 2014). Upwelled,

nutrient-rich water drives primary production and cools surface waters on the shelf, favouring higher phytoplankton biomass. Chlorophyll-a (chl-*a*), a proxy for phytoplankton abundance, is positively correlated with krill abundance (Lavaniegos *et al.*, 2019; Cimino *et al.*, 2020) and growth (Pinchuk & Hopcraft, 2007; Shaw *et al.*, 2010; Robertson & Bjorkstedt, 2020). Seawater temperature is inversely related to both krill abundance and growth (Marinovic & Mangel, 1999; Lavaniegos *et al.*, 2019; Cimino *et al.,* 2020), and may even lead to negative growth (apparent shrinkage) at temperatures > 19° C (Marinovic & Mangel, 1999). Finally, large-scale climate oscillations are also known to influence krill abundance in the CCE, including the 2- to 7-year frequency El Niño Southern Oscillation (ENSO; Marinovic *et al*., 2002), the Pacific Decadal Oscillation (PDO; Brinton & Townsend, 2003), and marine heatwave (MHW) conditions (Brodeur *et al.,* 2019; Cimino *et al.*, 2020), with low krill abundance occurring during warm periods.

MHWs are regional phenomena associated with prolonged anomalously warm sea surface temperatures and can have a profound impact on ecosystems (Hobday *et al.,* 2016). In the CCE, a severe MHW, called the Northeast Pacific Blob, originated in late 2013 and lasted through fall 2016 (Gentemann *et al.*, 2017). Anomalously high sea level pressure in the North Pacific led to warm SST anomalies in the northern CCE beginning in spring and summer 2014 (Bond *et al.*, 2015). These conditions persisted through 2015 and into 2016, but were intensified by the 2015-2016 El Niño (DiLorenzo & Mantua, 2016) and aggravated by a delayed, weakened 2015 upwelling season (Gentemann *et al.,* 2017). The 2014-2016 MHW was associated with substantial and pervasive ecosystem-wide effects, including a reduction in the abundance of krill (Brodeur *et al.,* 2019; Cimino *et al.,* 2020). However, the impact of MHWs on krill body size has not been well documented (except see Robertson & Bjorkstedt, 2020) despite its importance for

understanding mechanisms underlying observed die offs of krill predators (Jones *et al.*, 2018; Piatt *et al.,* 2020) and shifts in their foraging behaviour (Barlow *et al.,* 2020; Santora *et al.,* 2020). Understanding krill size response to MHWs may aid in predicting the response of zooplankton communities to future extreme events in the region and globally, which are expected to increase in frequency with climate change (Frölicher *et al*., 2018).

To better understand the effect of MHWs on krill body size in the CCE, we examined drivers of spatial and temporal variability in adult krill length using samples collected by the NOAA-NMFS Rockfish Recruitment and Ecosystem Assessment Survey (RREAS) throughout the California portion of the CCE from 2011 to 2018 (Sakuma *et al*., 2016), spatially expanding on prior work conducted at regional scales (Robertson & Bjorkstedt, 2020). This period includes both positive and negative ENSO phases as well as conditions before, during, and after the 2014-2016 MHW dominated the system. We hypothesized that (a) krill body length declined during 2014-2016, and (b) this was due to a combination of anomalously high temperatures, below average upwelling, and low food availability. To test these hypotheses, we modelled variability in the length of adults of three krill species (*E. pacifica, T. spinifera,* and *N. difficilis*) interannually and across a range of environmental conditions in 2015, during the peak of the MHW, and throughout the time series. In attempting to identify environmental drivers of MHW effects on krill body size, this work aims to inform expectations for MHWs beyond the 2014-2016 Northeast Pacific event.

MATERIALS AND METHODS

NMFS Juvenile Rockfish Survey

Krill samples were obtained from the RREAS. Generally, annual surveys were conducted from May through mid-June, with krill sampling occurring at night. We examined specimens collected from 2011 through 2018, except for 2014 (samples unavailable), from three of the five RREAS regions (core, south central, and south; Sakuma *et al.,* 2016) each with distinct oceanographic regimes (Checkley & Barth, 2009). In each region, RREAS sampling was conducted along multiple transects, each with stations spanning the continental shelf and slightly beyond. To characterize cross-shelf krill communities, we chose one station onshore (generally <200 m deep, ~ 3 km from shore) and one offshore (generally >200 m, ~45 km from shore) from each transect line (Figure 1; station metadata are available in Appendix A Table 1). Krill were sampled using a modified Cobb midwater trawl with a 26 m headrope and 9.5 mm mesh codend. This mesh size was used to target juvenile fish (Sakuma *et al*., 2006) and did not adequately sample krill smaller than 10 mm. Krill larvae transition to adults at 10-11 mm in length (Brinton, 1976; Tanaisichuk, 1998), so most larvae and some small adults were likely excluded by extrusion through the 9.5 mm mesh codend. To account for size selectivity of our gear, we omitted all krill <10 mm from our dataset and limit our analysis to adults. While this could result in overestimation of population mean lengths, we expect this effect is negligible and unlikely to impact comparisons among samples collected using identical methods. Krill were preserved in 10% buffered formaldehyde to minimize body shrinkage of specimens during storage (Krag *et al*., 2014).

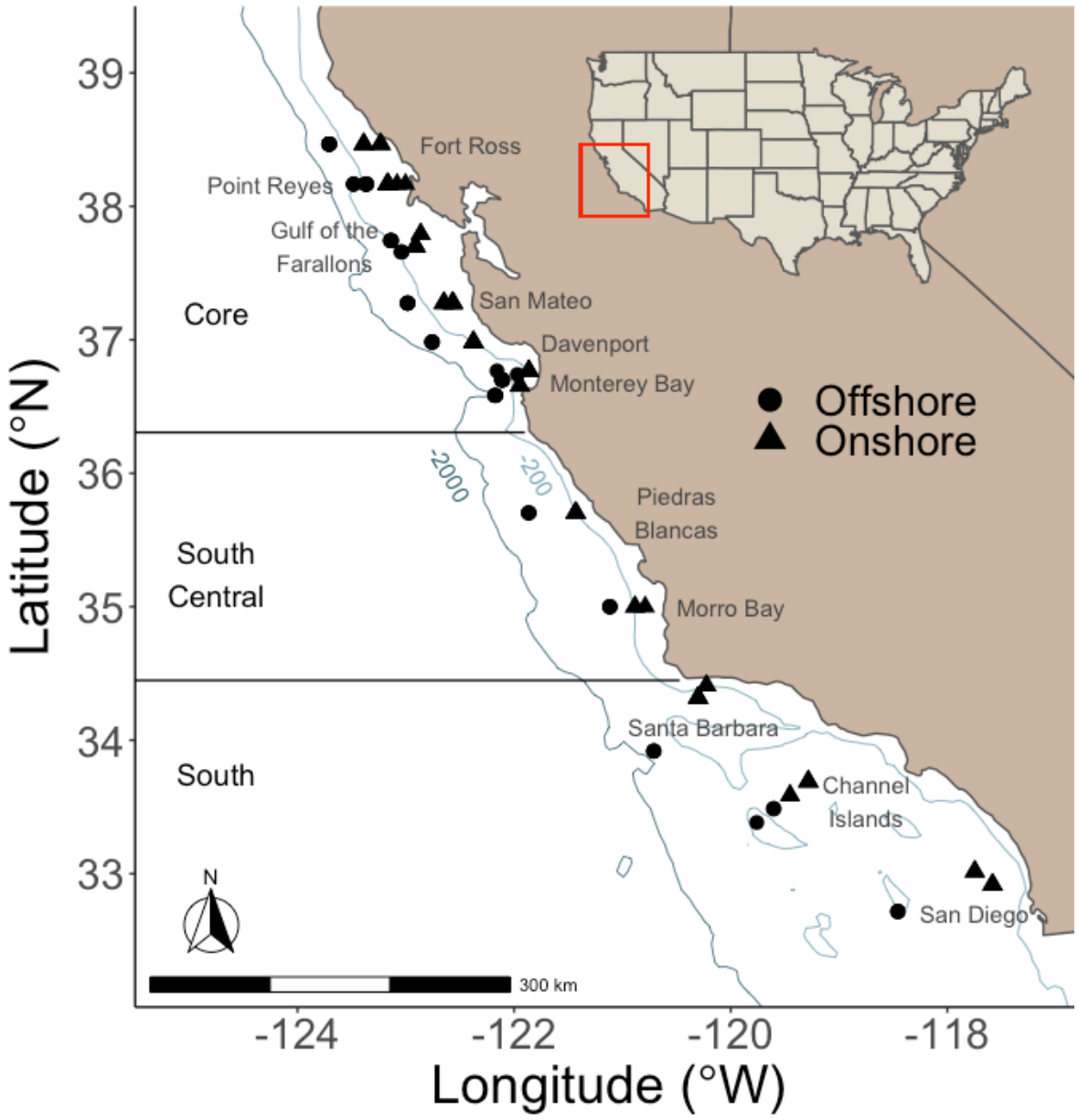

Figure 1. Points show the location of sampling stations and transects included in the study. Point shape denotes whether the station was designated as an 'offshore' or 'onshore' location. -200 m and -2,000 m isobaths are shown in light and dark blue respectively.

Krill Lengths

Krill samples were split using a Folsom Splitter to aliquots of the original 200 mL RREAS sample volume depending on the number of krill in the sample. All individuals in the aliquot were identified to species and sex using a dissecting microscope and a key for Pacific euphausiid identification (Baker *et al.*, 1990; Brinton *et al.,* 2000). To ensure that enough individuals were measured to create representative length frequency distributions, we sought to identify at least (1) 90 of the most common species and (2) 40 of the second most common species in each sample, and continued identifying intact individuals from successive aliquots until we had achieved both benchmarks. We excluded samples from our analysis in cases where we were unable to measure at least 40 individuals of a given species. Once identified and sexed, krill were placed on a petri dish, alongside a ruler for scale, and photographed using a Canon EOS 3000N camera. We used ImageJ (Reuden *et al*., 2017) to measure adult krill total length using the segmented line tool along the dorsal side of the body from the foremost part of the carapace, generally the tip of the rostrum, to the most posterior point on the telson (Brinton & Wyllie, 1976).

Environmental Predictors

To model adult krill length, we chose predictor variables for environmental models of length based on our hypotheses and drivers that likely impact adult krill body size in the CCE, including seawater temperature, food availability, upwelling, and ocean climate (Table 1). We accounted for daily vertical migrations (on day-night cycles) for all three species by using both temperature at 2 m depth (sea surface temperature; SST) and temperature at 100 m depth (subsurface temperature) to represent conditions affecting krill. Mean daily surface and subsurface temperatures were extracted from the Regional Ocean Modeling System (ROMS)

Nowcast (10km resolution) for each station using the virtual sensor tool available on the CenCOOS Data Portal (https://data.cencoos.org/). Daily mean satellite chl-*a* values (4 km^2 minimum spatial resolution) were extracted for each station via the THREDDS data server from the European Space Agency Ocean Color Climate Change Initiative (version 4.2; accessible at https://rsg.pml.ac.uk/thredds/) and log transformed (Sathyendranath *et al*., 2020). In addition to chl-*a,* we tested the impact of the standard deviation of SST (SST SD) on krill length, which may be an indicator of food availability as a proxy for the horizontal presence of fronts and has been associated with *T. spinifera* abundance in the region (Cimino *et al.,* 2020). SST SD values were assigned to each station by taking the standard deviation of ROMS 2 m temperatures over a chosen period prior to sampling (see below). We used the daily Cumulative Upwelling Transport Index (CUTI; accessed at http://mjacox.com/upwelling-indices/) as an indicator of regional coastal upwelling intensity and duration at each station. CUTI incorporates vertical transport due to both Ekman flux and cross-shore geostrophic transport, providing a local (1° latitude, 0-75 km from shore) estimate of recent upwelling conditions experienced by krill prior to collection (Jacox *et al*., 2018). Finally, we included the multivariate ocean climate index (MOCI; accessed at http://www.faralloninstitute.org/moci) as a measure of regional ocean conditions and low-frequency climate oscillation (see García-Reyes & Sydeman, 2017 for details). Each station was assigned the corresponding MOCI value for its region (MOCI regions: north, central, and southern California) during the spring months (April-June). High (low) MOCI values are indicative of warm (cold) and low (high) productivity conditions in the CCE.

To determine the number of days over which to average each predictor, we modelled adult krill length against each predictor averaged over increasing durations (1-30 days) such that length~$predictor_i$, where *i* is the number of days over which the predictor was averaged. We

chose a value for *i* by selecting the model with the highest R^2 for a given predictor (Figure S2). All environmental predictors and krill length were scaled (means and variances equate to 0 and 1, respectively) for analysis and interpretation.

Modelling

Statistical modelling of lengths was conducted in R version 3.6.2 (R Core Team, 2019) using a hierarchical linear mixed modelling approach with varying intercepts. This method allowed us to examine the effects of interannual variation and environmental predictors on body length of adult krill throughout the CCE while accounting for differences in the effect of sampling location (Gelman & Hill, 2007). We designed three families of models to examine (1) interannual variability in adult krill length; (2) the role of upwelling, SST, and chl-a in determining adult krill length during the peak of the MHW in 2015; and (3) environmental drivers of spatial and temporal variability in adult krill length throughout our time series (Table 1). All models were constructed using the lme4 package (Bates *et al*., 2015), and figures and tables were made using the packages ggplot2 (Wickham, 2016), superheat (Barter & Yu, 2017) and kableExtra (Zhu, 2020). Data and analyses are publicly available online (https://doi.org/10.17605/osf.io/c8hr3).

Table 1. Environmental and biological predictors and grouping factors included in linear mixed-effects models of krill body length off California from 2011 to 2018. Temporal and spatial averaging columns indicate the domain over which predictors were averaged. *Chl-*a* values were accessed from the Ocean Color Initiative, which merges multiple satellite chlorophyll products with variable (4 km^2 minimum) spatial resolution.

Predictor	Variable	Description	Purpose	Temporal Averaging	Spatial Averaging	Source
Sea Surface Temperature	temp_2	Temperature at 2 m depth	Direct impact of temperature on body size	10 days	10 km^2	Regional Ocean Modeling System 10 km Nowcast
Subsurface temperature	temp_100	Temperature at 100 m depth	Direct impact of temperature on body size	5 days	10 km^2	Regional Ocean Modeling System 10 km Nowcast
SST Standard Deviation	sst_sd	Standard deviation of temperature at 2 m depth	Food availability	17 days	10 km^2	Regional Ocean Modeling System 10 km Nowcast
Chlorophyll-a	chl-a	Log chlorophyll-a content	Food abundance	27 days	4 km^2*	Sathyendranath *et al*., 2020
Multivariate Ocean Climate Index	moci	Multivariate index capturing regional atmospheric and oceanographic variability	Regional, seasonal oceanographic variability including low-frequency oscillations	3 months	Regional	García-Reyes & Sydeman, 2017
Coastal Upwelling Transport Index	cuti	Local upwelling strength as a function of Ekman and geostrophic transport	Local upwelling intensity	9 days	1 degree latitude	Jacox *et al*., 2018
Sex	sex	Krill sex	Sexual dimorphism	NA	NA	NA

Predictor	Variable	Description	Purpose	Temporal Averaging	Spatial Averaging	Source
Station	station	Station number	Grouping variable for random intercept and regression estimation, captures station-level variation in habitat type and distance from shore	NA	NA	RREAS

To test our first hypothesis that mean adult krill length declined during 2014-2016, we constructed two sets of mixed-effect models with a variable intercept for station. The first set of models included sex as a predictor to determine whether sexes were impacted differently by year. The second set did not include sex as a predictor to estimate the effect of year on adult krill length across males and females. Both sets included one model for each of the three species. Model structure followed the form (Gelman & Hill, 2007):

Equation 1

$$l_i = \alpha_{j[i]} + X_i\beta + \epsilon_i$$

$$\text{where } \alpha_j \sim N(\mu_\alpha, \sigma_\alpha^2)$$

$$\text{and } \epsilon_i \sim N(0, \sigma^2)$$

where $\boldsymbol{l}$ is a vector of length n, representing standardized krill lengths for n individuals, indexed as i. $\boldsymbol{\alpha}$ is a vector of random intercepts associated with station j and is normally distributed with a mean of μ_α and variance of σ_α^2. $\boldsymbol{X}$ is the matrix (n x p) for p fixed terms of year, sex, and year by sex interaction. $\boldsymbol{\beta}$ is the vector (p x 1) of fixed term coefficients and $\boldsymbol{\epsilon}$ is the vector (n x 1) of error terms with a zero mean and variance of σ^2.

To test our second hypothesis that changes in mean adult krill length during the MHW were driven by upwelling, SST, and chl-*a,* we constructed species-specific mixed-effects models of krill length with varying intercepts for each of three years before (2013, average MOCI = -1.28), during (2015, average MOCI = 1.41) and after (2017, average MOCI = 0.77) the MHW. We also examined differences in the impact of predictors on male and female krill by including interaction terms of sex and environmental predictors in the 2015 model. Model structure used the same form as Equation 1, where $\boldsymbol{X}$ is the matrix ($n \times p$) for p fixed terms of SST, upwelling, chl-*a*, sex, and their two-way interactions terms.

To explore environmental drivers of adult krill length more generally across the whole time series, and to investigate regional variability in drivers of adult krill size, we constructed three species-specific mixed-effects models with varying intercepts and slopes. Model structure followed the form (Gelman & Hill, 2007):

Equation 2

$$l_i \sim N\left(\alpha_{j[i]} + \gamma_{j[i]}\tau_i + X_i\beta, \sigma^2\right), \text{for } i = 1, \dots, \text{n}$$

$$\text{where } \begin{pmatrix}\alpha_j \\ \gamma_j\end{pmatrix} \sim N\left(\begin{pmatrix}\mu_\alpha \\ \mu_\gamma\end{pmatrix}, \begin{pmatrix}\sigma_\alpha^2 & \rho\sigma_\alpha\sigma_\gamma \\ \rho\sigma_\alpha\sigma_\gamma & \sigma_\gamma^2\end{pmatrix}\right), \text{for } j = 1, \dots, \text{J}$$

where $\boldsymbol{\alpha}$ is an intercept estimated for each station j, $\boldsymbol{\gamma}_j$ is the station-specific SST coefficient, and $\boldsymbol{\tau}$ is SST. $\boldsymbol{X}$ is a matrix (n x p) containing vectors for sex, the set of environmental predictors described in Table 1, and interactions between sex and environmental predictor; $\boldsymbol{\beta}$ is the vector (p x 1) of estimated coefficient for each fixed term. Variable intercepts and slopes for station were modelled as normal distributions with means ($\boldsymbol{\mu_\alpha}$, $\boldsymbol{\mu_\gamma}$) and variances ($\boldsymbol{\sigma_\alpha^2}$, $\boldsymbol{\sigma_\gamma^2}$) including a between-station correlation parameter, **ρ.** We excluded fixed terms from species-specific models of environmental drivers across the whole time series in two cases based on data structure

considerations. First, we excluded subsurface temperature from the *T. spinifera* model because a large proportion of individuals were collected at stations with depths ≤ 100 m (37%). Secondly, the term $\boldsymbol{\gamma_{j[i]}\tau_i}$ was left out of the *N. difficilis* model because too few individuals were measured to estimate station-specific temperature coefficients. We used an information theoretic approach (Grueber *et al*., 2011) and the MuMIn package (Bartón, 2020) to select a single top-performing model for each species. Model performance was evaluated by comparing Akaike Information Criterion (AIC) values associated with each fixed and random effect structure. We selected the model with the lowest AIC value. Collinearity was assessed graphically and by calculating the variance inflation factor associated with each top-performing model.

RESULTS

We measured 11,284 *E. pacifica,* 5,865 *T. spinifera,* and 1,636 *N. difficilis* individuals (total n = 18,785). Table 2 shows count data for krill included in the analysis by species, sex, year, and region. Mean length of adult krill varied by species. The mean length of adult *E. pacifica* was 20.92 mm with a 95% confidence interval (CI) of 20.87 to 20.96 mm; adult *T. spinifera* mean length was 24.06 mm (CI: 23.97 to 24.16 mm); and adult *N. difficilis* mean length was 22.41 mm (CI: 22.27 to 22.55 mm). After confirming that the distributions of each species-sex were normal, a two-sample t-test showed that females were larger than males by 0.94 mm ($t = 6.03$, $p < 0.001$) for *E. pacifica* and by 2.63 mm ($t = 6.87$, $p < 0.001$) for *T. spinifera*. *N. difficilis* females were 0.86 mm larger than males, but the result was not statistically significant ($t = 1.53$, $p = 0.14$).

Table 2. Sample size of krill measured for each year and region off California from 2011 to 2018, with totals in the bottom row. Columns show species and sex totals for the core (C), south central (SC), and south (S) regions as defined in Figure 1.

	E. pacifica						*T. spinifera*						*N. difficilis*					
	Female			Male			Female			Male			Female			Male		
year	C	SC	S	C	SC	S	C	SC	S	C	SC	S	C	SC	S	C	SC	S
2011	1250	55	0	732	58	0	565	67	0	667	22	0	31	0	0	16	0	0
2012	538	131	545	396	38	302	554	58	169	235	12	84	37	0	44	23	0	1
2013	553	0	0	394	0	0	582	0	0	398	0	0	49	0	0	12	0	0
2015	276	156	359	168	30	182	0	28	165	0	28	102	35	0	285	16	0	46
2016	678	241	50	457	131	36	143	0	0	164	0	0	153	59	85	21	25	15
2017	515	323	238	317	232	125	470	74	84	152	102	24	100	36	193	52	11	39
2018	737	163	266	379	67	166	435	70	19	321	21	50	0	0	232	0	0	20
Total	**4547**	**1069**	**1458**	**2843**	**556**	**811**	**2749**	**297**	**437**	**1937**	**185**	**260**	**405**	**95**	**839**	**140**	**36**	**121**

Interannual variability in krill length

Total length of adult krill varied interannually for all three species. Species-specific mean length varied by year up to 9.6%, 19.5%, and 14.7% for *E. pacifica, T. spinifera*, and *N. difficilis*, respectively (Figure 2). We expected that krill would be smaller during 2015 and 2016 (no length data available for 2014). Results of our interannual linear mixed modelling analysis show that in 2015 *E. pacifica* and *T. spinifera* mean lengths were smaller than average, but *N. difficilis* mean length was larger than average (Figure 3A; full results available in Appendix A tables 2-4). From 2016 to 2018, *E. pacifica* and *T. spinifera* mean lengths were larger than average and *N. difficilis* mean length was smaller than average.

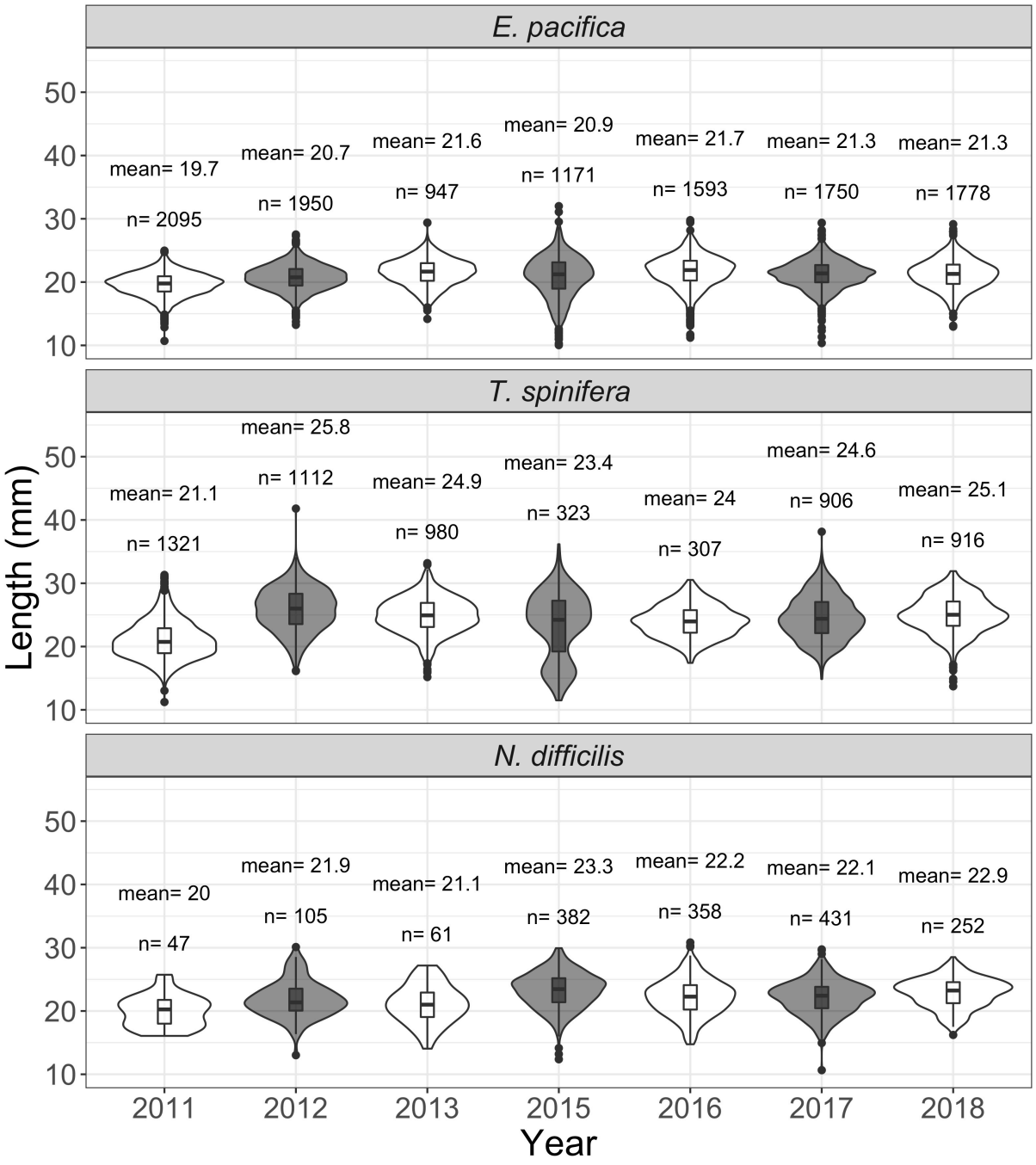

Figure 2. Raw length frequency distributions for three krill species collected off California from 2011-2018. Mean values indicated by inset box-and-whisker plots.

We also found that the impact of year on mean total length of adult krill differed for males and females (Figure 3B; full results available in Appendix A tables 5-7). In all years but 2015, mean total length of females was greater than males. In 2015, mean total length of adult

males was larger than females for both *T. spinifera* and *N. difficilis*. *E. pacifica* females remained larger than males in 2015, but the species exhibited a 39% reduction in size-based sexual dimorphism relative to 2013 (Figure 3C). From 2016 onward, we observed a return to the pre-heatwave pattern of larger females and smaller males for all three species.

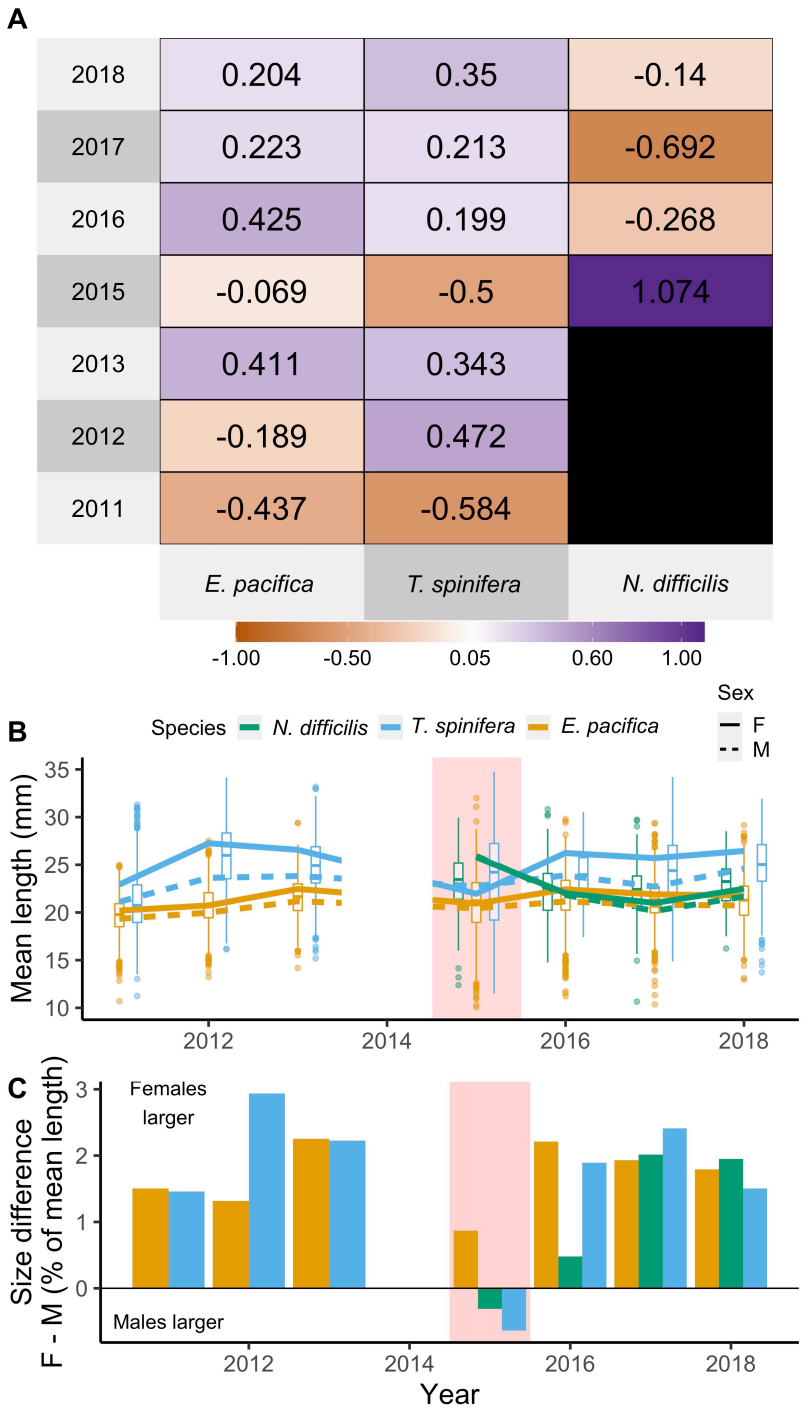

Figure 3. (A) Coefficient estimates of year impact on krill length derived from linear mixed effects models with a variable intercept for station and fixed effects for year. Values and colors indicate deviation from the overall population mean length in units of standard deviation. Estimates for *N. difficilis* from 2011-2013 not shown due to low sample size. (B, C) Simulated data from linear mixed effects model with a variable intercept for station and fixed effects of year, sex, and year:sex. The peak of the MHW is shaded red. (C) Size difference between male and female krill across all years. Bars above the zero line indicate females were larger.

Environmental drivers of adult krill body length

The period when samples were collected was marked by substantial interannual environmental variability in the CCE. Cool conditions with negative MOCI values prevailed in 2011-2013 but shifted to warmer conditions by 2014 (Figure 4K, L) with the onset of the MHW. In 2015, positive MOCI values, warm surface and subsurface temperatures, and average to below average upwelling were associated with reduced chl-*a* concentrations. By the time samples were collected in 2016 (May-June), surface and subsurface temperatures as well as upwelling had begun to return to a pre-heatwave state. MOCI values declined through 2017 and 2018, and other covariates returned to average values for the study period.

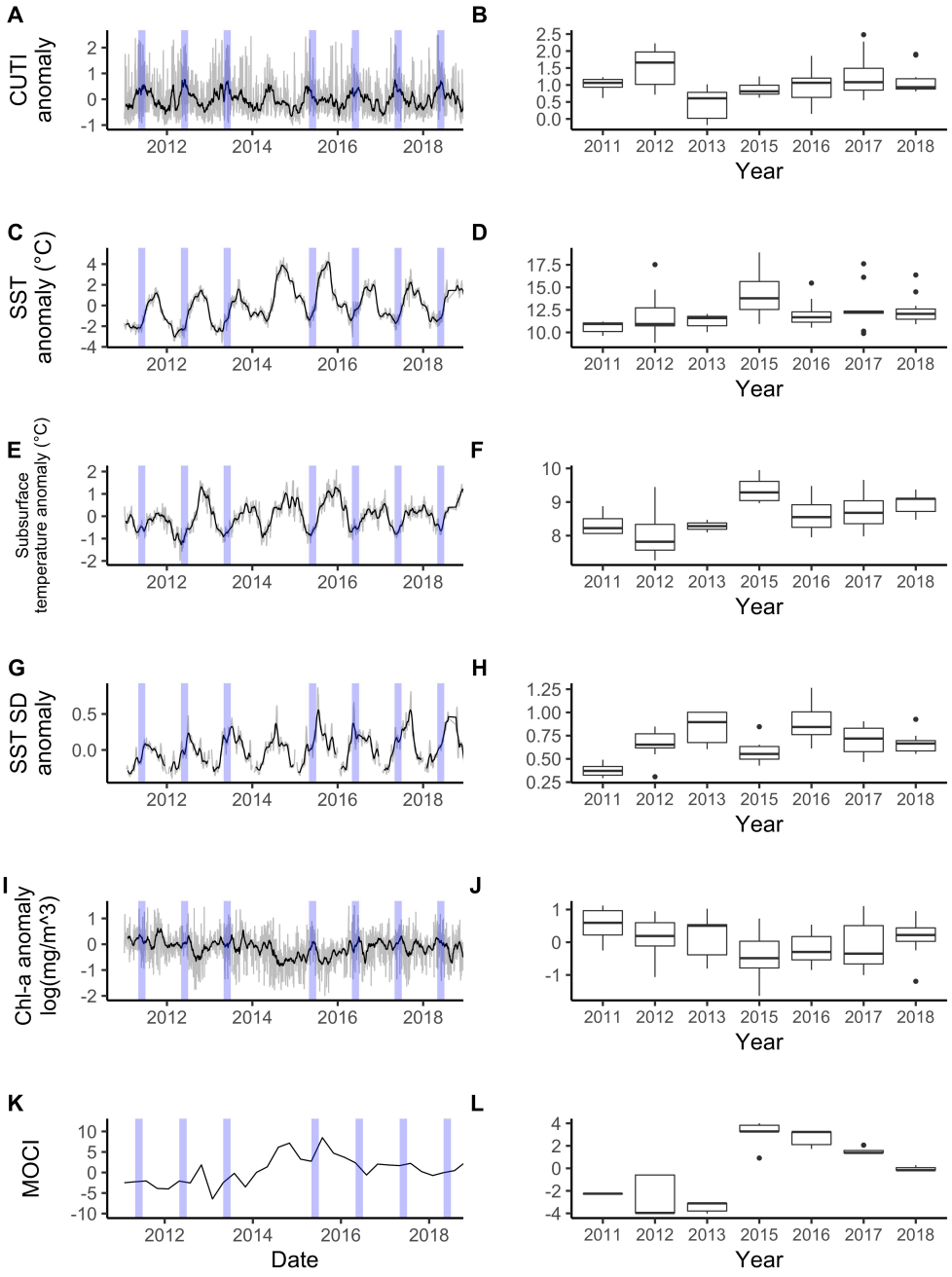

Figure 4. Time series of environmental covariates used in environmental models of krill length off California from 2011-2018, including CUTI (A, B), SST (C, D), subsurface temperature (E, F), SST SD (G, H), chl-*a* (I, J), and MOCI (K, L). Plots in the left column show conditions averaged across representative stations indicated in S1. The gray line shows daily average values, and the black line shows a 30-day moving average. RREAS sampling periods indicated by blue bars, excluding 2014. Boxplots in the right column show covariate values (based on timing and location of sample collection) included in linear mixed effects models of environmental drivers of krill length.

Euphausia pacifica

Our hypothesis that decreases in krill length during 2014-2016 were driven by elevated SST and reduced upwelling and primary productivity was not supported for *E. pacifica.* We found that adult *E. pacifica* length was not significantly associated with SST, CUTI, or chl-*a* during 2015, and we did not observe significant differences between sexes in length response to the three predictors (Figure 5, Table 3). When considering the impact of the environment on krill length throughout the time series (2011-2018) we found that *E. pacifica* size was moderately positively associated with increases in SST SD and moderately negatively associated with increases in CUTI and chl-*a* (Figure 6; confidence intervals available in Appendix A table S8). The influence of SST and subsurface temperature differed by sex, but not substantially.

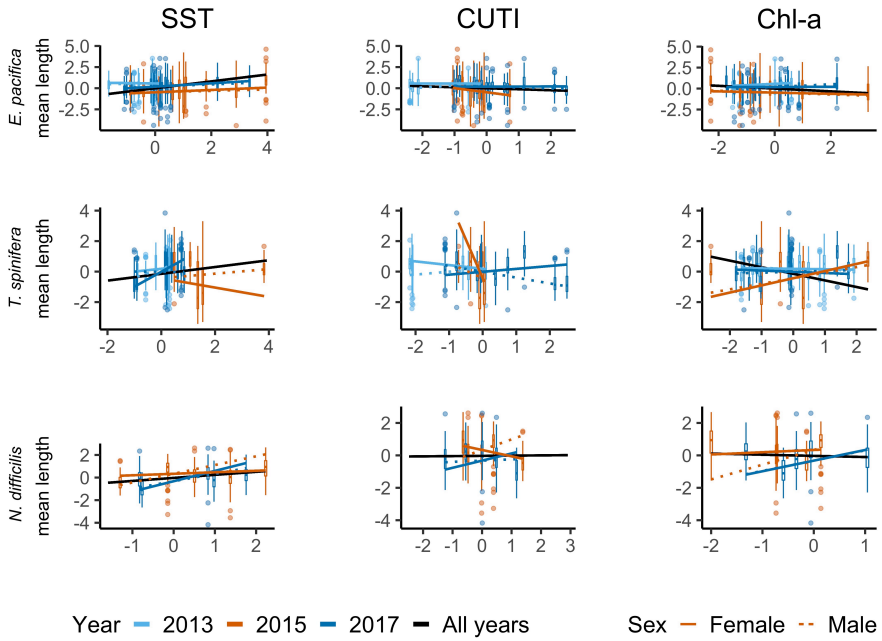

Figure 5. Annual, species-specific linear mixed effects models of krill length with SST, CUTI, chl-*a,* and sex two-way interaction terms as fixed effects and variable intercepts for station. SST, CUTI, and chl-*a* trends are shown before the heatwave (2013, light blue line), during the heatwave (2015, orange line), after the heatwave (2017, dark blue line), and across all years (2011-2018, black line). Solid lines show trends for females and dotted lines show trends for males. Boxplots show the distribution of raw data for each year, station. All length and predictor values are standardized such that means are 0 and variances are 1.

Table 3. Coefficient estimates of fixed effects (SST, CUTI, chl-*a*, and sex two-way interaction) from annual, species-specific linear mixed-effects models of krill length with variable intercepts for station. Estimates shown above 95% confidence intervals. Bolded values indicate estimates for which the 95% confidence interval does not cross 0. The number of stations (variable intercepts) in each model, marginal R^2 (R^2 of model with only fixed effects), and conditional R^2 (R^2 of model with fixed and station-level effects) are shown in the three columns to the right.

Species	CUTI	SST	Chl-a	Sex:CUTI	Sex:SST	SEX:Chl-a	Stations	marginal R^2	conditional R^2
2013									
E. pacifica	0.01 (-0.26 - 0.27)	-0.05 (-0.42 - 0.33)	0.16 (-0.09 - 0.41)	**0.24 (0.17 - 0.30)**	0.10 (-0.16 - 0.36)	**0.31 (0.12 - 0.39)**	8	0.127	0.145
T. spinifera	**-0.24 (-0.49 - 0.00)**	0.18 (-0.44 - 0.81)	-0.03 (-0.25 - 0.20)	**0.43 (0.37 - 0.50)**	**0.40 (0.12 - 0.68)**	-0.03 (-0.13 - 0.07)	10	0.191	0.318
2015									
E. pacifica	-0.49 (-1.32 - 0.35)	0.14 (-0.19 - 0.47)	-0.07 (-0.38 - 0.24)	-0.02 (-0.28 - 0.25)	-0.05 (-0.18 - 0.07)	-0.04 (-0.17 - 0.09)	10	0.109	0.278
T. spinifera	**-5.07 (-9.30 - -0.84)**	-0.31 (-1.36 - 0.75)	0.47 (-0.27 - 1.21)	**4.07 (2.90 - 5.33)**	**0.46 (0.22 - 0.69)**	-0.11 (-0.38 - 0.17)	5	0.233	0.523
N. difficilis	-0.39 (-2.51 - 1.73)	-0.13 (-1.56 - 1.82)	0.14 (-1.77 - 2.05)	**1.04 (0.47 - 1.62)**	**0.64 (0.10 - 1.18)**	**0.77 (0.11 - 1.43)**	5	0.058	0.474

Species	CUTI	SST	Chl-a	Sex:CUTI	Sex:SST	SEX:Chl-a	Stations	marginal R^2	conditional R^2
T. spinifera	0.19 (-0.22 - 0.60)	**0.98 (0.19 - 1.77)**	-0.08 (-0.37 - 0.21)	**-0.57 (-0.73 - - 0.41)**	**-1.00 (-1.27 - - 0.72)**	**0.14 (0.03 - 0.25)**	10	0.260	0.496
N. difficilis	**0.44 (0.11 - 0.78)**	**0.92 (0.56 - 1.27)**	**0.66 (0.36 - 0.95)**	-0.37 (-0.85 - 0.12)	-0.26 (-0.76 - 0.24)	-0.02 (-0.40 - 0.35)	5	0.144	0.157

We used estimated variable intercepts and slope coefficients from our model of krill length and environmental conditions (2011-2018) to interpret the effect of station on adult krill length (Figure 7A, B). Variable intercepts, which estimate mean length at each station, showed that *E. pacifica* tended to be slightly larger onshore than offshore (unpaired two-sample Wilcoxon test: W = 99, p = 0.064). SST variable slope coefficients, which estimate station-level differences in the response of adult krill length to changes in SST showed that krill length in the core region was more positively associated with increases in SST than in the south region (Kruskal-Wallis test: $X^2 = 6.92$, p = 0.031).

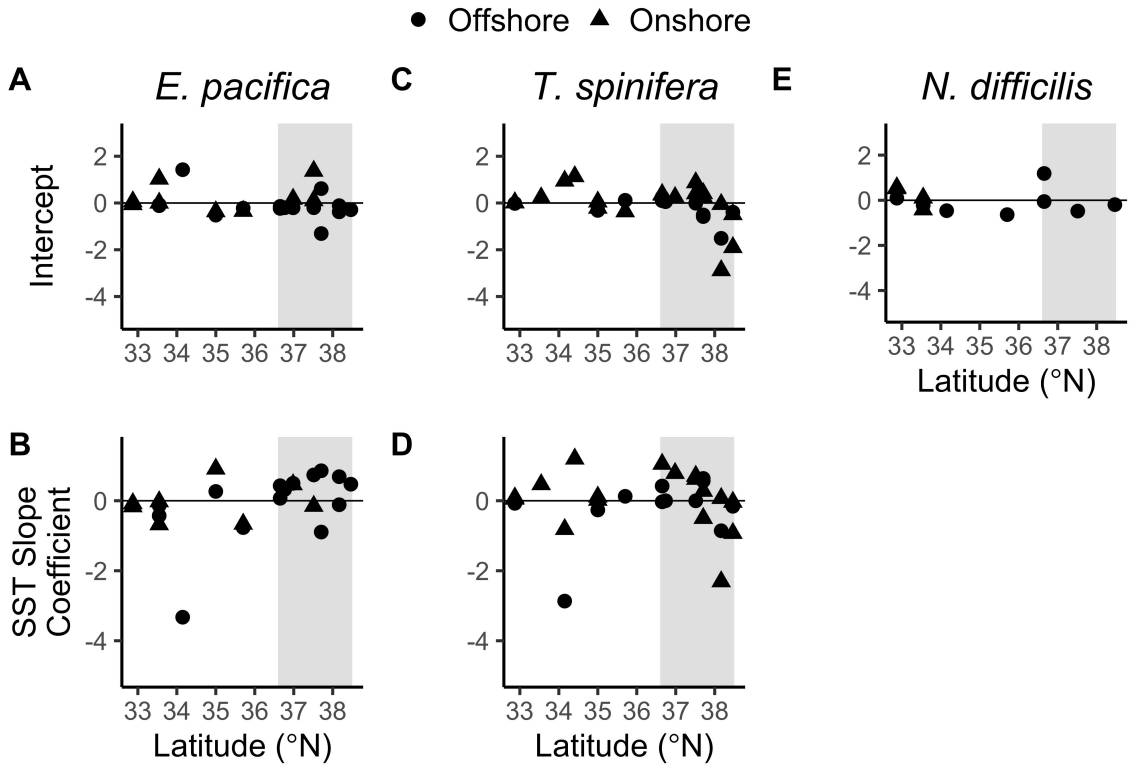

Figure 7. Station-level variable intercepts (A, C, E) and slopes (B, D) estimated by linear mixed effects models of environmental drivers of krill lengths across all years (2011-2018). Point share denotes offshore stations (>200 m deep, ~45 km from shore) and onshore stations (<200 m deep, ~3 km from shore). Gray shading shows the location of the North Central region.

Thysanoessa spinifera

In 2015, *T. spinifera* body size was not associated with SST or primary productivity, but it was inversely associated with CUTI, failing to support our hypotheses for the first two variables and contradicting our hypothesis for the third (Figure 5, Table 3). However, *T. spinifera* males showed a much weaker relationship with CUTI than females. Throughout the time series (2011-2018), lengths of adult *T. spinifera* females and, to a lesser extent, males were strongly negatively associated with increases in chl-*a*. *T. spinifera* length was moderately positively associated with increases in SST SD. Female, but not male, length was moderately negatively associated with the MOCI (Figure 7; confidence intervals available in Appendix A table 9). There was moderate variability in the effect of station on *T. spinifera* length (7C). Variable intercept estimates indicated that adult *T. spinifera* were smallest at the northernmost stations (Point Reyes and Fort Ross, Figure 1) but size varied little throughout the rest of the study area. Slope coefficients for SST were highly variable. Excluding the two northernmost transects, *T. spinifera* onshore responded more positively to increases in SST than offshore (unpaired two-sample Wilcoxon test: $W = 40$, $p = 0.05$) (Figure 7D).

Nematoscelis difficilis

In 2015, adult *N. difficilis* male, but not female, length was positively associated with CUTI, partially supporting our hypothesis for the role of upwelling in determining krill size during 2014-2016. Female *N. difficilis* showed no relationship with SST but males showed a positive association, contradicting our hypothesis for the role of SST in determining krill size during the 2014-2016. Finally, only male *N. difficilis* length was positively associated with chl-*a,* partially supporting our hypothesis for primary productivity (Figure 5, Table 3). Throughout the time series (2011-2018), adult *N. difficilis* were strongly positively associated with increases in

MOCI and CUTI, and moderately positively associated with increases in chl-*a* (Figure 6; confidence intervals available in Appendix A Table 10). However, the sample size of *N. difficilis* was considerably smaller than the other two species so model estimates may be biased. There was little variability in the effect of station on length (Figure 7E). *N. difficilis* were only present onshore in the south region, where the species is most abundant, and were infrequently present north of 34.5° N. Consequently, few station intercepts were estimated for the core region.

DISCUSSION

Previous warm periods in the CCE have been linked to reduced krill abundance (Brinton & Townsend, 2003; Fleming *et al*., 2016; Cimino *et al*., 2020), but it has been unclear how such periods have impacted krill body length, critical to understanding available biomass for krill predators in the ecosystem. Here we show some of the first evidence that 1) adult *E. pacifica* and *T. spinifera* lengths declined and adult *N. difficilis* lengths increased throughout the region during the peak of the 2014-2016 Northeast Pacific MHW and the beginning of the 2015-2016 El Niño, confirming patterns in *E. pacifica* and *T. spinifera* length observed off Trinidad Head during the same period (41° N; Robertson & Bjorkstedt, 2020); 2) the effect of the MHW/El Niño and environmental conditions on adult krill length differed strongly by sex; and 3) adult krill length and its response to increases in SST differed regionally and across the shelf. These results relate exclusively to adult krill >10 mm, and it is likely that interannual variation and environmental drivers of krill length differ for smaller age/size classes (Robertson & Bjorkstedt, 2020). Nonetheless, as adults comprise a large portion of available krill biomass and constitute the breeding part of the population, documenting drivers of adult krill length is useful for understanding both krill trophic ecology and population dynamics.

This study indicates how extreme climate events impact krill biomass over broad spatial and temporal scales by investigating changes in mean population length. However, it is important to note that individual growth is not the only factor that can influence mean population length. Low growth/shrinkage as well as an increase in recruitment of juveniles (small size classes) to the adult stage can reduce mean population length. For instance, we found that mean adult length was smallest during 2011 and 2015 (Figure 3A). This was surprising given that the two years were very different in key indicators of ocean condition (Figure 4). A strong La Niña occurred in 2011 with negative MOCI values and negative SST anomalies (generally indicators for high productivity) throughout the CCE. In contrast, 2015 was characterized by positive MOCI values and some of the highest SST anomalies (generally indicators for low productivity) in the time series. Consequently, it is unlikely that shared environmental conditions across the two years led to low growth. High levels of spawning in early 2011 (Jan-Mar), triggered by elevated primary production, may have led to a large cohort of juveniles recruiting to the adult stage by the time RREAS sampling took place (May-Jun), resulting in lower mean population length of adults >10 mm. This is supported by the observation that krill abundance was anomalously high in 2011 (Cimino *et al*., 2020). However, in 2015, when krill abundance was anomalously low (Cimino *et al.,* 2020), low growth due to adverse environmental conditions, rather than an influx of juveniles, is more likely to have caused observed declines in population mean length. As changes in both age structure and growth are viable mechanisms for shifts in population mean length, future observational studies could expand on this work by quantifying or controlling for both processes concurrently (Shaw *et al.,* 2021).

Krill length 2014-2016

While it is unfortunate that we were not able to report on krill length in 2014, when the beginnings of the MHW were first felt in our study area, we did observe interesting differences in krill body size across 2015 and 2016. *E. pacifica* and *T. spinifera* size declined dramatically in 2015 and recovered in 2016 while *N. difficilis* displayed the opposite pattern. Ocean conditions and the evolution of the MHW also differed in 2015 and 2016. Anomalously warm SSTs peaked in 2015 (Gentemann *et al*., 2017) with the northward propagation of an El Niño and subsequent re-intensification of the MHW in the winter of 2014/15 (DiLorenzo & Mantua, 2016). *N. difficilis* were exceptionally large during this period, perhaps due to the species' adaptation to subtropical-tropical as well as temperate waters (Brinton, 1962) and poleward advection linked to the El Niño (Lilly & Ohman, 2021). By the winter of 2015/16, SSTs in our study region were still warm but not as warm as in 2015 (Gentemann *et al*., 2017). Moreover, in the weeks leading up to 2016 krill sampling, upwelling, and chl-*a* content were more similar to pre- and post-MHW conditions (Figure 4). Therefore, declines in *E. pacifica* and *T. spinifera* size, such as that observed in 2015, may be linked more to the intensity than the duration of extreme climate events like the MHW, and length frequency distributions may be able to recover quickly as extreme events elapse.

Length-based sexual dimorphism

Our findings confirm well-established knowledge that female krill are larger than males (Nemoto, 1966; Tanasichuk, 1998a). However, in 2015, adult female:male length ratios declined for all three species and even inverted for *T. spinifera* and *N. difficilis* (Figure 3C) driven by a disproportionate reduction in female length. Hence, conditions associated with the MHW may

have disrupted energy allocation for growth by adult female krill, but not males, during or prior to sample collection (May and June).

All three species spawn in the spring and summer (Brinton & Wyllie, 1976; Feinberg *et al.,* 2003), and it is expected that female krill allocate more energy towards reproduction than males during this period (Pond *et al.,* 1995; Tanasichuk, 1998b). As female krill are unlikely to be smaller from prioritising reproductive investment over growth (see above discussion around spawning during 2015), observed reductions in female length are more likely due to low growth or shrinkage when food availability was low, water temperatures were high, and energy was required to sustain even very limited reproductive output. This could also help explain low krill abundance in 2015 and 2016 as smaller females tend to produce smaller brood sizes for both *E. pacifica* and *T. spinifera* (Ross *et al.,* 1982; Feinberg *et al.,* 2007; Gómez-Gutiérrez *et al.,* 2006). To evaluate the effect of extreme climate events on krill, future studies should consider the concurrent abundance, length, and reproductive state of individuals. Such an approach would be particularly helpful in differentiating between fluctuations in length due to reproductive output vs. growth, both of which are impacted by environmental change (Pinchuk & Hopcraft, 2007; Shaw *et al.,* 2021).

Environmental drivers of krill body length

Sea Surface Temperature

There is strong evidence that *E. pacifica* length declines with rising temperature (Robertson & Bjorkstedt, 2020), particularly when temperatures exceed 14° C and metabolic efficiency declines (Iguchi & Ikeda, 1995; Alonzo & Mangel, 2001). *E. pacifica* in the CCE are even known to shrink with successive moults when *in situ* SST increases above 19° C (Marinovic & Mangel, 1999). Nonetheless, adult length in our study was not strongly associated

with SST before, during, or after 2014-2016 for any of the three species (though it was strongly associated with SST SD, see Appendix A). Incongruence between our findings and prior work may be because 10-day averaged surface temperature derived from a 10 km^2 gridded numerical ocean model (ROMS) does not adequately capture conditions experienced by krill *in situ*. However, we believe these data are a reasonable approximation of *in situ* conditions experienced by krill over the temporal scale of krill moulting, with intermoult periods on the order of several days (Marinovic & Mangle, 1999; Pinchuk & Hopcraft, 2007; Shaw *et al*., 2010).

In 2017, mean body length of all three species increased with SST (Table 3). *E. pacifica* length was also weakly positively associated with SST when we modelled length across all years (2011-2018; Figure 6). These trends directly contradict previously documented relationships between temperature and length. However, SSTs in our study domain were infrequently above the 14°C threshold identified by Iguchi and Ikeda (1995), suggesting that krill may have rarely (except in 2015) been exposed to water temperatures that directly curtail growth or cause shrinkage. In a *post hoc* test examining whether adult *E. pacifica* length exhibits a different relationship with SSTs above and below 14°C, we compared model performance of nonlinear and linear models of SST and mean *E. pacifica* length (Figure S12). The nonlinear model showed a more positive association between SST and length at temperatures below 14°C than above the threshold. Hence, elevated SST may result in larger adult *E. pacifica* up to approximately 14°C with diminishing returns at higher SST values. Alternatively, krill species may show longer mean length with moderate SST increases as a result of reduction in reproductive effort (Feinberg *et al.,* 2007) or selective mortality of smaller individuals, but we did not quantify reproductive effort or cohort survival in our study.

Upwelling and Food Availability

Upwelling was not strongly linked to adult mean length in 2015 for either *E. pacifica* or *N. difficilis*, but it was strongly negatively associated with female *T. spinifera* mean length (Table 3). This latter trend was driven by two stations off Santa Barbara where female *T. spinifera* were substantially smaller than males following a period of typical upwelling intensity. During a year of otherwise below average upwelling, this localized pulse of upwelling may have stimulated an increase in energy allocation to reproduction by females, resulting in shrinkage or low growth of females but not males (Smiles & Pearcy, 1971; Feinberg *et al.,* 2007).

The same process may be responsible for the strongly negative relationship observed across all years (Figure 6) between chl-*a* and mean length of *E. pacifica* and *T. spinifera*. The size of adult *E. pacifica* size tends to peak prior to spawning (Robertson & Bjorkstedt, 2020), which is timed to overlap with phytoplankton blooms, as indicated by chl-*a* content peaks (Feinberg *et al.,* 2010; Shaw *et al.,* 2021). Adult length may have declined with increasing chl-*a* content as a result of elevated spawning rather than lack of food (Shaw *et al*., 2021). It is worth noting that satellite chlorophyll-*a* content (4 km^2 resolution) may not be a reliable indicator of food availability for krill. Satellite derived data may differ from *in situ* concentrations, and it cannot indicate subsurface chlorophyll concentrations, which also play a role in determining food availability for vertically migrating krill (Shaw *et al.,* 2021). In addition, chl-*a* does not reflect the full complement of food resources available to krill. As opportunistic heterotrophs, krill feed on phytoplankton, marine snow (Dilling 1998), and other planktonic invertebrates (copepods; Ohman 1984), and heterotrophic feeding might ameliorate the impact of low phytoplankton availability on the body size reduction of adult krill.

Regional variation in krill body length response to temperature

A major benefit of using a mixed-effects modelling approach to examine species trends over large spatial scales is that it allowed us to look at both ecosystem-wide and local drivers of krill length. For example, *E. pacifica* and *T. spinifera* response to SST varied regionally throughout the CCE. Krill length onshore (*T. spinifera*) and in the core region (*E. pacifica*) responded more positively to increasing SSTs than in other regions (Figure 7B, D). Strong, persistent springtime upwelling yields high pelagic productivity in these zones but also cooler surface waters. Therefore, adult *E. pacifica* and *T. spinifera* body size in localities with high upwelling intensity may be limited less by food availability and more by thermal limits on metabolic efficiency (Marinovic & Mangel, 1999), allowing them to benefit from limited increases in SST. Such a mechanism would help to explain why adult krill were of average length in 2016, when SSTs were still high relative to other years in the time series but CUTI had increased relative to 2015. Moreover, local variability could partially explain why the relationship between SST and adult length is different in other regions of the CCE (Robertson & Bjorkstedt, 2020).

Regional differences in krill length response to environmental variability may be key to understanding how ocean warming will impact this numerically and trophically important taxon. Spatial and temporal fluctuations in krill biomass during the 2014-2016 MHW have been linked to seabird reproductive failures (Jones *et al*., 2018), reduced fishery recruitment (McClatchie *et al*., 2016) and increased whale mortality (Santora *et al*., 2020). In turn, indirect effects of the MHW on krill predators have had system-wide ecological and socioeconomic consequences. Future studies could expand on our work by investigating regional variation in the response of krill biomass response to environmental change, perhaps identifying high-risk locations where

krill are particularly sensitive to warming or refugia that help to mitigate the effects of extreme climate events for both krill and their predators. These insights may prove invaluable for managers seeking to enact ecosystem-based fishery management in the region (Harvey *et al*., 2019).

CONCLUSION

We demonstrated that the observed 2014-2016 Northeast Pacific MHW/El Niño had a strong impact on the adult body size of three common krill species in the CCE, particularly in 2015 (no length data available for 2014). Adult krill length declined for two temperate species (*E. pacifica* and *T. spinifera*) adapted to cool, highly productive waters, but increased for one temperate-subtropical species (*N. difficilis*) adapted to warmer conditions. We also show evidence that female size declined relative to male size for all three species, indicating that heatwave conditions made reproductive energy allocation more costly to females in terms of somatic growth. Finally, we found that high SST and low upwelling and primary productivity were not strong predictors of reduced krill size during 2014-2016, but drivers of krill size appear to vary by location providing early evidence that some locations may serve as refugia for krill from the worst effects of extreme climate events. Making multispecific comparisons across large spatial and long temporal scales is a powerful approach that provided new insights into the effect of extreme climate events and environmental drivers on krill populations with cascading consequences for key predators in pelagic ecosystems. Our observations offer a guide to how we may expect krill biomass to be impacted by future climate change, including the increasing frequency of MHWs (Frölicher *et al*., 2018).

CHAPTER 1 LITERATURE CITED

Alonzo, S., and Mangel, M. 2001. Survival strategies and growth of krill: Avoiding predators in space and time. Marine Ecology Progress Series, 209: 203-217.

Baker, A. d. C., Boden, B., and Brinton, E. 1990. A practical guide to the euphausiids of the World, Natural History Museum Publications, London.

Barlow, D. R., Bernard, K. S., Escobar-Flores, P., Palacios, D. M., and Torres, L. G. 2020. Links in the trophic chain: modeling functional relationships between in situ oceanography, krill, and blue whale distribution under different oceanographic regimes. Marine Ecology Progress Series, 642: 207-225.

Barter, R., and Yu, B. 2017. superheat: A graphical tool for exploring complex datasets using heatmaps. [Online] Available: https://cran.r-project.org/web/packages/superheat/index.html.

Bartón, K. 2020. MuMIn: Multi-model inference. [Online] Available: https://cran.r-project.org/web/packages/MuMIn/index.html.

Bates, D., Mächler, M., Bolker, B., and Walker, S. 2015. Fitting linear mixed-effects models using lme4. Journal of Statistical Software; Vol 1, Issue 1.

Bond, N. A., Cronin, M. F., Freeland, H., and Mantua, N. 2015. Causes and impacts of the 2014 warm anomaly in the NE Pacific. Geophysical Research Letters, 42: 3414-3420.

Brinton, E. 1960. Changes in the distribution of euphausiid crustaceans in the region of the California Current. California Cooperative Oceanic Fisheries Investigations Reports, 7: 137-146.

Brinton, E. 1962. The distribution of Pacific euphausiids. Bulletin of the Scripps Institution of Oceanography, 8: 21-270.

Brinton, E., Ohman, M. D., Townsend, A., Knight, M. D., and Bridgeman, A. L. 2000. Euphausiids of the world oceans, series: World biodiversity database CD-ROM Series. Expert Center for Taxonomic Identification, Amsterdam, Netherlands.

Brinton, E., and Townsend, A. 2003. Decadal variability in abundances of the dominant euphausiid species in southern sectors of the California Current. Deep Sea Research Part II: Topical Studies in Oceanography, 50: 2449-2472.

Brinton, E., and Wyllie, J. G. 1976. Distributional atlas of euphausiid growth stages off southern California, 1953-1956. 24.

Brodeur, R. D., Auth, T. D., and Phillips, A. J. 2019. Major shifts in pelagic micronekton and macrozooplankton community structure in an upwelling ecosystem related to an unprecedented marine heatwave. Frontiers in Marine Science, 6: 212.

Checkley, D. M., and Barth, J. A. 2009. Patterns and processes in the California Current System. Progress in Oceanography, 83: 49-64.

Cimino, M. A., Santora, J. A., Schroeder, I., Sydeman, W., Jacox, M. G., Hazen, E. L., and Bograd, S. J. 2020. Essential krill species habitat resolved by seasonal upwelling and ocean circulation models within the large marine ecosystem of the California Current System. Ecography, 43: 1536-1549.

Di Lorenzo, E., and Mantua, N. 2016. Multi-year persistence of the 2014/15 North Pacific marine heatwave. Nature Climate Change, 6: 1042-1047.

Dilling, L., Wilson, J., Steinberg, D., and Alldredge, A. 1998. Feeding by the euphausiid *Euphausia pacifica* and the copepod *Calanus pacificus* on marine snow. Marine Ecology Progress Series, 170: 189-201.

Feinberg, L. R., and Peterson, W. T. 2003. Variability in duration and intensity of euphausiid spawning off central Oregon, 1996–2001. Progress in Oceanography, 57: 363-379.

Feinberg, L. R., Peterson, W. T., and Tracy Shaw, C. 2010. The timing and location of spawning for the Euphausiid *Thysanoessa spinifera* off the Oregon coast, USA. Deep Sea Research Part II: Topical Studies in Oceanography, 57: 572-583.

Feinberg, L. R., Shaw, C. T., and Peterson, W. T. 2007. Long-term laboratory observations of *Euphausia pacifica* fecundity: comparison of two geographic regions. Marine Ecology Progress Series, 341: 141-152.

Field, J. C., and Francis, R. C. 2006. Considering ecosystem-based fisheries management in the California Current. Marine Policy, 30: 552-569.

Field, J. C., Francis, R. C., and Aydin, K. 2006. Top-down modeling and bottom-up dynamics: Linking a fisheries-based ecosystem model with climate hypotheses in the Northern California Current. Progress in Oceanography, 68: 238-270.

Fleming, A. H., Clark, C. T., Calambokidis, J., and Barlow, J. 2016. Humpback whale diets respond to variance in ocean climate and ecosystem conditions in the California Current. Global Change Biology, 22: 1214-1224.

Frölicher, T. L., Fischer, E. M., and Gruber, N. 2018. Marine heatwaves under global warming. Nature, 560: 360-364.

García-Reyes, M., Largier, J. L., and Sydeman, W. J. 2014. Synoptic-scale upwelling indices and predictions of phyto- and zooplankton populations. Progress in Oceanography, 120: 177-188.

García-Reyes, M., and Sydeman, W. J. 2017. California Multivariate Ocean Climate Indicator (MOCI) and marine ecosystem dynamics. Ecological Indicators, 72: 521-529.

Gelman, A., and Hill, J. 2007. Data analysis using regression and multilevel/hierarchical models, Cambridge University Press, Cambridge, United Kingdom.

Gentemann, C. L., Fewings, M. R., and García-Reyes, M. 2017. Satellite sea surface temperatures along the West Coast of the United States during the 2014–2016 northeast Pacific marine heat wave. Geophysical Research Letters, 44: 312-319.

Gómez-Gutiérrez, J., Feinberg, L. R., Shaw, C., and Peterson, W. 2006. Variability in brood size and female length of *Euphausia pacifica* among three populations in the North Pacific. Marine Ecology-Progress Series, 323: 185-194.

Grueber, C. E., Nakagawa, S., Laws, R. J., and Jamieson, I. G. 2011. Multimodel inference in ecology and evolution: challenges and solutions. Journal of Evolutionary Biology, 24: 699-711.

Harvey, C., Garfield, N., Williams, G., Tolimieri, N., Schroeder, I., Andrews, K., Barnas, K., et al. 2019. Ecosystem status report of the California Current for 2019: A summary of ecosystem indicators compiled by the California Current Integrated Ecosystem Assessment team (CCIEA).

Hipfner, J. M. 2009. Euphausiids in the diet of a North Pacific seabird: Annual and seasonal variation and the role of ocean climate. Marine Ecology Progress Series, 390: 277-289.

Hobday, A. J., Alexander, L. V., Perkins, S. E., Smale, D. A., Straub, S. C., Oliver, E. C. J., Benthuysen, J. A., et al. 2016. A hierarchical approach to defining marine heatwaves. Progress in Oceanography, 141: 227-238.

Iguchi, N., and Ikeda, T. 1995. Growth, metabolism and growth efficiency of a euphausiid crustacean *Euphausia pacifica* in the southern Japan Sea, as influenced by temperature. Journal of Plankton Research, 17: 1757-1769.

Jacox, M. G., Edwards, C. A., Hazen, E. L., and Bograd, S. J. 2018. Coastal upwelling revisited: Ekman, Bakun, and improved upwelling indices for the U.S. West Coast. Journal of Geophysical Research: Oceans, 123: 7332-7350.

Jones, T., Parrish, J. K., Peterson, W. T., Bjorkstedt, E. P., Bond, N. A., Ballance, L. T., Bowes, V., et al. 2018. Massive mortality of a planktivorous seabird in response to a marine heatwave. Geophysical Research Letters, 45: 3193-3202.

Koehn, L. E., Essington, T. E., Marshall, K. N., Kaplan, I. C., Sydeman, W. J., Szoboszlai, A. I., and Thayer, J. A. 2016. Developing a high taxonomic resolution food web model to assess the functional role of forage fish in the California Current ecosystem. Ecological Modelling, 335: 87-100.

Krag, L. A., Herrmann, B., Iversen, S. A., Engås, A., Nordrum, S., and Krafft, B. A. 2014. Size selection of Antarctic krill (*Euphausia superba*) in trawls. Plos One, 9: e102168.

Lavaniegos, B. E., Jiménez-Herrera, M., and Ambriz-Arreola, I. 2019. Unusually low euphausiid biomass during the warm years of 2014–2016 in the transition zone of the California Current. Deep Sea Research Part II: Topical Studies in Oceanography, 169-170: 104638.

Lilly, L. E., and Ohman, M. D. 2021. Euphausiid spatial displacements and habitat shifts in the southern California Current System in response to El Niño variability. Progress in Oceanography, 193: 102544.

Marinovic, B., and Mangel, M. 1999. Krill can shrink as an ecological adaptation to temporarily unfavourable environments. Ecology Letters, 2: 338-343.

Marinovic, B. B., Croll, D. A., Gong, N., Benson, S. R., and Chavez, F. P. 2002. Effects of the 1997–1999 El Niño and La Niña events on zooplankton abundance and euphausiid

community composition within the Monterey Bay coastal upwelling system. Progress in Oceanography, 54: 265-277.

McClatchie, S., Goericke, R., Leising, A., Auth, T. D., Bjorkstedt, E., Robertson, R., Brodeur, R., et al. 2016. State of the California Current 2015-16: Comparisons with the 1997-98 El Niño. California Cooperative Oceanic Fisheries Investigations Reports, 57: 5-61.

Nakagawa, Y., Ota, T., Endo, Y., Taki, K., and Sugisaki, H. 2004. Importance of ciliates as prey of the euphausiid *Euphausia pacifica* in the NW North Pacific. Marine Ecology Progress Series, 271: 261-266.

Nemoto, T. 1966. *Thysanoessa* euphausiids, comparative morphology, allomorphosis and ecology. Scientific Reports of the Whales Research Institute, 20: 109-155.

Nickels, C. F., Sala, L. M., and Ohman, M. D. 2018. The morphology of euphausiid mandibles used to assess selective predation by blue whales in the southern sector of the California Current System. Journal of Crustacean Biology, 38: 563-573.

Ohman, M. D. 1984. Omnivory by *Euphausia pacifica*: the role of copepod prey. Marine Ecology Progress Series, 19: 125-131.

Piatt, J. F., Parrish, J. K., Renner, H. M., Schoen, S. K., Jones, T. T., Arimitsu, M. L., Kuletz, K. J., et al. 2020. Extreme mortality and reproductive failure of common murres resulting from the northeast Pacific marine heatwave of 2014-2016. Plos One, 15: e0226087.

Pinchuk, A. I., and Hopcroft, R. R. 2007. Seasonal variations in the growth rates of euphausiids (*Thysanoessa inermis*, *T. spinifera*, and *Euphausia pacifica*) from the northern Gulf of Alaska. Marine Biology, 151: 257-269.

Pond, D., Watkins, J., Priddle, J., and Sargent, J. 1995. Variation in the lipid content and composition of Antarctic krill *Euphausia superba* at South Georgia. Marine Ecology Progress Series, 117: 49-57.

R Core Team 2019. R: A language and environmental for statistical computing. Vienna, Austria. [Online] Available: https://www.r-project.org/.

Robertson, R. R., and Bjorkstedt, E. P. 2020. Climate-driven variability in *Euphausia pacifica* size distributions off northern California. Progress in Oceanography, 188: 102412.

Ross, R., and Quetin, L. 2000. Reproduction in Euphausiacea. In Krill: biology, ecology and fisheries. Ed. by I. Everson. Blackwell Science, Cambridge, United Kingdom.

Rueden, C., Schindelin, J., Hiner, M., Dezonia, B., Walter, A., and Eliceiri, K. 2017. ImageJ2: ImageJ for the next generation of scientific image data. BMC Bioinformatics, 18.

Sakuma, K. M., Field, J. C., Mantua, N. J., Ralston, S., Marinovic, B. B., and Carrion, C. N. 2016. Anomalous epipelagic micronekton assemblage patterns in the neritic waters of the California Current in spring 2015 during a period of extreme ocean conditions. California Cooperative Oceanic Fisheries Investigations Reports, 57: 163-183.

Sakuma, K. M., Ralston, S., and Wespestad, V. G. 2006. Interannual and spatial variation in the distribution of young-of-the-year rockfish (*Sebastes spp*): Expanding and coordinating a survey sampling frame. California Cooperative Oceanic Fisheries Investigations Reports, 47: 127-139.

Santora, J. A., Mantua, N. J., Schroeder, I. D., Field, J. C., Hazen, E. L., Bograd, S. J., Sydeman, W. J., et al. 2020. Habitat compression and ecosystem shifts as potential links between marine heatwave and record whale entanglements. Nature Communications, 11: 536.

Sathyendranath, S., Jackson, T., Brockmann, C., Brotas, V. C., B., Chuprin, A., Clements, O., Cipollini, P., et al. 2020. ESA Ocean Colour Climate Change Initiative (Ocean_Colour_cci): Global chlorophyll-a data products gridded on a sinusoidal projection. 4.2 edn.

Shaw, C., Peterson, W., and Feinberg, L. 2010. Growth of *Euphausia pacifica* in the upwelling zone off the Oregon coast. Deep Sea Research Part II: Topical Studies in Oceanography, 57: 584-593.

Shaw, C. T., Bi, H., Feinberg, L. R., and Peterson, W. T. 2021. Cohort analysis of *Euphausia pacifica* from the Northeast Pacific population using a Gaussian mixture model. Progress in Oceanography, 191: 102495.

Smiles, M. C., and Pearcy, W. G. 1971. Size structure and growth rate of *Euphausia pacifica* off the Oregon coast. Fisheries Bulletin, 69.

Sydeman, W. J., Thompson, S. A., Santora, J. A., Koslow, J. A., Goericke, R., and Ohman, M. D. 2015. Climate–ecosystem change off southern California: Time-dependent seabird predator–prey numerical responses. Deep Sea Research Part II: Topical Studies in Oceanography, 112: 158-170.

Tanasichuk, R. W. 1998(a). Interannual variations in the population biology and productivity of *Euphausia pacifica* in Barkley Sound, Canada, with special reference to the 1992 and 1993 warm ocean years. Marine Ecology Progress Series, 173: 163-180.

Tanasichuk, R. W. 1998(b). Interannual variations in the population biology and productivity of *Thysanoessa spinifera* in Barkley Sound, Canada, with special reference to the 1992 and 1993 warm ocean years. Marine Ecology Progress Series, 173: 181-195.

Thayer, J. A., Field, J. C., and Sydeman, W. J. 2014. Changes in California Chinook salmon diet over the past 50 years: Relevance to the recent population crash. Marine Ecology Progress Series, 498: 249-261.

Trathan, P. N., and Hill, S. L. 2016. The importance of krill predation in the Southern Ocean. In Biology and ecology of Antarctic krill, 1 edn. Ed. by V. Seigel. Springer International, Switzerland.

Wells, B. K., Santora, J. A., Schroeder, I. D., Mantua, N., Sydeman, W. J., Huff, D. D., and Field, J. C. 2016. Marine ecosystem perspectives on Chinook salmon recruitment: A synthesis of empirical and modeling studies from a California upwelling system. Marine Ecology Progress Series, 552: 271-284.

Wickham, H. 2016. ggplot2: Elegant graphics for data analysis. [Online] Available: https://cran.r-project.org/package=ggplot2.

Zhu, H. 2020. kableExtra: Construct complex table with ‘kable’ and pipe syntax. [Online] Available: https://cran.r-project.org/package=kableExtra.

CHAPTER 2

Behavior regulates nearshore retention and cross-shelf transport of fish larvae in an upwelling region

ABSTRACT

The larvae of diverse coastal species exhibit depth preferences that regulate dispersal patterns and population connectivity, however the prevalence of such behaviors among larval fishes is not well understood in the California Current upwelling region. We collected larval fishes at four depths along two cross-shelf transects in the northern California Current during peak upwelling season (Mar-July, 2017-2019) at Bodega Head (38.3° N) and Stewarts Point (38.6° N). Larval distributions were used to test the hypothesis that ichthyoplankton exhibit ontogenetically variable, and environmentally cued depth preferences akin to those observed among other the larvae of other coastal taxa. Over 75% of larvae of 51 fish taxa were retained within 6 km of shore despite strong alongshore wind stress and upwelling-driven offshore transport of surface waters. Larvae of 10 species were concentrated close to shore beneath the mixed layer, seven species were almost exclusively neustonic, seven species were transported shoreward and to the surface during upwelling, and three species conducted a reverse ontogenetic vertical migration. Larvae of another 15 species, from predominantly mid- and outer-shelf habitats, were distributed across the continental shelf below the mixed layer. Thus, behavioral regulation of dispersal is common among nearshore fish species in the California Current and likely is in other upwelling regions where cross- and alongshore flows are vertically stratified. Behavioral patterns documented in this study would improve biophysical- and individual-based dispersal models used to predict spatial population connectivity, recruitment, and the design of marine protected areas linked by planktonic dispersal.

INTRODUCTION

Connectivity among biological populations allows for exchange of individuals and genes, generating spatial and temporal population dynamics. In marine systems, many species are sessile, sedentary or have a limited home range, so dispersive planktonic larvae provide all or most of the connectivity between spatially disparate populations (Weersing & Toonen, 2009). Consequently, understanding larval dispersal, connectivity and recruitment are of central importance to both marine ecology (Cowen et al., 2007) and management (Shanks et al., 2003; Hastings & Botsford, 2006; White et al., 2010). Larval dispersal is notoriously difficult to study though, as larvae are miniscule and develop for weeks to months in a vast and dynamic ocean. Moreover, because larval swimming abilities are generally limited relative to ambient current speeds, many studies in planktonic connectivity adopt a null model of dispersal, treating larvae as passive drifters. Such studies frequently use mean ocean currents (Siegel et al., 2008; Watson et al., 2010; Nishimoto et al., 2019) and pelagic larval duration (Hedgecock et al., 2007) as indicators of dispersal kernals. However, decades of laboratory studies and larval surveys of a wide variety of taxa in settings around the world show that larvae are not passive drifters and exhibit active swimming and depth preference behaviors that influence their dispersal patterns and thus larval connectivity (Leis et al., 1996; Epifanio & Garvine, 2001; Paris & Cowen, 2004; Morgan, 2006).

Larval behavior plays a particularly important role in regions with stratified flow, such as in upwelling systems, where larvae may move vertically either avoiding or increasing exposure to currents (Lenarz et al., 1991; Morgan et al., 2018). In the California Current Ecosystem (CCE), a seasonal atmospheric high-pressure system in the North Pacific brings strong alongshore, northwesterly winds to the U.S. West Coast during the boreal spring and summer

months. These winds drive equatorward surface flow that is redirected offshore by Ekman forces, lowering nearshore sea surface height and drawing deep, cold, nutrient-rich waters to the photic zone. Persistent upwelling in this region also results in the formation of a coastal equatorward geostrophic jet bounded on the landward side by the coastline and seaward by an upwelling front (Strub et al., 1987). Alongshore flows are, however, damped within a narrow coastal boundary layer (CBL), out to 6 km from shore, where friction with the benthos slows equatorward transport (Nickols et al., 2012). During the peak upwelling season in this region, dominant flows are thus vertically stratified cross-shore and equatorward alongshore and are periodically interrupted by relaxation events where flow velocities slow or reverse.

Despite strong offshore transport of surface waters in the California Current, larvae of most species of nearshore invertebrates are retained close to shore (Fisher et al., 2014; Hameed et al., 2018; Morgan et al., 2018) and many taxa exhibit directed onshore swimming (Drake et al., 2018) and/or depth preferences that limit advection offshore or facilitate the return of pre-settlement larvae after developing offshore (reviewed by Morgan, 2014). For example, some species maintain proximity to shore throughout development by remaining beneath the surface mixed layer where offshore currents are strongest. Other species conduct daily vertical migrations (DVM), ascending to the surface at night when onshore winds occur. And still others change their depth distribution according to developmental stage: descending late in development where they are exposed to shoreward upwelling currents, completing an ontogenetic vertical migration (OVM) or ascending late in development where they are transported shoreward on internal tides or waves in a reverse ontogenetic vertical migration (ROVM).

Simulations of larval dispersal in numerical circulation models have shown that these behaviors impact connectivity by reducing alongshore transport (Drake et al., 2013) and increasing settlement rates (Drake et al., 2015). While these behaviors have been well documented in the California Current for many invertebrates (especially, crustaceans), they have only rarely been explored in larval fishes. Like nearshore invertebrate larvae, ichthyoplankton of nearshore species are most abundant on the inner continental shelf, even during peak upwelling season (Laroche & Richardson, 1979; Watson, 1982; Marliave, 1986). Moreover, there is evidence that some species exhibit depth preference behaviors similar to sympatric invertebrate larvae, including remaining beneath the surface mixed layer (Marliave, 1986) and by conducting DVM (Robards et al., 1999; Sakuma et al., 1999) or OVM (Sakuma & Larson, 1995; Allen & Leos, 2001). A full assessment of how widespread these behaviors are among ichthyoplankton and evaluation of the impact of behaviors on dispersal outcomes, however, requires cross-shelf, depth-stratified sampling of the full ichthyoplanktonic assemblage across a variety of upwelling states.

From 2017-2019, we surveyed ichthyoplankton across the continental shelf during peak upwelling season on the central coast of California to better understand the degree to which larval fish dispersal is regulated by swimming and depth preference behaviors in an advective environment. Our primary goal was to test the hypothesis that local retention of the larvae of nearshore fishes is facilitated by the existence of species-specific depth regulation behaviors akin to those that have been documented in sympatric invertebrate larvae. Existing regional ichthyoplankton surveys, such as the National Marine Fisheries Service midwater trawl survey or CalCOFI, have been unable to adequately test this hypothesis because cruises occur too infrequently or target only late-stage larvae. Our survey also differed from prior surveys in that

we used a depth-stratified sampling approach to map vertical variation in larval density, and we targeted both upwelling and relaxation events to understand the role of environmental forcing in vertical and cross-shelf distributions. Our secondary goal was to examine how behavior may regulate transport of the larvae of species living across the shelf, beyond nearshore habitats. Consequently, this study provides novel natural history information and valuable insights needed to improve dispersal estimation for a wide range species, including economically and ecologically important fishes.

MATERIALS & METHODS

Study system

The region between Point Reyes and Point Arena varies spatially in upwelling frequency and duration (Largier et al., 1993). In the north, near Point Arena, an upwelling center, upwelling is typically persistent and strong throughout the spring and summer. Farther south, Bodega Bay is subject to somewhat less frequent bouts of upwelling, and more frequent relaxation events when prevailing wind and current directions reverse. We collected plankton samples at 10 stations along two transects, at Stewarts Point and Bodega Head, spanning the width of the continental shelf (Figure 1). Sampling took place during peak upwelling (March-July) from 2017 to 2018. We sampled each transect five times and chose cruise dates to coincide with upwelling and relaxation events in order to characterize the impact of these phenomena on ichthyoplankton distributions. We identified these sampling windows using regional marine weather forecasts and conditions monitored offshore at National Data Buoy Center 46013. We collected all samples between sunset (~20:00 PDT) and sunrise (~6:00 PDT) when fish larvae are less likely to avoid

collection (McGurk, 1992). Some cruises were truncated due to a worsening sea state, equipment failure, or crew illness. In these cases, we present results from partial transects.

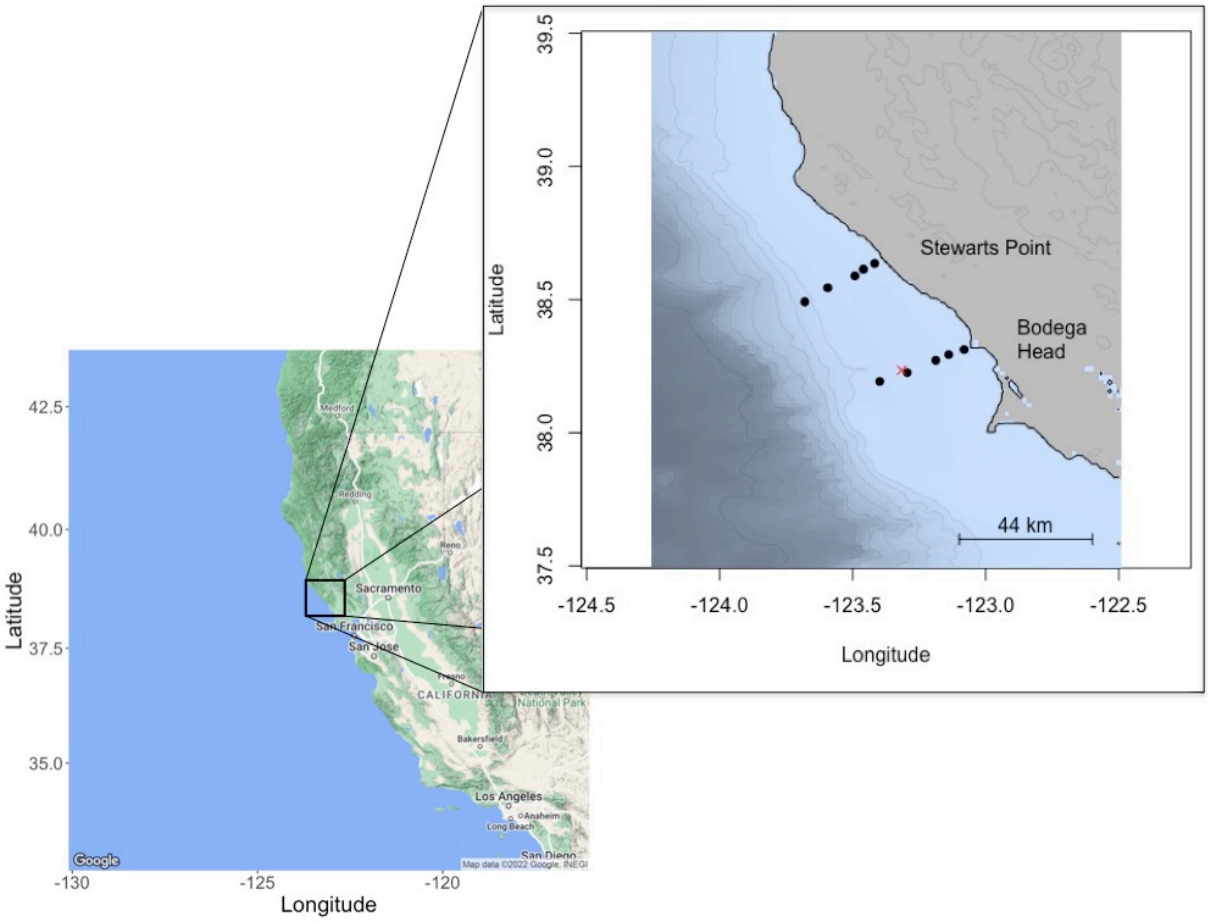

Figure 1. Inset map shows the study location on the coast of California, USA from San Francisco Bay to Point Arena. Points show station locations. A red 'X' marks the location of NOAA buoy 46013, where offshore wind was monitored.

In addition to these 10 nighttime, cross-shelf expeditions, we conducted cruises every 12 h over 48 h from April 1-3, 2019 to detect diel changes in ichthyoplankton distributions. We sampled only the two stations nearest to shore, where larval density is typically highest, along the Bodega Head transect. The sampling and laboratory methods that follow were the same for both the 10 nighttime and four diel cruises.

Ichthyoplankton sampling

At each station, we sampled four discrete depth bins. We collected plankton samples from the surface using a neuston net (0.5 m^2 opening) and from the subsurface using an electronically tripped and obliquely towed Tucker Trawl equipped with three nets (all 1 m^2 opening), a temperature probe, and a depth sensor. We also equipped all nets with mechanical flowmeters (General Oceanics) to estimate the volume of water sampled. All four nets had a 505-μm mesh and codend and were darkly colored to target ichthyoplankton >3 mm while minimizing net avoidance. To minimize extrusion of larvae, nets were towed at 2 - 5 kn depending on the sea state. When a thermocline was apparent, samples were collected above (categorically referred to as 'top'), within ('mid-water'), and below ('bottom') the thermocline to 100 m; when no thermocline was apparent, we sampled evenly binned depths to 100 m.

We fixed plankton samples in the field using 95% ethanol and brought them back to Bodega Marine Laboratory for sorting and enumeration. Once sorted, we visually identified all ichthyoplankton to the lowest possible taxonomic level and to developmental stage using meristics and morphology as described in available keys (Ahlstrom, 1962; Richardson & Washington, 1980; Washington, 1981; Kendall & Vinter, 1984; Matarese et al., 1989; Moser, 1996; Matarese et al., 2013). Most specimens were identifiable to species, but some were only visually identifiable to genus (e.g., *Sebastes*). Efforts are currently underway to extend this analysis by identifying all *Sebastes* to species level using molecular methods.

To examine interspecific differences in larval behavior and distribution related to adult cross-shore habitat preference, we classified ichthyoplankton into three groups: larvae of fishes living in depths <50 m (hereafter referred to only as 'nearshore' species), larvae of fishes living in depths of 50-200 m (hereafter 'mid-shelf' species), and larvae of coastal pelagic species and

fishes living in depths >200 m (hereafter 'offshore' species). Additional detail on species classifications and grouping methods are available in the B. We also pooled developmental stages such that 'early' larvae included all stages from hatching or parturition through flexion of the posterior end of the vertebral column. 'Late' larvae included postflexion and transformation individuals. We did not identify fish eggs. Unidentifiable specimens (<1% of all collected specimens) and pelagic juveniles, likely under sampled by our nets, were excluded from our analysis.

Environmental data

Prior to plankton collection at each station, we deployed a CTD (SeaBird) to measure temperature, salinity, and chlorophyll-a fluorescence from the surface to the benthos or 100 m. These *in situ* measurements were used to create cross-shelf profiles of water column structure during sampling. We also used hourly wind speeds and direction, collected at National Data Buoy Center 46013 (38.235, -123.317; Figure 1), to calculate average daily wind velocity throughout the sampling period following the methods of Grange (2014). We then calculated alongshore wind stress (τ) using the equation $\boldsymbol{\tau = \rho c_D u^2}$, where u is wind speed rotated along a 320° axis, ρ is air density of 1.3 kg/m^3, and c_D is a dimensionless drag coefficient of 0.0014. To create average daily current velocities, we averaged hourly high frequency radar (HF radar) surface current measurements (6 km resolution) for both Bodega Head (38.1369, -123.4273) and Stewarts Point (38.3843, -123.9052) and present the alongshore and cross-shore components for each time series. HF-radar data were provided by the U.S. Integrated Ocean Observing System (IOOS) HF Radar Network and available via the Coastal Observing R&D Center (cordc.ucsd.edu/projects/mapping). We extracted mean daily SSTs from the Regional Ocean Modeling System (ROMS) Nowcast (10-km resolution) for both Bodega Head (38.2835, -

123.1147) and Stewarts Point using the CenCOOS Data Portal (https://data.cencoos.org/). Finally, to characterize regional upwelling conditions, we used the daily Coastal Upwelling Transport Index (CUTI; accessed at http://mjacox.com/upwelling-indices/), which incorporates both Ekman and geostrophic transport and provides a 1° latitudinal estimate of upwelling/relaxation activity (Jacox et al., 2018). Environmental data were used in concert to identify upwelling and relaxation events that coincided with sampling and to interpret the influence of these processes on ichthyoplankton distributions. We considered upwelling events as periods where alongshore wind stress <-0.5 Pa, and CUTI was ≥1.5 on average over the 72-h period preceding each cruise, and when a shoaling thermocline was present in CTD profiles.

Statistical analyses

Larval distributions are reported as larval concentrations (number per m^3) and densities (number per m^2). Densities were calculated by dividing larval concentration by the depth of the water column to account for the possible dilution of larvae in a deepening water column across the shelf. Doing so, however, may inflate estimates of larvae in offshore environments if larvae are concentrated in the upper water column, as was the case for our two previous studies on crustacean larvae (Morgan et al. 2009, 2018). We used both measures on a log scale and evaluated their relative value for characterizing three-dimensional larval distributions.

To determine where larvae are most concentrated, we computed taxon-specific mean depth (ZCM) and cross-shelf (XCM) centers of mass and associated standard error using the method for standard error of weighted averages described by Gatz & Smith (1995). ZCM and XCM values were then used to identify and group taxon-specific larval behaviors. We used nonparametric analysis of similarity (ANOSIM) with a Bray-Curtis dissimilarity matrix to examine whether ichthyoplankton assemblages were structured by depth or distance from shore

and whether transects differed from each other. We then used nonmetric multidimensional scaling (NMDS) and resultant species scores to determine how strongly assemblages differed according to depth and distance from shore. ANOSIM and NMDS analyses were conducted using the vegan package (Oksanen et al., 2019). All data processing, analyses, and figure generation, using the ggplot2 package (Wickham, 2018), were conducted in R version 3.6.2 (R Core Team, 2019), and are available online (https://osf.io/pv43u/).

RESULTS

Local and regional environment

One nighttime cruise across the shelf was conducted in late July of 2017, and the other nine of these cruises were conducted during 2018. We sampled ichthyoplankton during five upwelling events in 2018 (March 28, April 3, May 3, May 23, and June 18) and five periods of upwelling relaxation (July 24 in 2017 and April 25, May 8, May 16, July 5 in 2018; Figure 2). Upwelling and relaxation cruises were roughly evenly distributed across the two transects. The cruise conducted July 24, 2017 occurred during a period of relaxation with near-zero alongshore wind stress, a stratified water column, and a nearshore peak in surface chlorophyll (Figures 2, 3). Cruises on March 23 and April 3, 2018 took place at the beginning and end of a single upwelling event, interrupted by a brief relaxation of alongshore wind stress (Figure 2). Shoaling of the thermocline nearshore and development of an offshore peak in surface chlorophyll consistent with the upwelling of cold, nutrient-rich waters was apparent across the two dates (Figure 3). We sampled at the end of multi-day upwelling events on May 3, 23 and June 18, 2018 (Figure 2). The remaining 2018 cruises took place following two to four days of relaxed alongshore wind stress and coincided with near zero CUTI values (Figure 2). Cross-shelf profiles (Figure 3)

revealed thermal stratification and variability in the distance of peak surface chlorophyll from shore. All four diel cruises, April 1-3, 2019, occurred during a period of relaxation when alongshore wind stress was minimal and SSTs were 1.5° above the mean (Figure 2).

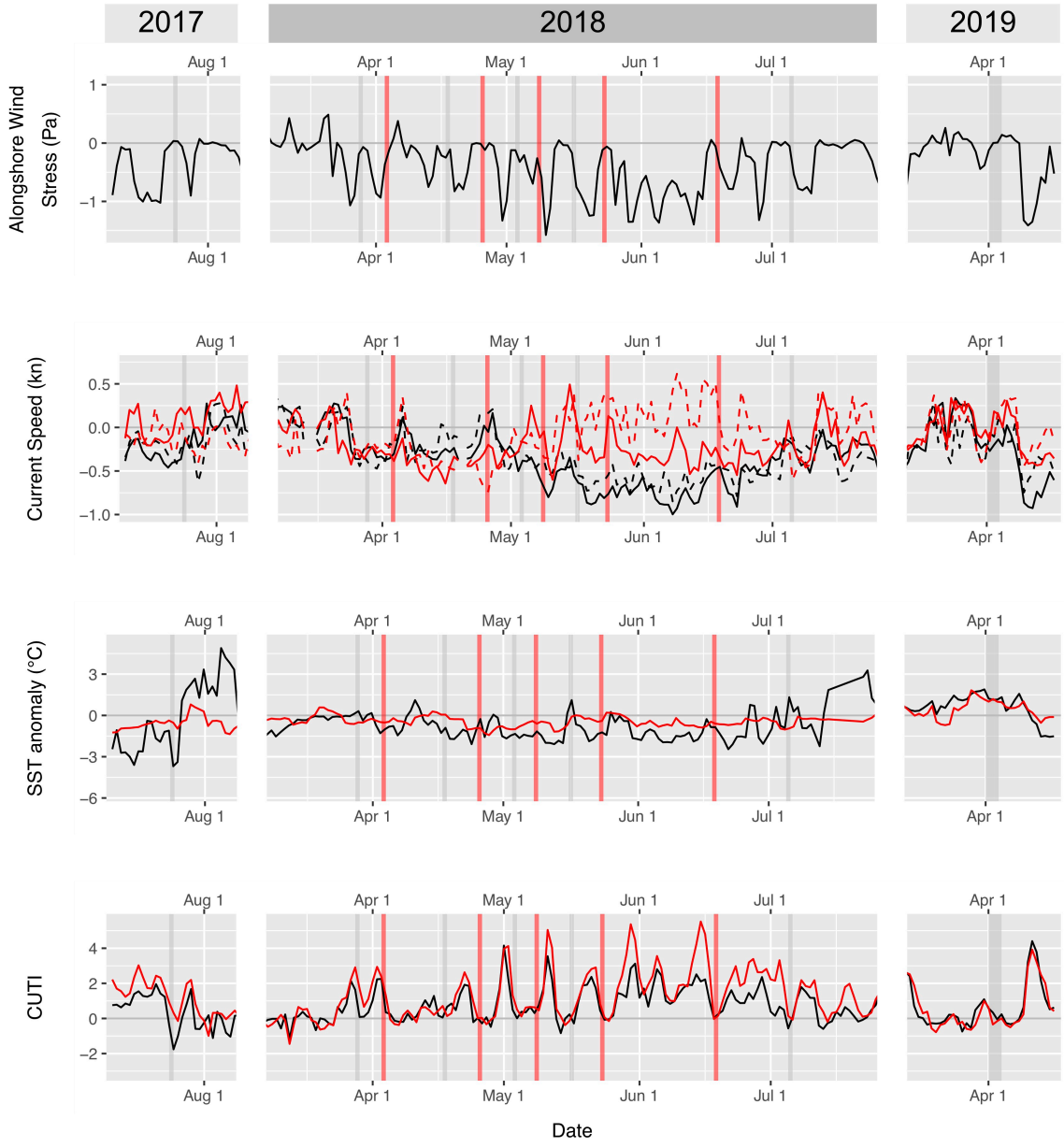

Figure 2. Time series of environmental conditions during the sampling period. Black lines show data collected near Bodega Head, and red lines show data collected near Stewarts Point. Gray (red) bars indicate when samples were collected at Bodega Head (Stewarts Point). The final gray bar shows the 48-h period when diel cruises were conducted. Negative alongshore wind stress values signify northwesterly winds using data collected at National Data Buoy Center 46013. High-frequency radar surface currents are shown as cross-shore (solid lines) and alongshore (dashed lines) component vectors, where negative values indicate offshore and southward flow, respectively. SST anomaly was calculated using 2011-2021 mean 2-m temperature from ROMS Nowcast data. Positive CUTI values indicate upwelling.

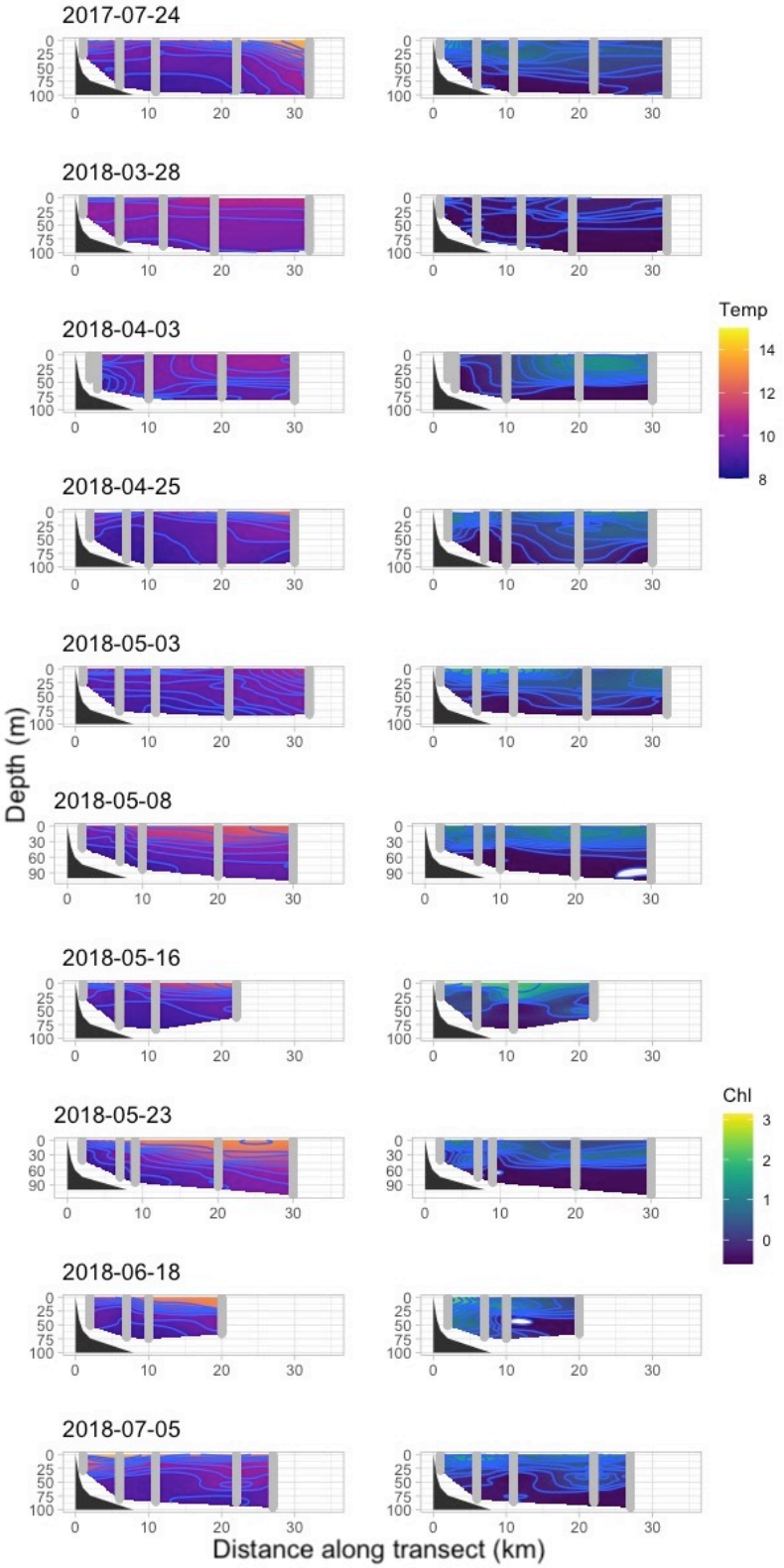

Figure 3. *In situ* CTD temperature (left column) and chlorophyll fluorescence (right column_ data. Gray lines indicate the cross-shelf locations of each cast. Values between casts were interpolated linearly. The black polygon at left of each plot shows approximate bathymetry.

Cross-shelf ichthyoplankton assemblage at night

Over the course of our 10 cross-shelf, nighttime cruises, we collected 941 ichthyoplankters of 80 taxa from Bodega Head and 1,365 ichthyoplankters of 71 taxa from Stewarts Point (total N = 2,306, total taxa = 102). We statistically analyzed and mapped distributions only for taxa observed more than twice (51 taxa). Most observed larval taxa were classified as nearshore (48), followed by offshore (26) and mid-shelf (15) (see Appendix B for classification approach).

Twenty-eight percent of early and late stages of all larval taxa were found <6 km from shore at Bodega Head and 52% occurred <6 km from shore at Stewarts Point. Larvae of nearshore fishes were most concentrated within the CBL at both transects (Table 1). Larvae of mid-shelf species were most concentrated over the continental shelf (Bodega Head) and within the CBL (Stewarts Point). Larvae of offshore species were relatively evenly distributed across the shelf at both transects.

Table 1. Percentage of larvae collected across the continental shelf at Bodega Head and Stewarts Point by the adult distributions of species (nearshore, mid-shelf, and offshore; see Appendix B for classification approach) with stages pooled.

Species distributions	Transect	CBL (% <6 km)	Mid-shelf (% 6-20 km)	Outer shelf (% >20 km)
Nearshore	Bodega Head	52	43	5
	Stewarts Point	90	7	3
Mid-shelf	Bodega Head	20	62	18
	Stewarts Point	73	19	8
Offshore	Bodega Head	14	39	47
	Stewarts Point	34	29	37

Plots of larval concentration (individuals per m^3) were highest within the CBL at both transects, but this pattern was less pronounced in plots of larval densities (individuals per m^2) standardized by the depth of the water column (Figure 4). We also observed that larvae were more concentrated near the surface regardless of total water column depth. Indeed, at Stewarts Point, 78% of all ichthyoplankton at station 4 (total depth = 154 m) and 60% of all ichthyoplankton at station 5 (total depth = 660 m) were found <50 m deep, suggesting that standardizing larval densities by the depth of the water column depth inflated densities offshore

somewhat diminishing cross-shore structure in larval distributions. Hence, we used non-standardized larval concentrations in subsequent analyses.

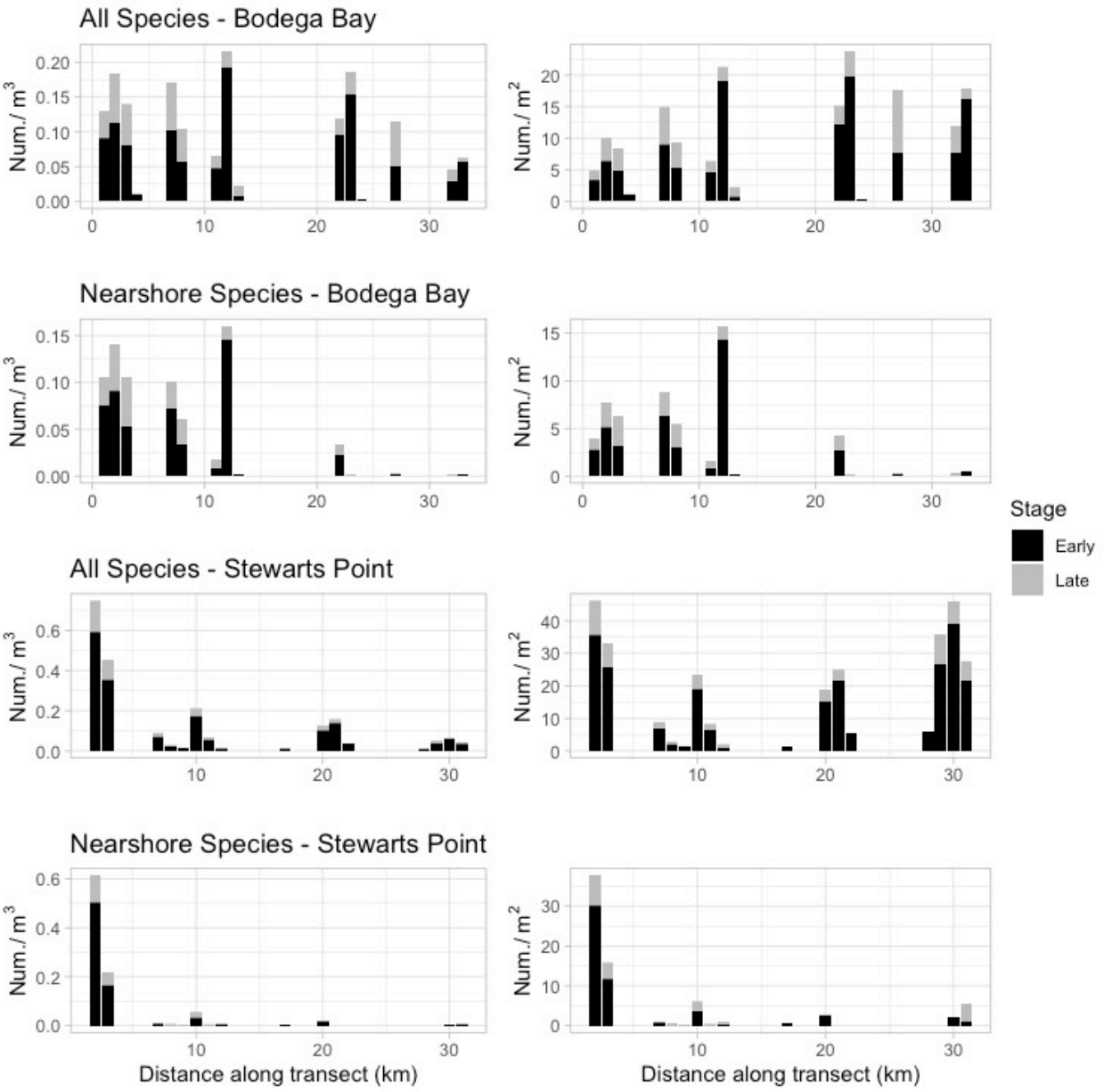

Figure 4. Total and nearshore species only ichthyoplankton densities across the shelf at Bodega Head and Stewarts Point. Concentrations (number per cubic meter) are reported in the left column, and densities (number per square meter standardized by water column depth) are shown in the right column. Bars show both early (black) and late (gray) stages of development.

We used ANOSIM to test for spatial differences in the ichthyoplankton assemblage by depth, distance from shore, and across the two transects. Larval taxa differed by depth (neuston, top, midwater, and bottom; ANOSIM statistic R = 0.29, $p = 0.001$) and distance from shore (station 1-5; R = 0.33, $p = 0.001$), but not by transect (R = 0.01, $p = 0.314$). Consequently, we pooled data across the two transects for subsequent ordination analyses and visualization of larval distributions.

We used NDMS to compare assemblage composition among depths and distances from shore (Figure 5). The ichthyoplankton assemblage found in the top (mean center = 9.72 m) and mid-water (31.86 m) depth bins were largely similar to one another, and both showed some overlap with the bottom depth bin (51.57 m) assemblage. However, the composition of the assemblage in the neuston was distinct. Species scores indicated members of the Hexagrammidae family, *Scorpaenichthys marmoratus*, and *Sardinops sagax* were strongly associated with the neuston assemblage. Ichthyoplankton also varied by distance from shore. The inshore (station 1) and shelf break (station 5) assemblages were most dissimilar with no overlap in ordination space. Intermediate stations filled in the cross-shelf gradient.

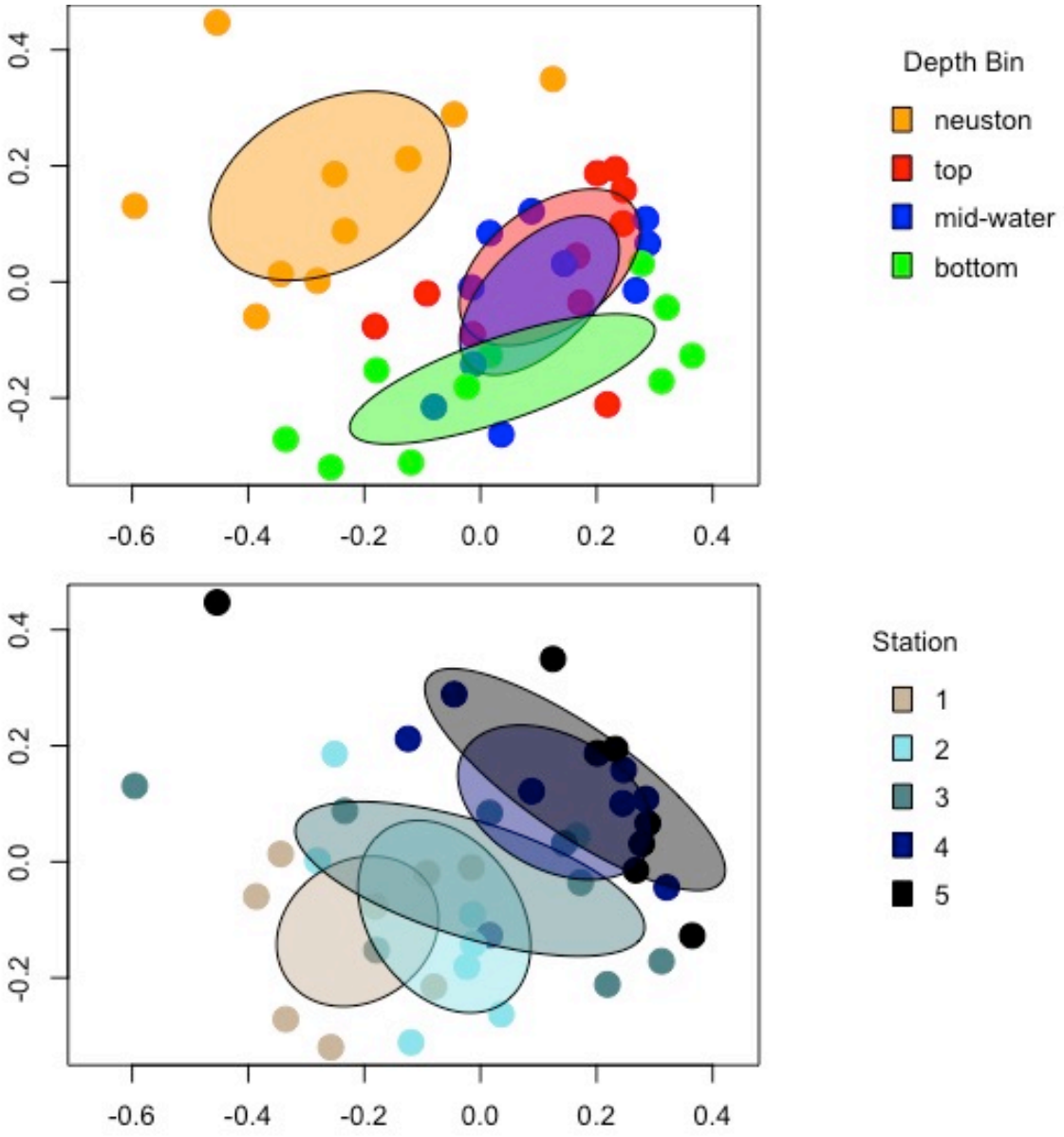

Figure 5. Nonmetric multi-dimensional scaling plots for the ichthyoplankton assemblage, pooled across all sampling dates and both transects. Circular points show the two-dimensional projection of each sample in the ordination space. Red crosses show species scores used in creating the projection. (A) Points are colored by sampling depth, ellipses show a standard deviation corresponding with each depth. (B) Points are colored by station (a categorical proxy for distance from shore), ellipses show a standard deviation corresponding with each cross-shelf location.

Larval behaviors

We visually and quantitatively examined the distribution of the most abundant ichthyoplankton taxa and identified five distinct patterns of larval behavior (Figures 6-10). Eight nearshore species and two mid-shelf species showed a preference for deeper water (Combined ZCM 9.07-35.87 m; Table 2, Figure 6). Larvae of nearshore species remained on the inner shelf and larvae of mid-shelf species either moved closer to shore or were retained there after adults migrated shoreward for spawning (Combined XCM 1.61-3.13 km). One species showing a preference for subsurface waters, *Orthonopias triacis,* was found at the edge of the CBL (Combined XCM = 6.45 km). Seven species, including five nearshore species, one mid-shelf species, and one offshore species, were strongly affiliated with the wind-driven neuston layer (Combined ZCM <0.5-2.53 m; Table 3, Figure 7). All were concentrated within 10 km from shore except the three *Hexagrammos* spp., which were found farther offshore (Combined XCM = 24.06 km). Seven nearshore species were concentrated deep in the water column across the shelf during relaxation (ZCM 17.57-56.02 m, XCM 2.56-4.87 km; Table 4, Figure 8) but were nearer to the surface and more abundant during upwelling conditions (ZCM 12.20-24.66 m, XCM 2.35-5.95 km). Three nearshore species showed evidence of ROVM by ascending into the neuston late in development and moving closer to shore (ZCM 0.5 – 1.01 m, XCM 4.26-10.66 km; Table 5, Figure 9) from deeper, mid-shelf waters early in development (ZCM 2.59-25.13 m, XCM 1.91-6.01 km). These species were retained on the inner shelf (XCM < 11 km). A fifth group of ichthyoplankton, including three nearshore, five mid-shelf, and seven offshore species, were affiliated with mid-water depths (Combined ZCM 13.57-56.61 m; Table 6, Figure 10) and occurred from the outer margin of the CBL to the outer shelf (Combined XCM 4.66 – 18.93).

Engraulis mordax were found in somewhat shallower waters (ZCM = 6.87 m) but showed a similar cross-shelf distribution.

Table 2. Larvae of 10 species of fishes collected on the inner shelf (<6 km) largely below the mixed layer off Bodega Head and Stewarts Point. Reported are cross-shelf species distributions (adults), common names, mean depth (m) center of mass (ZCM ± SE) at both transects separately and combined and mean cross-shelf (km) center of mass (XCM ± SE) at both transects combined. Larval stages and upwelling conditions were combined because larval distributions were similar,

Species distributions	Taxa	Common name	Bodega Head ZCM	Stewarts Point ZCM	Combined ZCM	Combined XCM
Nearshore	*Ruscarius* spp. (n=2)	Sculpin	16.2 ± 5.67	31.93 ± 1.41	29.61 ± 2.58	2.35 ± 0.27
	Cebidichthys violaceus	Monkeyface prickleback	9.07 ± 6.14	NaN ± NaN	9.07 ± 6.14	1.75 ± 0.21
	Cottus asper	Prickly sculpin	28.1 ± NaN	32.76 ± 0	30.96 ± 1.73	1.61 ± 0.37
	Orthonopias triacis	Snubnose sculpin	24 ± NaN	33.77 ± NaN	30.03 ± 4.62	6.45 ± 4.26
	Platichthys stellatus	Starry flounder	11.4 ± 5.34	15.26 ± 8.29	13.56 ± 4.82	2.75 ± 0.63
	Icelinus quadriseriatus	Thornback sculpin	14.26 ± 7.67	42.72 ± 1.32	35.87 ± 5.24	2.07 ± 0.17
	Lepidogobius lepidus	Bay goby	21.78 ± 6.41	NaN ± NaN	21.78 ± 6.41	3.13 ± 1.34
Mid-shelf	*Liparis pulchellus*	Showy snailfish	46.36 ± 23.38	30.19 ± 7.23	32.02 ± 6.37	2.32 ± 0.33
	Odontopyxis trispinosa	Pygmy poacher	14.64 ± 2.3	22.42 ± 8.07	20.38 ± 6.04	2.17 ± 0.13

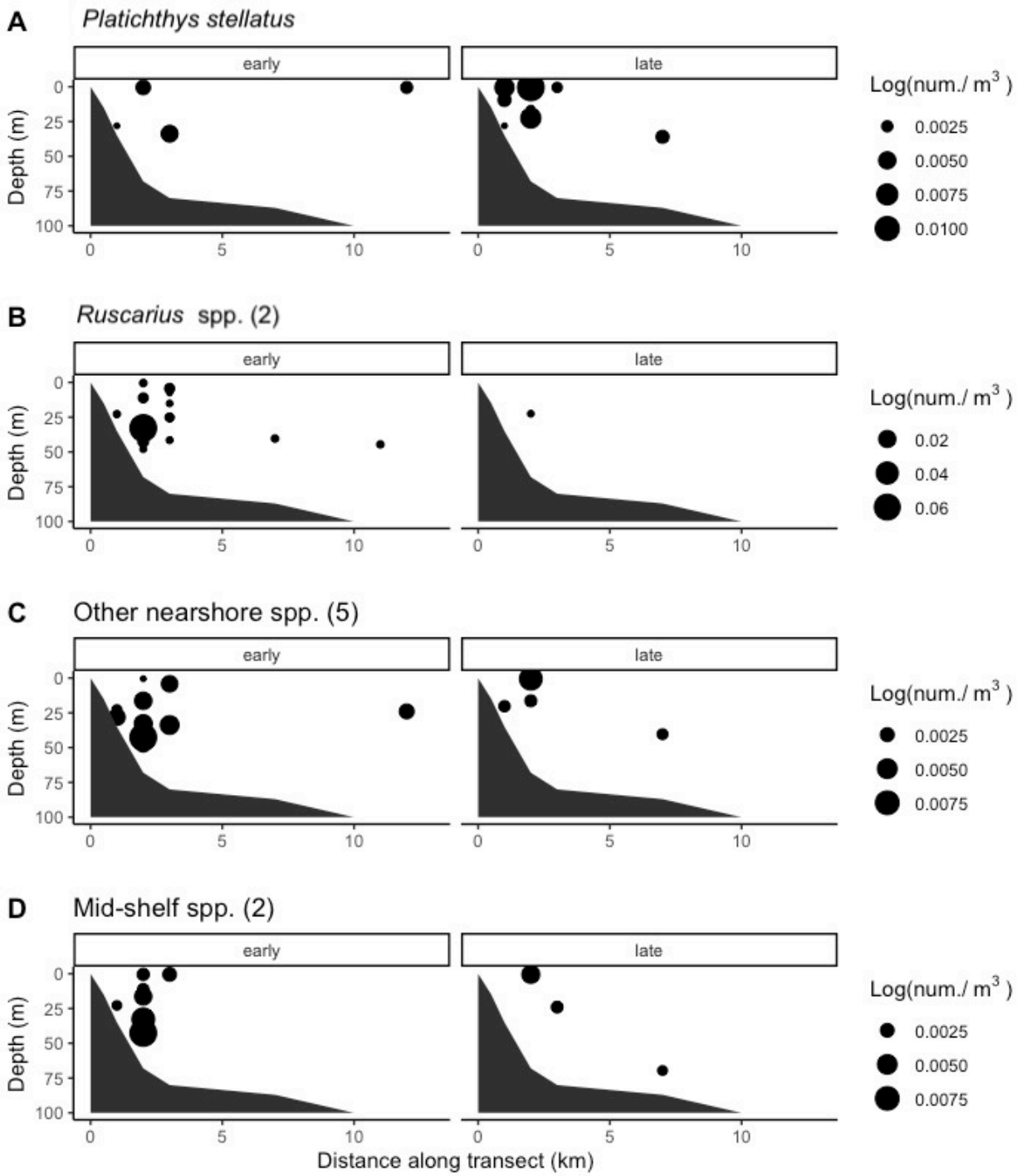

Figure 6. Cross-shelf ichthyoplankton distributions for species that occurred on the inner shelf (<6 km) largely below the mixed layer, corresponds with Table 2. Early and late stages of all taxonomic groups are shown separately.

Table 3. Larvae of seven species of fishes collected in the neuston off Bodega Head and Stewarts Point. Reported are cross-shelf species distributions (adults), common names, mean depth (m) center of mass (ZCM ± SE) at both transects separately and combined and mean cross-shelf (km) center of mass (XCM ± SE) at both transects combined. Larval stages and upwelling conditions were combined because larval distributions were similar.

Species distributions	Taxa	Common name	Bodega Head ZCM	Stewarts Point ZCM	Combined ZCM	Combined XCM
	Hexagrammos spp. (n=3)	Greenling	0.5 ± NaN	0.5 ± 0	0.5 ± 0	24.06 ± 3.9
Nearshore	*Oxylebius pictus*	Painted greenling	11.15 ± NaN	0.5 ± 0	2.23 ± 2.02	2.73 ± 0.24
	Scorpaenichthys marmoratus	Cabezon	3.33 ± 2.97	0.82 ± 0.37	2.02 ± 1.4	6.31 ± 1.64
Mid-shelf	*Cryptacanthodes aleutensis*	Dwarf wrymouth	0.5 ± NaN	0.5 ± 0	0.5 ± 0	9.43 ± 2.59
Offshore	*Sardinops sagax*	Pacific sardine	3.57 ± 2.2	1.6 ± 0.73	2.53 ± 1.03	6.57 ± 1.65

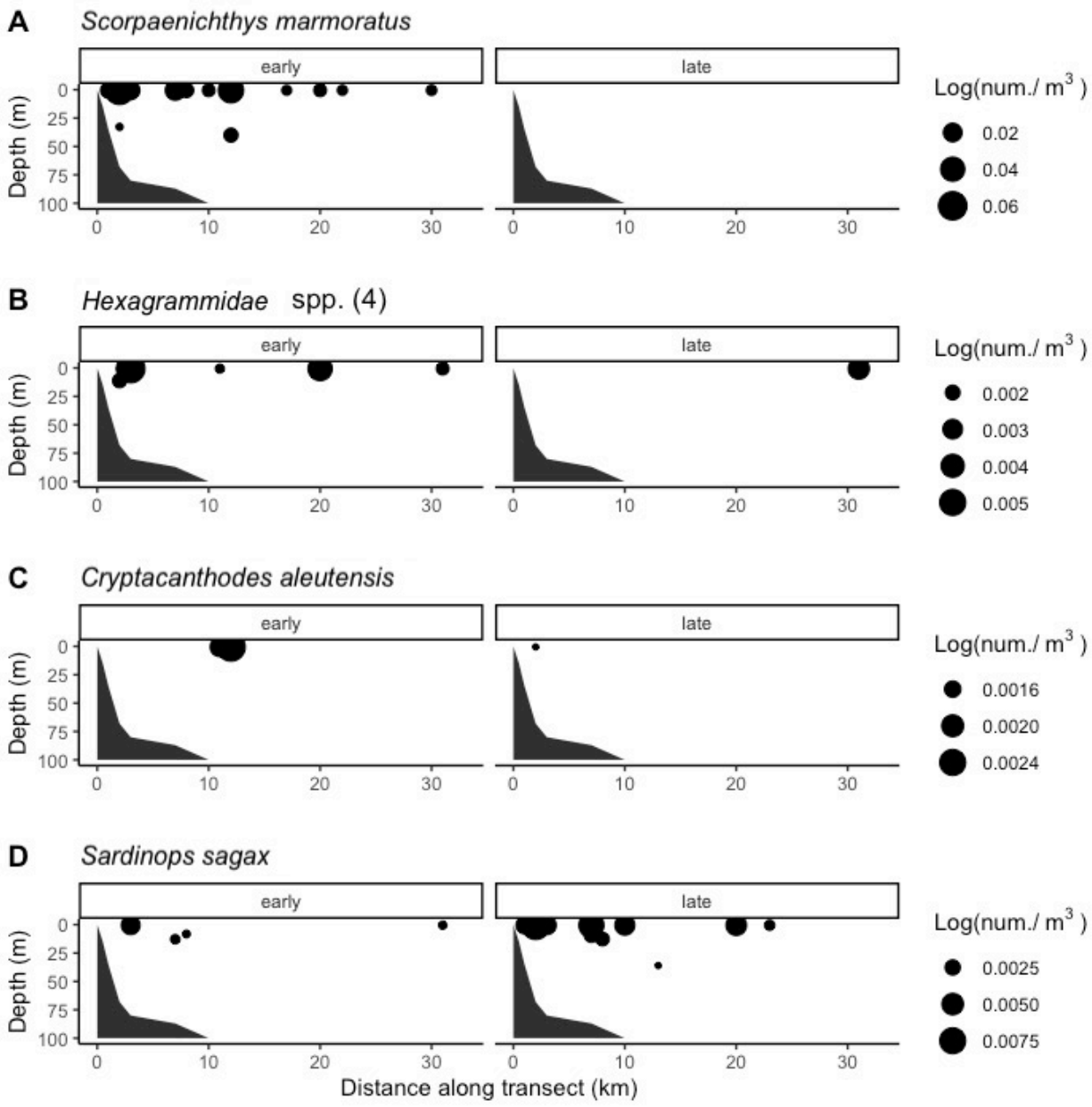

Figure 7. Cross-shelf ichthyoplankton distributions for species that occurred predominantly in the neuston, corresponds with Table 3. Early and late stages of all taxonomic groups are shown separately.

Table 4. Larvae of seven species of fishes collected closer to shore during upwelling than relaxation off Bodega Head and Stewarts Point. Reported are cross-shelf species distributions (adults), common names, mean depth (m) center of mass (ZCM ± SE) at both transects separately and combined and mean cross-shelf (km) center of mass (XCM ± SE) at both transects combined. Transects and larval stages were combined because larval distributions were similar

Species distributions	Taxa	Common name	Upwelling ZCM	Relaxation ZCM	Upwelling XCM	Relaxation XCM
Nearshore	*Parophrys vetulus*	English sole	13.43 ± 2.84	45.52 ± 10.07	5.95 ± 1.15	4.87 ± 1.84
	Ammodytes hexapterus	Pacific sand lance	12.2 ± 11.38	56.02 ± 13.79	2.35 ± 0.34	4.43 ± 2.5
	Chitonotus pugetensis	Roughback sculpin	12.24 ± 4.64	18.38 ± 6.31	4.11 ± 0.78	2.56 ± 0.49
	Artedius spp. (n=3)	Sculpin	21.48 ± 3.01	20.9 ± 4.44	3.54 ± 3.01	4.05 ± 4.44
	Rathbunella alleni	Stripefin ronquil	24.66 ± 4.04	17.57 ± 3.83	3.37 ± 0.79	2.73 ± 0.48

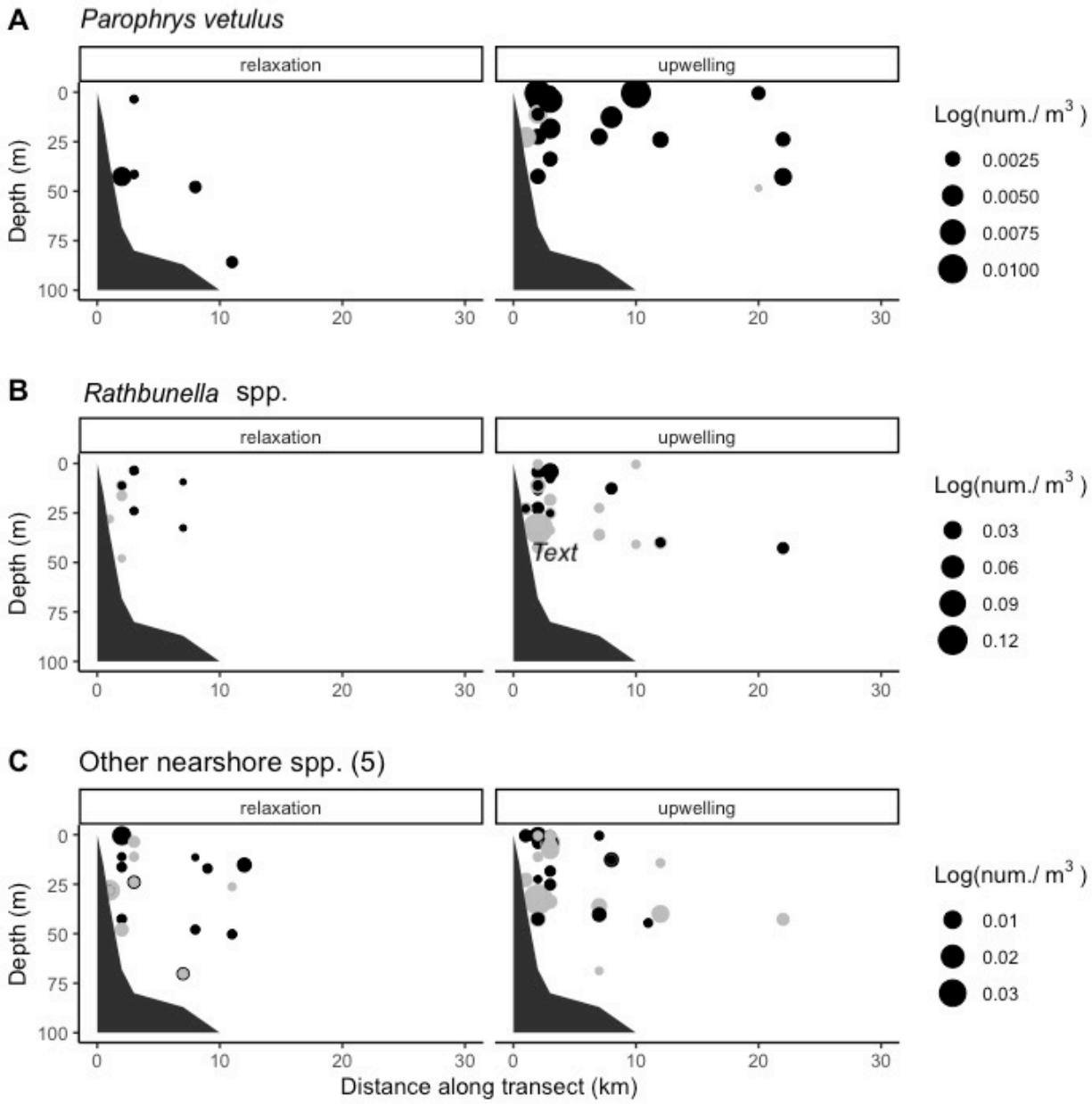

Figure 8. Cross-shelf ichthyoplankton distributions for species that exhibited changes in distribution according to upwelling state, corresponds with Table 4. Point shading shows developmental stage for all taxonomic groups: early (black) and late (gray). Distributions during upwelling and relaxation conditions are shown separately.

Table 5. Larvae of three species of fishes that migrate to the neuston late in development off Bodega Head and Stewarts Point. Reported are species distributions (adults), common names, mean depth (m) center of mass (ZCM ± SE) for early (through flexion), late and all stages combined and mean cross-shelf (km) center of mass (XCM ± SE) at both transects combined. Transects and upwelling conditions were combined because larval distributions were similar

Species distributions	Taxa	Common name	Early stages ZCM	Late stages ZCM	Early stages XCM	Late stages XCM
	Ophiodon elongatus	Lingcod	2.59 ± 1.28	0.5 ± 0	6.01 ± 1.52	5.17 ± 1.82
Nearshore	*Leptocottus armatus*	Pacific staghorn sculpin	13.82 ± 8.45	0.5 ± 0	1.91 ± 0.44	4.26 ± 2.5
	Citharichthys stigmaeus	Speckled sanddab	25.13 ± 13.71	1.01 ± 0.58	NaN ± NaN	10.66 ± 3.65

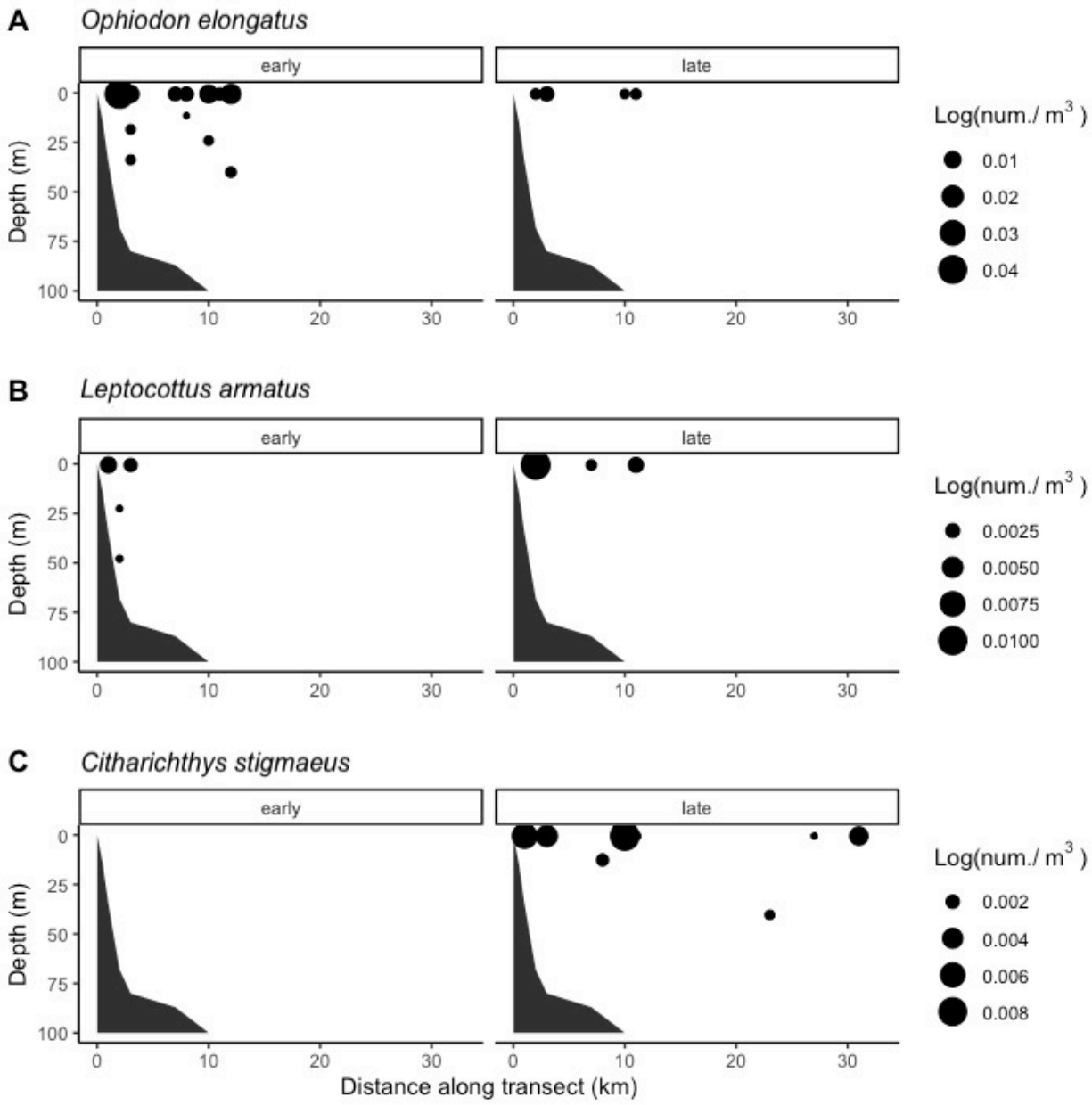

Figure 9. Cross-shelf ichthyoplankton distributions for species that exhibited changes in distribution according to developmental stage, corresponds with Table 5. Early and late stages of all taxonomic groups are shown separately.

Table 6. Larvae of 15 species of fishes collected in the upper water column off Bodega Head and Stewarts Point. Reported are cross-shelf species distributions (adults), common names, mean depth (m) center of mass (ZCM ± SE) at both transects separately and combined and mean cross-shelf (km) center of mass (XCM ± SE) at both transects combined. Larval stages and upwelling conditions were combined because larval distributions were similar

Species distributions	Taxa	Common name	Bodega Head ZCM	Stewarts Point ZCM	Combined ZCM	Combined XCM
Nearshore	*Radulinus asprellus*	Slim sculpin	83 ± NaN	45.02 ± 9.14	49.57 ± 10.67	8.1 ± 4.33
	Liparis mucosus	Slimy snailfish	4.75 ± 3.09	25.24 ± 11.54	15.64 ± 8.93	4.66 ± 1.8
	Hemilepidotus spinosus	Brown Irish lord	18.1 ± 17.75	0.5 ± NaN	13.57 ± 12.46	5.53 ± 2.6
Mid-shelf	*Liparis fucensis*	Slipskin snailfish	52.82 ± 13.65	61.89 ± 16.19	56.61 ± 9.23	12.46 ± 3.23
	Plectobranchus evides	Bluebarred prickleback	38.96 ± 7.22	50.16 ± 18.45	44.27 ± 8.8	12.1 ± 0.73
	Citharichthys spp. (n=2)	Sole	23.26 ± 6.95	9.79 ± 5.29	19.9 ± 5.51	9.64 ± 1.09
	Psettichthys melanostictus	Pacific sand sole	25 ± 7.3	31.1 ± 2.9	27.57 ± 4.5	5.94 ± 1.46
Offshore	*Bathylagus ochotensis*	Eared blacksmelt	41.66 ± 7.98	58.56 ± 6.85	51.92 ± 5.83	15.71 ± 1.44
	Engraulis mordax	Northern anchovy	15.58 ± 5.62	0.5 ± 0	6.87 ± 3.98	4.88 ± 1.59
	Merluccius productus	North Pacific hake	29.52 ± 8.25	44.15 ± 9.04	35.72 ± 6.62	18.93 ± 2.91
	Lyopsetta exilis	Slender sole	30.83 ± 3.75	23.28 ± 5.81	27.93 ± 3.39	10.66 ± 1.3
	Zaniolepis	Shortspine	24.1 ±	18.38 ±	22.49 ±	9.47 ±

Species distributions	Taxa	Common name	Bodega Head ZCM	Stewarts Point ZCM	Combined ZCM	Combined XCM
	frenata	combfish	16.24	NaN	10.28	2.73
	Xeneretmus spp. (n=2)	Poacher	34.83 ± 7	0.5 ± NaN	28.2 ± 10.35	10.07 ± 2.39

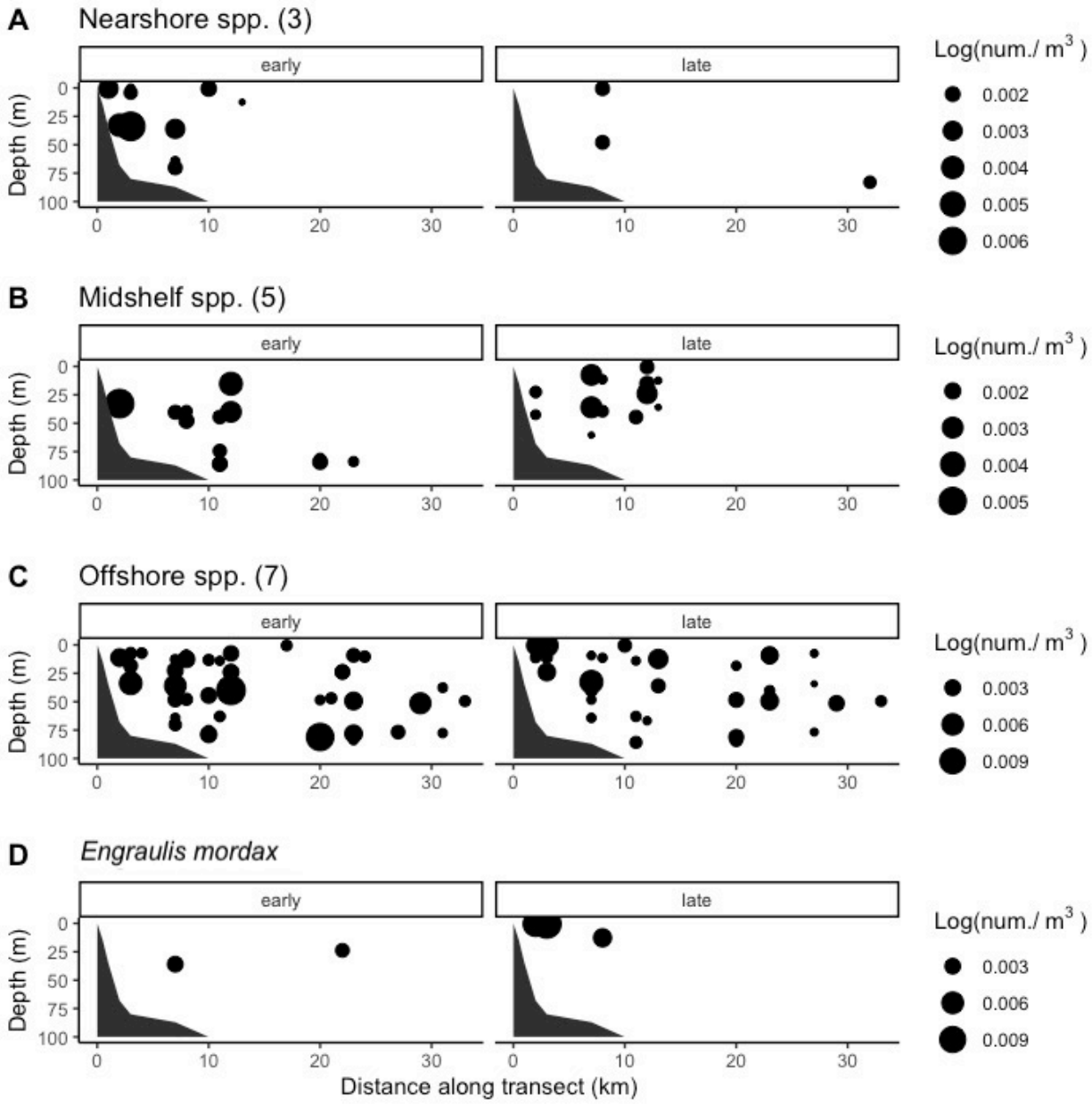

Figure 10. Cross-shelf ichthyoplankton distributions for species that occurred predominantly below the mixed layer and across the shelf, corresponds with Table 6. Early and late stages of all taxonomic groups are shown separately.

3.4 Diel variation of inner shelf ichthyoplankton assemblage

In addition to our nighttime sampling across the shelf, we conducted four diel cruises at the two nearshore stations from August 1-3, 2019 to investigate the prevalence of DVM. We captured 236 ichthyoplankters of 28 taxa during the four cruises. Unfortunately, we collected too few larvae to utilize rigorous statistical approaches to detect diel behaviors. Among species that

were sampled more than twice during the four cruises cruises (32 total samples), five appeared to avoid surface waters during the day. Early stage *Ophiodon elongatus* were observed in the neuston at night (n = 3) and at 10 m during the day (n = 1), whereas *Scorpaenichthys marmoratus* (n = 36) were present in the neuston at night but were absent during the day. Late-stage larvae of two species (*Engraulis mordax* and *Parophrys vetulus*) and early-stage larvae of one species (*Cebidichthys violaceus*) also showed a strong diel signal being abundant in night samples and absent in day samples. Conversely, early-stage *Psettichthys melanostictus* larvae were found in depths <20 m during the day and >20 m at night. We did not detect a diel signal for five other species (*Lepidogobius Lepidus*, *Paralichthys californicus*, *Platichthys stellatus*, *Pleuronichthys coenosus*, and *Rathbunella alleni*).

DISCUSSION

The primary goal of our investigation was to examine the role of behavior in facilitating nearshore retention of the larvae of fishes living on the inner shelf. Many of these species are economically, recreationally, and ecologically important and their recruitment has been assumed to be limited by advection away from nearshore settlement sites. We showed that larvae of a diverse assemblage of nearshore fishes were most abundant on the inner shelf during peak upwelling season on the central coast of California, indicating they are largely retained there despite the potential for offshore advection. Furthermore, we demonstrated that these larvae exhibited an array of vertical positioning behaviors that likely limited their cross-shore and alongshore transport. Our survey also allowed us to collect the larvae of mid- and outer-shelf fishes, providing the opportunity to gain new insights into how behavior regulates transport of these species as well. Together, these findings support our central conjecture that dispersal of

fish larvae is frequently behaviorally regulated in the highly advective California Current upwelling system.

Larval behavior of nearshore fishes

One way that nearshore larvae escape advection offshore is by remaining below surface waters where Ekman transport is strongest (Table 2). All stages of nearshore species employing this "strategy", including five sculpins, one prickleback, one flounder, and one goby, were found within or adjacent to the CBL (<7 km from shore). Therefore, these species completed development close to natal and settlement sites. Our study is the first to document avoidance of surface waters for all species in this assemblage with the exception of *Orthonopias triacis* (snubnose sculpin) larvae, which have previously been found exclusively in epibenthic, shallow waters (Feeney, 1992).

Larvae of other nearshore species were found offshore of the CB. These species exhibited behaviors that mitigate cross-shelf transport by delivering late stage larvae to suitable inner shelf settlement habitats. Seven nearshore species, including four sculpins, one sole, one sand lance, and one ronquil, were broadly distributed in mid-deep water (ZCM 17.6-56 m, Table 1) during relaxation periods but were much more abundant and higher in the water column (ZCM 12.2-24.66 m) during upwelling. These species likely rode in from deeper waters on upwelling currents becoming concentrated in shallow nearshore waters. Only early stage *Parophrys vetulus* (English sole) displayed evidence of subsequent offshore advection. Three other nearshore species – lingcod, one sole (*Citharichthys stigmaeus*), and three species of sculpins (*Artedius* spp.) – were present in the neuston or close to the surface late in development but were distributed more broadly throughout the water column early in development (we did not sample any preflexion *C. stigmaeus*, but transformation stage individuals were more neustonic than

postflexion individuals). This ROVM has previously been observed for larvae of sympatric nearshore benthic crustaceans during upwelling season (Morgan et al., 2009, 2018). Early-stage larvae mitigated offshore advection by avoiding surface waters, and late-stage larvae ascended to the surface where they may have been exposed to internal waves and shoreward winds that occur during relaxation events, thereby facilitating return to suitable settlement sites (Pineda, 1994; Shanks, 1995). Interestingly, our findings build on prior surveys by suggesting that *C. stigmaeus* larvae may undergo two sequential ontogenetic shifts in depth preference. We found transformation-stage *C. stigmaeus* concentrated near the surface, but Sakuma and Larson (1995) showed that older *C. stigmaeus*, too large to have been sampled by our nets, descend in the water column where they are transported shoreward by upwelling currents. Crustacean larvae of the family Grapsidae also exhibit multiple ontogenetic shifts in depth preference (Morgan et al., 2009).

Larvae of only five nearshore species, four greenlings and cabezon, were found almost exclusively in the neuston, where the risk of offshore advection is greatest. Larvae of three of the greenling species (family *Hexagrammos*) occurred 10-35 km from shore in all stages, suggesting that these species may experience significant alongshore and cross-shelf transport during their planktonic larval stage. Other studies have even classified them as 'oceanic', being more abundant off the shelf than on it (Richardson & Pearcy, 1977). Nonetheless, these species settle in shallow water rocky habitats and so may rely on shoreward transport during relaxation events (Morgan et al., 2018) or directed onshore swimming (Drake et al., 2018) to reach suitable sites. Larvae of the two other species in this group were able to remain on the inner shelf: *Oxylebius pictus* stayed within the CBL (XCM = 2.73 ± 0.24 km) and *Scorpaenichthys marmoratus* were concentrated slightly farther offshore (XCM = 6.31 ± 1.64 km). Both species were

predominantly retained close to shore despite their neustonic distribution strongly suggesting that other behaviors, such as DVM (see below), directed swimming, or both, may play a role in limiting offshore advection.

Larval behavior of mid-shelf and offshore species

Identification of the entire ichthyoplankton assemblage provided opportunities to gain new insights into how behavior regulates the transport of fishes residing on the middle and outer shelf too. Larvae of most mid-shelf species (five of eight) and offshore species (seven of eight) were broadly distributed across the shelf (Combined XCM 4.88-18.93 km) and concentrated in the middle of the water column (Combined ZCM 19.9-56.61 m), except for *Engraulis mordax* larvae that were somewhat shallower. At these depths, cross- and alongshore flows tend to be weaker than either shallower or deeper in the water column (Largier et al., 1993). Larvae occupying this zone are therefore likely to experience reduced alongshore transport and avoid being swept off the continental shelf or toward shore, maintaining their position over potential settlement sites on the shelf.

Determination of spawning and settlement locations

We used information about the spawning sites and preferred settlement locations to classify species as nearshore, mid-shelf, and offshore (Appendix B). And while the spawning and settlement locations of some species in our region are known, these basic life history data are lacking for many species, particularly those that are not fished commercially or recreationally. When spawning and settlement locations were unknown, we assumed that these species start and end their larval stage wherever adults are known to occur. This assumption is reasonable for most species but not all. Some species are known to conduct migrations from deep water habitats to spawn in shallow waters, such as *Liparis fucensis* (Marliave & Peden, 1989) and *Parophrys*

vetulus (Laroche & Richardson, 1979; Matarese et al., 1989). Furthermore, juveniles of some species are spawned where adults reside but settle in nurseries that are distinct from adult habitats, as is the case for *Hemilepidotus spinosus* (Richardson & Washington, 1980) and *Paralichthys californicus* (Kucas & Hassler, 1986).

Depth-stratified sampling approaches can be useful in revealing potential adult spawning or juvenile settlement locations when this information is uncertain. For example, *Liparis pulchellus* and *Odontopyxis trispinosa* are two species found in deep water, soft bottom habitats as adults but little is known about their early life history or spawning habits. In our survey, early and late stages of both species were concentrated very nearshore (Combined XCM <3 km, Table 2), deep in the water column (Combined ZCM >20 m) suggesting that larvae may be spawned or settle to nearshore habitats before moving deeper as settled juveniles. Complete life history information can be difficult to gather for cryptic species or species that are not fished and absent from fishery-independent surveys as adults. However, adult habitat preferences and behaviors can be inferred from larval distributions and support marine spatial planning efforts that are based on species biogeography.

Retention and recruitment in an upwelling region

Populations of marine species with a dispersive larval stage were commonly thought to be 'open' over small scales, such that recruitment to a particular location depends on larval supply and is decoupled from local reproductive output (Roughgarden, 1988). This study builds on recent work by demonstrating that larvae of species living on exposed coasts, including the larvae of fishes, are typically retained nearshore such that decoupling between reproduction and recruitment may be uncommon. Where there are high rates of local retention, populations are less likely to be regulated by larval supply from distant locations and less likely to exhibit

metapopulation dynamics. Prior work on retention mechanisms of larval fishes in upwelling systems have identified upwelling fronts (Woodson et al., 2012; Tiedemann & Brehmer, 2017), mesoscale structures (Santos et al., 2007; Roy, 2010; Moyano et al., 2014), and "upwelling shadows" created in the lee of headlands (Wing et al., 2003; Morgan & Fisher, 2010; Satterthwaite et al., 2021) as ingredients for local retention of larvae. In addition to these mechanisms, our survey identified a suite of behaviors that promote retention of nearshore fish larvae near natal sites. Indeed, 63% of the most abundant nearshore species were likely able to avoid significant cross-shore or alongshore transport by moving shoreward in deep upwelling currents (Table 4, Figure 8) or by remaining beneath the surface layer where offshore transport is strongest (Table 2, Figure 6).

While upwelling systems like the CCE present the potential for long-distance dispersal or advection from shore, they are also highly productive environments where upwelled waters promote phytoplankton blooms, supporting secondary and tertiary consumers like larval fish. To capitalize on this productivity, most nearshore fish species spawn during peak upwelling season. For these species, there is likely selective pressure to limit dispersal (Strathmann et al., 2002; Shanks & Eckert 2005; Burgess et al., 2016). Many of the nearshore species we observed produce egg masses that they fix to the benthos or structures such as kelp fronds, eliminating the potential for dispersal during a planktonic egg stage. Indeed, these modes of spawning have been shown to be more common in our region than elsewhere along the West Coast (Parrish et al., 1981). Moreover, nearshore larvae tend to have shorter pelagic larval durations (PLDs), allowing feeding plankton to benefit from upwelling productivity but reducing the time they spend in the water column. Eighty-one percent of nearshore species for which we were able to identify a PLD from available literature have a PLD of three months or less, whereas mid-shelf and offshore

species tended to have longer PLDs (6-12 months). The suite of larval behaviors identified here are likely yet another way in which these species are adapted to life in a productive but advective environment.

Finally, adaptations for life in an upwelling regime are important to understand as the environment changes. In the Eastern Pacific region, climate change poses a threat to marine systems through a variety of oceanographic and physical drivers (Collins et al., 2010; DiLorenzo & Mantua, 2016), including changes in upwelling frequency and intensity (Bakun et al., 2015). It is expected that the alongshore peak in upwelling intensity on the North American West Coast will shift northward, with reduced upwelling equatorward (Garcia Reyes et al., 2015). Such a shift could lead to reduced recruitment of northern nearshore fishes by increasing rates of advection where upwelling intensity grows (e.g., Santos et al., 2007), but our findings suggest that this effect could be mitigated for species where cross-shelf dispersal is behaviorally mediated. These same behaviors though could prove to be maladaptive in cases where local retention inhibits species' ability to track changing climate envelopes (Bashevkin et al., 2020).

Diel vertical migration

Our diel surveys of larval distributions suggested that five species (*Cebidichthys violaceus, Engraulis mordax, Ophiodon elongatus, Parophrys vetulus,* and *Scorpaenichthys marmoratus*) may undergo DVM. Larvae of these species were more abundant near the surface during the night than during the day. Adults of these species inhabit the inner shelf or in intertidal and estuarine habitats. Consequently, DVM could play an important role in facilitating nearshore retention by reducing exposure of these larvae to wind-driven offshore transport during the daytime and increasing exposure to landward seabreezes at night (Shanks, 1995;

Woodson et al., 2007). The one exception is *Engraulis mordax*, which is a coastal pelagic species that occurs across the shelf. DVM may help retain larvae on the shelf.

While our observed distributions suggest that larvae may undergo DVM, they also highlight a challenge of collecting *in situ* ichthyoplankton data. As larvae develop, they become more competent swimmers and are presumably better able to detect and avoid an approaching net. Consequently, late-stage larvae and juveniles are frequently under sampled relative to early-stage larvae (Hewitt, 1980; McGurk, 1992; Thompson et al., 2017). We strove to minimize under sampling by conducting most of our trawling at night with a darkly colored net, reducing the chance that larvae would see the net, and by using a large mesh size (505 μm), reducing the pressure head that develops in front of the net, which can trigger escape behaviors in larvae.

Two lines of evidence suggest that late-stage larvae of some species were, nonetheless, under sampled by our survey. First, we collected few late-stage *O. elongatus* and no late-stage *S. marmoratus* during nighttime and diel surveys. Both species spawn in winter and early spring (CDFW, n.d.) and have pelagic larval durations of 90 d (*O. elongatus*) and 120 d (*S. marmoratus*). Therefore, late-stage larvae should have been present at the time of sampling. That few late-stage larvae of either species were collected could suggest these individuals were able to evade the net. Data on swimming speeds of *O. elongatus* and *S. marmoratus* larvae are lacking, but it is interesting to note that both were strongly affiliated with the neuston throughout development where strong swimming abilities could help reduce offshore advection by surface currents. Secondly, in our diel surveys, late-stage *E. mordax* and *P. vetulus* were absent in daytime samples but abundant in nighttime samples suggesting that these individuals may have been able to see and avoid the net during the day. Indeed, prior surveys have collected 20 times more late-stage *E. mordax* larvae at night than during the day (Hewitt, 1980) and late-stage

individuals are competent swimmers (Thompson et al., 2017). Another coastal pelagic species, *Sardinops sagax*, which were also present in the neuston during our 10 nighttime cruises but were not sampled during our diel survey, are also known to be strong swimmers that may reach nearshore nursery sites by directed onshore swimming (Weber et al., 2015). These cases highlight the likelihood that late-stage larvae may have been regularly under sampled in our survey for many species, though the cause of and degree to which under sampling occurs likely varies by species (McGurk, 1992).

CONCLUSION

We have shown that the larvae of most nearshore species of fishes are retained on the inner continental shelf, near settlement sites, during peak upwelling season off the central coast of California in spite of the potential for offshore advection. Larvae of many nearshore species are maintained close to shore by exhibiting a suite of depth preference behaviors that exploit vertical shear in cross-shore currents. Larvae of mid-shelf and offshore species also exhibited depth preference behaviors that likely influence dispersal trajectories. Together, these findings substantially expand our knowledge of the early life history of a diverse assemblage of marine fishes in the California Current Ecosystem and highlight the value of depth-stratified sampling, targeting a range of environmental conditions, in understanding variability of planktonic distributions. Future research should integrate depth preferences with other behaviors, such as directed swimming (Burgess et al., 2015, Drake et al. 2018), and explore the impact of behavior on larval dispersal. Biophysical modeling studies that account for larval behavior will be an important next step in understanding recruitment variability among fished species (Kuparinen et

al., 2014; He & Field, 2019) as well as realized connectivity within networks of protected areas (Shanks et al., 2003; Hastings & Botsford, 2006; White et al., 2010).

CHAPTER 2 LITERATURE CITED

Ahlstrom EH (1962) Kinds and abundance of fishes in the California Current region based on egg and larval surveys. CalCOFI Report 10

Allen MJ, Leos R (2001) Sanddabs. California's marine living resources: A status report. California Department of Fish and Wildlife

Bashevkin SM, Dibble CD, Dunn RP, Hollarsmith JA, Ng G, Satterthwaite EV, Morgan SG (2020) Larval dispersal in a changing ocean with an emphasis on upwelling regions. Ecosphere 11:e03015

Burgess SC, Baskett ML, Grosberg RK, Morgan SG, Strathmann RR (2016) When is dispersal for dispersal? Unifying marine and terrestrial perspectives. Biological Reviews 91:867-882

Burgess SC, Bode M, Leis JM, Mason LB (2022) Individual variation in marine larval-fish swimming speed and the emergence of dispersal kernels. Oikos:e08896

California Department of Fish and Wildlife (n.d.) Life history information for selected California marine fishes. Accessed 7 April 2022. https://wildlife.ca.gov/Conservation/Marine/Life-History-Fish

Collins M, An S-I, Cai W, Ganachaud A, Guilyardi E, Jin F-F, Jochum M, Lengaigne M, Power S, Timmermann A, Vecchi G, Wittenberg A (2010) The impact of global warming on the tropical Pacific Ocean and El Niño. Nature Geoscience 3:391

Cowen RK, Gawarkiewicz G, Pineda J, Thorrold SR, Werner FE (2007) Population Connectivity in Marine Systems An Overview. Oceanography 20:21

Di Lorenzo E, Mantua N (2016) Multi-year persistence of the 2014/15 North Pacific marine heatwave. Nature Climate Change 6:1042-1047

Drake PT, Edwards CA, Morgan SG (2015) Relationship between larval settlement, alongshore wind stress and surface temperature in a numerical model of the central California coastal circulation. Marine Ecology Progress Series 537

Drake PT, Edwards CA, Morgan SG, Dever EP (2013) Influence of larval behavior on transport and population connectivity in a realistic simulation of the California Current System. Journal of Marine Research 71:317-350

Drake PT, Edwards CA, Morgan SG, Satterthwaite EV (2018) Shoreward swimming boosts modeled nearshore larval supply and pelagic connectivity in a coastal upwelling region. Journal of Marine Systems 187:96-110

Epifanio CE, Garvine RW (2001) Larval transport on the Atlantic continental shelf of North America: a review. Estuarine Coastal and Shelf Science 52:51-77

Feeney RF (1992) Post-yolksac larval development of two southern California sculpins, Clinocottus analis and Orthonopias triacis (Pices: Cottidae). Fisheries Bulletin 90:454-468

Fisher JL, Peterson WT, Morgan SG (2014) Does larval advection explain latitudinal differences in recruitment across upwelling regimes? Marine Ecology Progress Series 503

Gatz DF, Smith L (1995) The standard error of a weighted mean concentration—I. Bootstrapping vs other methods. Atmospheric Environment 29

Hameed SO, Elliott ML, Morgan SG, Jahncke J (2018) Interannual variation and spatial distribution of decapod larvae in a region of persistent coastal upwelling. Marine Ecology Progress Series 587

Hastings A, Botsford LW (2006) Persistence of spatial populations depends on returning home. Proceedings of the National Academy of Sciences of the United States of America 103:6067-6072

He X, Field JC (2019) Effects of recruitment variability and fishing history on estimation of stock-recruitment relationships: Two case studies from U.S. West Coast fisheries. Fish Res 217

Hedgecock D, Barber PH, Edmands S (2007) Genetic Approaches to Measuring Connectivity. Oceanography 20:79

Hewitt R (1980) Atlas 28: Distributional atlas of fish larvae in the California Current region: northern anchovy, Engraulis mordax (Girard), 1966-1979. CalCOFI

Jacox MG, Edwards CA, Hazen EL, Bograd SJ (2018) Coastal upwelling revisited: Ekman, Bakun, and improved upwelling indices for the U.S. West Coast. Journal of Geophysical Research: Oceans 123:7332-7350

Kendall AW, Vinter B (1984) Development of Hexagrammids (Pisces: Scorpaeniformes) in the Northeastern Pacific Ocean. NOAA Technical Report

Kucas ST, Hassler TJ (1986) Species profiles: Life histories and environmental requirements of coastal fishes and invertebrates (Pacific Southwest). Fish and Wildlife Service

Kuparinen A, Keith DM, Hutchings JA (2014) Increased environmentally driven recruitment variability decreases resilience to fishing and increases uncertainty of recovery. ICES J Mar Sci 71

Largier JL, Magnell BA, Winant CD (1993) Subtidal circulation over the northern California shelf. Journal of Geophysical Research 98:18

Laroche JL, Richardson SL (1979) Winter-spring abundance of larval English sole, Parophrys vetulus, between the Columbia River and Cape Blanco, Oregon during 1972–1975 with notes on occurrences of three other pleuronectids. Estuarine and Coastal Marine Science 8

Leis JM, Sweatman HPA, Reader SE (1996) What the Pelagic Stages of Coral Reef Fishes Are Doing out in Blue Water: Daytime Field Observations of Larval Behavioural Capabilities. Marine and Freshwater Research 47

Lenarz WH, Larson RJ, Ralston S (1991) Depth distributions of late larvae and pelagic juveniles of some fishes of the California Current. California Cooperative Oceanic Fisheries Investigations Reports 32:41-46

Marliave JB (1986) Lack of planktonic dispersal of rocky intertidal fish larvae. Transactions of the American Fisheries Society 115:149-154

Marliave JB, Peden AE (1989) Larvae of Liparis fucensis and Liparis callyodon: Is the “cottid bubblemorp” phylogenetically significant? Fish Bull 87:735-743

Matarese AC, Blood DM, Busby MS (2013) Guide to the identification of larval and early juvenile pricklebacks (Perciformes: Zoarcoidei: Stichaeidae) in the northeastern Pacific Ocean and Bering Sea. NOAA Professional Paper

Matarese AC, Kendall AW, Blood DM, Vinter BM (1989) Laboratory guide to early life history stages of Northeast Pacific fishes. NOAA Technical Report

McGurk MD (1992) Avoidance of towed plankton nets by herring larvae: a model of night-day catch ratios based on larval length, net speed and mesh width. Journal of Plankton Research 14

Morgan S (2006) Larval migration between the Hudson River estuary and New York Bight. In: Levington J (ed) The Hudson River Estuary. Oxford University Press

Morgan S, Fisher J (2010) Larval behavior regulates nearshore retention and offshore migration in an upwelling shadow and along the open coast. Marine Ecology Progress Series 404

Morgan SG (2014) Behaviorally Mediated Larval Transport in Upwelling Systems. Advances in Oceanography 2014:17

Morgan SG, Miller SH, Robart MJ, Largier JL (2018) Nearshore Larval Retention and Cross-Shelf Migration of Benthic Crustaceans at an Upwelling Center. Frontiers in Marine Science 5

Moser HG (ed) (1996) The early stages of fishes in the California Current region. CalCOFI Atlas 33

Moyano M, Rodríguez JM, Benítez-Barrios VM, Hernández-León S (2014) Larval fish distribution and retention in the Canary Current system during the weak upwelling season. Fisheries Oceanography 23

Nickols K, Gaylord B, Largier J (2012) The coastal boundary layer: predictable current structure decreases alongshore transport and alters scales of dispersal. Marine Ecology Progress Series 464

Nickols KJ, Miller SH, Gaylord B, Morgan SG, Largier JL (2013) Spatial differences in larval abundance within the coastal boundary layer impact supply to shoreline habitats. Marine Ecology Progress Series 494:191-203

Nishimoto MM, Simons RD, Love MS (2019) Offshore oil production platforms as potential sources of larvae to coastal shelf regions off southern California. B Mar Sci 95:535-558

Oksanen J, Blanchet FG, Friendly M, Kindt R, Legendre P, McGlinn D, Minchin PR, O'Hara RB, Simpson GL, Solymos P, Stevens MHH, Szoecs E, Wagner H (2019) vegan: Community ecology package.

Paris C, Cowen R (2004) Direct evidence of a biophysical retention mechanism for coral reef fish larvae. Limnology and Oceanography 49

Parrish RH, Nelson CS, Bakun A (1981) Transport mechanisms and reproductive success of fishes in the California Current. Biological Oceanography 1:175-203

Pineda J (1994) Spatial and temporal patterns in barnacle settlement rate along a Southern California rocky shore. Marine Ecology Progress Series 107

R Core Team (2019) R: A language and environmental for statistical computing. https://www.R-project.org/

Richardson S, Washington BB (1980) Guide to identification of some sculpin (Cottidae) larvae from marine and brackish waters off Oregon and adjacent areas in the Northeast Pacific. NOAA Technical Report

Richardson SL, Pearcy WG (1977) Coastal and oceanic fish larvae in an area of upwelling off Yaquina Bay, Oregon. Fish Bull 75

Robards MD, Willson MF, Armstrong RH, Piatt JF (1999) Sand lance: A review of biology and predator relations and annotated bibliography. USDA, Portland, OR

Roy C (1998) An upwelling-induced retention area off Senegal: a mechanism to link upwelling and retention processes. South African Journal of Marine Science 19

Sakuma KM, Larson RJ (1995) Distribution of pelagic metamorphic-stage sanddabs Citharichthys sordidus and C. stigmaeus within areas of upwelling off central California. Fish Bull 93:516-529

Sakuma KM, Ralston S, Roberts DA (1999) Diel vertical distribution of postflexion larval Citharichthys spp. and Sebastes spp. off central California. Fisheries Oceanography 8

Santos AMP, Chícharo A, Dos Santos A, Moita T, Oliveira PB, Peliz Á, Ré P (2007) Physical–biological interactions in the life history of small pelagic fish in the Western Iberia Upwelling Ecosystem. Prog Oceanogr 74

Satterthwaite EV, Ryan JP, Harvey JBJ, Morgan SG (2021) Invertebrate larval distributions influenced by adult habitat distribution, larval behavior, and hydrodynamics in the retentive upwelling shadow of Monterey Bay, California, USA. Marine Ecology Progress Series 661

Shanks AL (1995) Orientated swimming by megalopae of several eastern North Pacific crab species and its potential role in their onshore migration. Journal of Experimental Marine Biology and Ecology 186

Shanks AL, Eckert GL (2005) Population persistence of California Current fishes and benthic crustaceans: A marine drift paradox. Ecol Monogr 75

Shanks AL, Grantham BA, Carr MH (2003) Propagule Dispersal Distance and the Size and Spacing of Marine Reserves. Ecological Applications 13:S159-S169

Shanks AL, Morgan SG (2018) Testing the intermittent upwelling hypothesis. Ecol Monogr 88

Siegel DA, Mitarai S, Costello CJ, Gaines SD, Kendall BE, Warner RR, Winters KB (2008) The stochastic nature of larval connectivity among nearshore marine populations. PNAS 105

Strathmann RR, Hughes T, Kuris AM, Lindeman KC, Morgan SG, Pandolfi JM, Warner RR (2002) Evolution of Local Recruitment and its Consequences for Marine Populations. B Mar Sci 70:377-396

Strub PT, Allen JS, Huyer A, Smith RL (1987) Large-scale structure of the spring transition in the coastal ocean off western North America. Journal of Geophysical Research 92

Swearer SE, Shima JS, Hellberg ME, Thorrold SR, Jones GP, Robertson DR, Morgan SG, Selkoe KA, Ruiz GM, Warner RR (2002) Evidence of self-recruitment in demersal marine populations. B Mar Sci 70:251-271

Thompson AR, McClatchie S, Weber ED, Watson W, Lennert-Cody CE (2017) Correcting for bias in CalCOFI ichthyoplankton abundance estimates associated with the 1977 transition from ring to bongo net sampling. CalCOFI Reports, Book 58

Tiedemann M, Brehmer P (2017) Larval fish assemblages across an upwelling front: Indication for active and passive retention. Estuarine and Coastal Marine Science 187:118-133

Washington BB (1981) Identification and systematics of larvae of Artedius, Clinocottus, and Oligocottus (Scorpaeniformes:Cottidae). Master of Science, Oregon State University,

Watson JR, Mitarai S, Siegel DA, Caselle JE, Dong C, McWilliams JC (2010) Realized and potential larval connectivity in the Southern California Bight. Marine Ecology Progress Series 401:31-48

Watson W (1982) Development of eggs and larvae of the white croaker Genyonemus lineatus ayres (Pices: Sciaenidae) off the Southern California coast. Fish Bull 30

Weber ED, Chao Y, Chai F, McClatchie S (2015) Transport patterns of Pacific sardine Sardinops sagax eggs and larvae in the California Current System. Deep Sea Research Part I: Oceanographic Research Papers 100:127-139

Weersing K, Toonen RJ (2009) Population genetics, larval dispersal, and connectivity in marine systems. Marine Ecology Progress Series 393:1-12

White JW, Botsford LW, Hastings A, Largier JL (2010) Population persistence in marine reserve networks: incorporating spatial heterogeneities in larval dispersal. Marine Ecology Progress Series 398:49-67

Wickham H (2016) ggplot2: Elegant graphics for data analysis. https://ggplot2.tidyverse.org

Wing SR, Botsford LW, Ralston SV, Largier JL (1998) Meroplanktonic distribution and circulation in a coastal retention zone of the northern California upwelling system. Limnology and Oceanography 43

Woodson C, Eerkes-Medrano DI, Flores-Morales A, Foley M, Henkel S, Hessing-Lewis M, Jacinto D, Needles L, Nishizaki M, O'Leary J, Ostrander C, Pespeni M, Schwager KB, Tyburczy J, Thomas K, Kirincich AR, Barth JA, McManus MA, Washburn L, Mexico (2007) Local diurnal upwelling driven by sea breezes in northern Monterey Bay. Continental Shelf Research 27

CHAPTER 3

Small-scale topographic fronts along an exposed coast structure plankton communities and facilitate retention

ABSTRACT

Fronts are boundaries between distinct water masses that often aggregate flotsam, detritus, phytoplankton and zooplankton. Studies of large-scale (100-1000 m) offshore fronts that persist over the course of days affect ecological processes by concentrating prey for diverse planktivores and delivering larval recruits to settlement habitats. Less is known about the small-scale (1-10 m), ephemeral (<1 d) fronts that commonly occur along exposed coasts, yet these features may have outsized importance for the many animals that live or forage in these environments. We characterized the hydrodynamics and plankton community along a front at a small headland on the exposed coast of northcentral California using a Tucker trawl, CTD profiler, satellite imagery, and timelapse photography between June and October over 2 yr. The front formed as the result of topographically generated flow separation primarily occurring during upwelling relaxation but also during other flow conditions. Only barnacle cyprids (*Chthamalus* spp.) accumulated at the front. For other species, the front acted as a barrier inhibiting cross-frontal movement or altered the vertical position of plankton in the water column. Fronts occur on the windward (poleward) side many small headlands occurring along coasts in upwelling systems where they may structure plankton communities, facilitating larval retention and concentrating prey.

INTRODUCTION

Marine fronts occurring at the boundaries between water masses are common on the continental shelf where they are generated by a variety of physical processes. Fronts form as the result of strong density gradients where cold, saline waters encounter less dense water masses at surface upwelling fronts (Halpern, 1973) or at the edge of river plumes (Grimes & Kingsford, 1996). They can also be caused by vertical or horizontal current instabilities where currents pass irregular surfaces or along the edges of rotational masses such as submesoscale eddies (Owen, 1981; Wolanski & Hamner, 1988). Depending on their physical drivers, fronts may appear as horizontal density steps or filaments, where sloping isopycnals intersect with the surface, and may be associated with current velocity gradients where shear forces are stronger than horizontal cross-frontal mixing instabilities (McWilliams, 2021). Shear fronts are especially common close to shore where alongshore flow creates flow separations and eddies in the lee of headlands or islands (McCabe et al., 2006; Wijesekera et al., 2020). Finally, fronts are frequently associated with lines of foam and other visible differences in sea-surface characteristics, such as water color, turbidity, and roughness (Figure 1).

Figure 1. Photograph of a front poleward of Bodega Head on the northcentral coast of California. Image shows a foam line and slight gradient in water color across the front.

A large body of literature on different kinds of fronts has demonstrated that frontal features influence the abundance and distribution of organisms. Franks (1992) posited that fronts can create patchiness in plankton communities due to simple interactions between frontal flow regimes and the swimming abilities and behaviors of different plankton. In his analysis, these interactions lead either to plankton aggregation, via convergence/compression of plankton at the front, or the development of retention zones on either side of the front. When retention zones develop, concentrations tend to be higher on one side or the other with the front acting as a barrier to cross-frontal mixing of plankton (Woodson et al., 2012). Density-driven fronts (e.g., upwelling or river plume fronts) tend to aggregate planktonic organisms that are drawn towards the front by secondary flow structures (Bjorkstedt et al., 2002; Karati et al., 2018). Topographically generated fronts (e.g., internal wave fronts, surface slicks, and flow separations) can also create spatial structure in the plankton by, for example, concentrating some planktonic taxa while dispersing others away from frontal boundaries (Wolanski & Hamner, 1988; Lennert-Cody & Franks, 1999; Shanks et al., 2003; Weidberg et al., 2014; Weidberg et al., 2019). These dynamics can have important ecological implications. Aggregation of planktonic organisms can facilitate delivery of larvae to nearshore habitats, when and where fronts progress towards or intersect with the settlement habitats (Wolanski & Hamner, 1988; Clancy & Epifanio, 1989; Eggleston et al., 1998; Bjorkstedt et al., 2002; Weidberg et al., 2014;) with consequences for spatial variability in recruitment (Woodson et al., 2012) and population genetic structure (Galarza et al., 2009). Fronts can also create rich foraging habitats for planktivores and their predators and have even been used as a predictor of fishery productivity (Hobday & Hartog, 2014; Woodson & Litvin, 2015).

Topographic fronts are common in the upwelling system along the West Coast of North America, where equatorward alongshore flow regularly encounters topographic irregularities, such as headlands, seamounts, and bays (McCabe et al., 2006; Vander Woude et al., 2006). Drag around headlands and other promontories results in the formation of an offshore-directed jet (Barth et al., 2000) and a flow separation eddy in the lee of the headland (McCabe et al., 2006; Vander Woude et al., 2006), generating a shear front at their interface. Headland flow separations facilitate recruitment of larval marine organisms during periods of equatorward flow, particularly during spring and summer when upwelling and reproduction peak (Graham & Largier, 1997. Wing et al. 1998, Roughan et al., 2006; Mace & Morgan, 2006; Satterthwaite et al., 2021). However, equatorward flow in this region is periodically interrupted by alongshore flow reversals, during which alongshore wind stress weakens and flow shifts poleward approximately every 4-10 d (Largier et al., 1993). Yet, few have investigated the impact of flow separations on the windward sides of headlands that occur during flow reversals (e.g., Vander Woude et al., 2006).

Bodega Head is a small headland on the exposed coast of northcentral California, where equatorward flow during upwelling and poleward flow during wind relaxation or reversal alternate. Several studies have documented the existence of a headland eddy on the leeward (equatorward) side of Bodega Head (BH; Mace & Morgan, 2006; Dibble, 2020), but none has investigated circulation and frontogenesis on the windward (poleward) side of BH near Mussel Point (MP, Figure 2). In spring 2018, we began visual surveys of the waters around BH in search of fronts, slicks, and foam lines to investigate how alternating flow regimes influenced the formation of fronts around the headland. We regularly observed a foam line extending northwesterly of MP (Figure 2), at the poleward edge of BH. In summer 2019, we began

surveying the area around MP to test the hypothesis that this foam line is associated with a front formed by a topographically generated flow separation past MP during periods of poleward alongshore flow. We also examined whether the front had an observable impact on the distribution and abundance of zooplankton during the summer months, following the peak reproductive period. Specifically, we tested whether the front aggregated zooplankton or partitioned the zooplankton community into different species on either side of and within it. Our study adds to the sparse literature on the development and ecological impact of fronts on the windward side of headlands along the West Coast, and is one of the first to focus on small scale (<1 km) and ephemeral (<1 d) features.

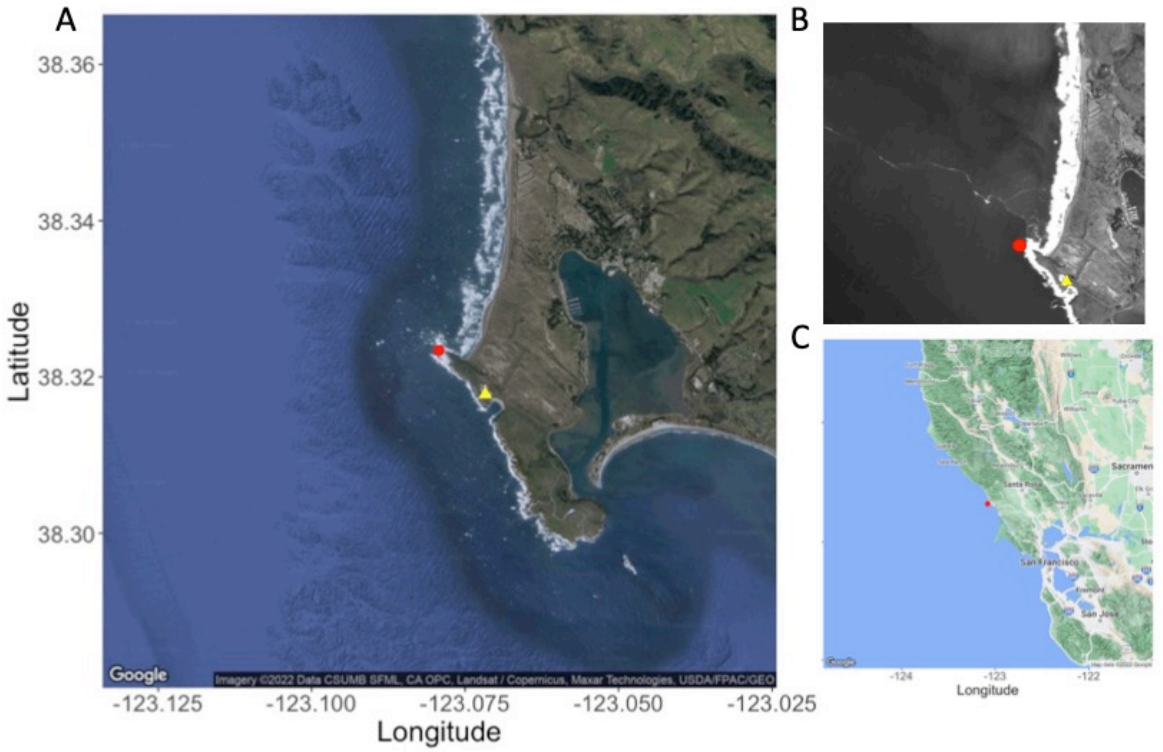

Figure 2. Images of the study area located on the northcentral coast of California. (A) Satellite image of Bodega Head indicating the location of Mussel Point (red circle) relative to the Bodega Marine Laboratory (yellow triangle). (B) Satellite image of Mussel Point (red circle) taken on 11 March 2019 showing a foam line and associated surface color discontinuity on Bodega Head. Image shown in grayscale to increase contrast. (C) Regional map showing the location of Mussel Point (red circle) relative to San Francisco Bay.

MATERIALS & METHODS

Surveys

BH is a prominent feature on the northcentral coast of California that is regularly exposed to alongshore flow reversals and predominant winds and wind waves from the northwest (Figure 2). The bluffs of BH slope seaward to a broad rocky subtidal shelf, extending approximately 15 km from shore (Kvitek et al., 2012; Johnson, 2015). Salmon Creek Beach (SCB), north of BH,

extends alongshore for about 4.3 km, and substrate offshore of SCB is sandy and shaped into channels by beach circulation currents.

Foam lines are common sights in the waters around BH (38.32 N, 123.075 W; Figure 2), particularly poleward of MP. We placed a GoPro camera on the bluffs above MP beginning in spring of 2019 to identify patterns in the formation of the foam line and its orientation with respect to the shoreline. In July 2019, we began boat-based surveys to examine whether the foam line was associated with a front and characterize the influence of the feature on the zooplankton community. We conducted 6 boat-based surveys between July 2019 and October 2020 (15 August and 20 September in 2019, and in 2020 on 23 and 30 June, 30 September, and 6 October). Each survey consisted of 3 components: surface-water mapping, vertical seawater profiles, and zooplankton collection. At the beginning of each survey, we mapped temperature and salinity at the surface using a conductivity, temperature, and depth profiler (CTD, SeaBird). The CTD was placed in a bucket into which water was pumped from the surface while the boat was underway. Generally, we mapped surface waters by moving between the 20 m and 40 m isobaths poleward parallel to SCB at ~2 kts. During mapping, we recorded local conditions and the location of the foam line relative to any observed gradient in seawater temperature or salinity. Next, we conducted vertical seawater profiles using a second CTD on either side of and within the front. If a front was not detectable during surface mapping, we positioned CTD casts relative to the foam line. The location of CTD profiles varied across survey dates because the position of the front was inconsistent. Data on surface water temperature, the location of CTD profiles and the location of zooplankton tows were not taken on 20 September 2019 and 23 June 2020, and CTD casts across the front were not taken on 15 August 2019 and 6 October 2020.

Zooplankton were collected along 3 transects within the front and on either side of the front using a mechanically triggered Tucker Trawl with a 0.25 m^2 opening and 300-µm mesh net and codend. Each net was equipped with a mechanical flowmeter (General Oceanics) to determine the volume of water sampled by the net and calculate zooplankton concentrations. Nets were towed obliquely at ~2 kts and sampled 2 discrete depth bins (surface: 0-5 m, and bottom: 5-10 m), as nearshore zooplankton are known to exhibit depth preferences (Morgan & Fisher 2010, Weidberg et al., 2019). Transects were oriented to follow or run parallel to the front and each depth was sampled for 5 min.

Zooplankton were preserved in the field in 95% ethanol and later enumerated at Bodega Marine Laboratory (BML). Samples were split using a Folsom Splitter into aliquots of variable fraction depending on sample density. All zooplankton in the aliquot selected were identified taxonomically and to developmental stage using available keys (Moser, 1996; Shanks, 2001). We then enumerated any additional taxa and stages in a larger aliquot (generally ½ depending on the density of the sample) to capture rare species. We pooled taxa and developmental stages based on the ease of identification and similarity in swimming behaviors/abilities. For instance, we pooled early (I-III) and late (IV-VI) stage barnacle nauplii because swimming abilities within either grouping are likely to be similar.

Environmental context

Surveys were contextualized using local and regional environmental data. We used high-frequency radar (HF-radar) to measure local hourly surface current velocities in the vicinity of BH (within the cell bounded by North 38.34 South 38.28, East -123.08, and West -123.12). HF-radar data were provided by the U.S. Integrated Ocean Observing System HF Radar Network and are available via the Bodega Ocean Observing Node (BOON) at

http://boonproducts.ucdavis.edu. Wind, sea surface temperature, and an upwelling index were used to determine recent upwelling conditions and infer the provenance of local water types. We used daily average wind data from both onshore (BOON, 38.32, -123.07) and offshore (National Data Buoy Center 46013, 38.24, -123.32) locations. We used the daily Coastal Upwelling Transport Index (CUTI; accessed at http://mjacox.com/upwelling-indices/), which incorporates both Ekman and geostrophic transport and provides a 1° latitudinal estimate of upwelling/relaxation activity (Jacox et al., 2018). Finally, we used daily averaged local seawater temperature collected at the BML seawater intake (BOON, 38.32, -123.07).

Statistical modeling

To investigate the effect of the front on zooplankton distributions, we modeled the abundance of zooplankton in a generalized linear mixed model (GLMM) with location relative to the front (levels: onshore, front, and offshore) as a fixed effect and date of survey as a random effect. We also included a fixed term for the interaction between location and depth (levels: surface, bottom) to examine whether the front alters the position of zooplankton within the water column. We created an individual model for each of the most common zooplankton species and developmental stage combinations (e.g., *Balanus crenatus* cyprid, hereafter referred to as zooplankton types), all of which were observed in >50% of all net samples. We selected from Poisson and negative binomial distributions, as well as their zero-inflated counterparts, for each GLMM depending on the degree of zero-inflation and overdispersion present in the data. Post-hoc pairwise comparisons were conducted for all models with significant estimates ($p < 0.05$ following Benjamini-Hochberg correction) for location. We then used pairwise comparisons to determine whether zooplankton were (1) aggregated at the front, (2) retained on either side such that the front acted as a barrier to onshore or offshore movement, or (3) unaffected by the front.

We then used non-metric multidimensional scaling (NMDS) and analysis of similarity (ANOSIM) with a Bray-Curtis dissimilarity matrix to investigate the role of the front, depth, and date on zooplankton assemblage, and computed the Shannon-Weiner diversity index for comparison across samples.

All data processing, analysis, and figure generation was conducted in R version 3.6.2 (R Core Team, 2019), and is available online (https://osf.io/pv43u/). GLMM analyses were conducted using the NBZIMM (Yi, 2020) and lme4 (Bates et al., 2015) packages, NMDS and ANOSIM were conducted using the vegan package (Oksanen et al., 2019), and figures were created using the ggplot2 package (Wickham, 2018).

RESULTS

Camera observations of the foam line

Timelapse footage obtained using a GoPro camera mounted in the bluffs above MP revealed that foam lines formed most often on a NW axis extending from the Point parallel to Salmon Creek Beach (Figure 2). NW foam lines were most common when alongshore flow adjacent to Bodega Head was poleward and when winds were low. Increases in wind speeds and wave heights, typical in the afternoon in the region, obscured the foam line. Foam line geometry evolved over the course of hours; we often observed changes in the angle between the foam line and the poleward edge of BH and meanders in the foam line indicative of cross-frontal vorticities. Surface slicks were also common and were presumably associated with internal waves shoaling on SCB. Slicks concentrated and entrained the foam line, shifting it toward the beach. Timelapse observations did not reveal an impact of tidal fluctuation on the foam line

position or geometry. Finally, we regularly observed patches or tendrils of foam in an eddy forming on the windward side of MP at the most equatorward point of SCB.

Survey observations of the front and foam line

We tested the hypotheses that (1) the foam line was associated with a front and (2) that the front was evident during periods of poleward alongshore flow by surveying environmental conditions near MP on 6 d in 2019 and 2020. Three surveys occurred during upwelling (15 August and 20 September 2019, and 30 June 2020; Figure 3), but these events were not associated with strong equatorward flow adjacent to Mussel Point. All but 1 survey (6 October 2020) occurred when BOON seawater temperatures were increasing. In the following sections, we describe environmental conditions and observations from each survey to describe the variability of frontal dynamics.

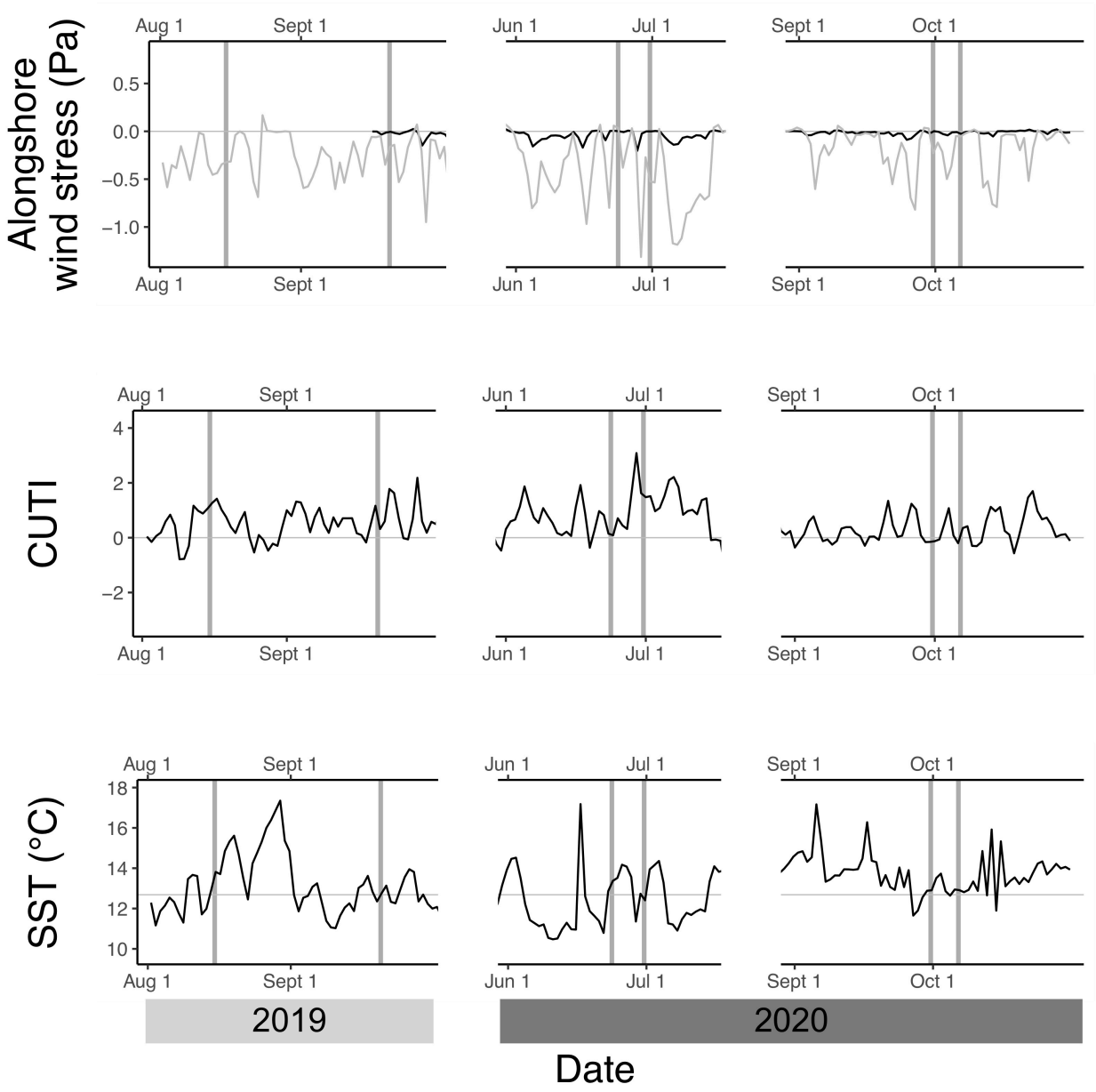

Figure 3. Regional environmental conditions during the survey period. Alongshore wind stress was calculated using wind data collected offshore at the National Data Buoy Center 46013 (gray line, 38.235, -123.317) and onshore at the Bodega Ocean Observing Node (black line, 38.31912, -123.07293). The Coastal Upwelling and Transport Index (CUTI) and sea surface temperature (SST) are also shown. The horizontal gray line in the SST plot represents mean SST throughout the survey period. Gray vertical bars show when surveys were conducted.

15 August 2019

We observed a thermal gradient that separated warmer onshore water from cooler offshore water (Figure 4) and coincided with a pronounced NW foam line. The front was also associated with a color differential. Birds were observed feeding in and around the foam line. HF-radar showed weak poleward alongshore flow during and in the hours preceding the survey and little cross-shore flow. The GoPro timelapse camera showed that surface slicks progressing onshore drove the foam line shoreward, toward SCB, in the hours following the survey.

20 September 2019

A NW foam line was present during the survey and coincided with a filament front where water within the front was cooler than water on either the onshore or offshore side, as evidenced by CTD profiles (Figure 4, surface-water data were not collected during this survey). Water within the front was colored by a local phytoplankton bloom and was darker than water on either the onshore or offshore side. Alongshore flow was weakly equatorward, and cross-shore flow was increasingly shoreward throughout the survey, which took place during a flood tide. Towards the end of the survey period, the foam line bifurcated such that the offshore segment ran parallel to the windward side of MP.

23 June 2020

The strongest poleward flow (>20 cm/s) and seaward flow (>20 cm/s) were observed during this survey (Figure 4), but the foam line was indistinct and irregular. Nonetheless, CTD profiles revealed a strong thermal gradient with warmer water offshore and isotherm deformation at the front. Surface slicks from internal waves progressed onshore throughout the survey.

30 June 2020

We observed a foam line oriented WNW relative to the point that coincided with a thermal gradient and a color differential. Water offshore of the front was warmer than onshore of the front. Weak equatorward flow prevailed throughout the survey, following a period of >12 h of poleward flow (Figure 4). Cross-shore flow was strongly seaward during an ebb tide.

30 September 2020

Like the survey on 23 June, foam was present during the survey but did not form a distinct and coherent line. However, we did observe a thermal gradient separating cooler onshore water from warmer offshore water (Figure 4). A change in water clarity and color co-occurred with the front (clearer water onshore). Surface flow during the survey was weakly poleward and very weakly seaward during an ebb tide.

6 October 2020

Patches of foam were present on the poleward side of MP but were not oriented in a line. A mixed flock of phalaropes and murres was present within and near the foam patches. Surface-water mapping revealed the presence of a thermal gradient separating cooler onshore water from warmer offshore water, but the front was not as distinct as in previous surveys. Water clarity declined offshore of the front, though not as much as on 30 September. Surface slicks progressed onshore throughout the survey and collided with the region of the front during zooplankton sampling. Surface flows were weakly poleward and shoreward during a flood tide following a 12-h period of weak alongshore and cross-shore flows (Figure 4).

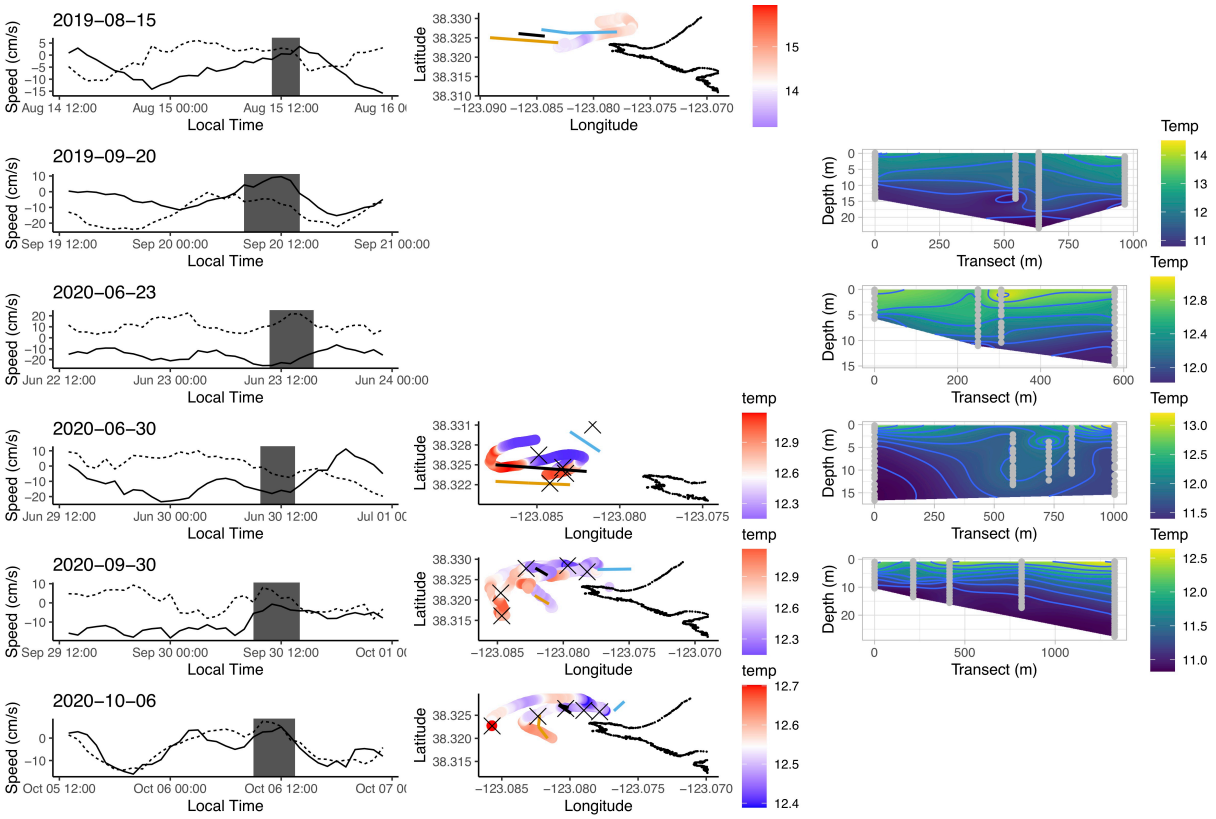

Figure 4. High-frequency radar current velocity and *in situ* temperature (°C) collected during the 6 surveys conducted at Mussel Point in northcentral California. The left column shows current speeds shoreward (black line) and poleward (dashed line) before, during, and after the survey (represented by the dark gray bar). The middle column shows surface water temperature, the location of CTD profiles (Xs), and the location of zooplankton tows (blue – onshore, black – front, orange – offshore). The right column shows the vertical temperature profile across the front with increasing distance from the onshore cast. Cast locations are indicated by gray points, intermediate values were linearly interpolated.

Zooplankton abundance across the front

We collected 36 zooplankton samples during the 6 surveys combined and identified 113 different types of 80 taxa. Seventeen types were present in 50% or more of our samples (Figure 5). We modeled the abundance of these using type-specific GLMMs. Larval concentration data for all types were overdispersed and zero-inflated (except for calanoid adults which were not zero-inflated). Consequently, we used zero-inflated negative binomial distributions in all models. The concentration of 24% of the most abundant zooplankton types was influenced by location

relative to the front (i.e., onshore, front, offshore; Table 1). Similarly, the position of zooplankton within the water column was influenced by the front for 24% of the most abundant zooplankton types, but this was not linked to zooplankton being more abundant on either side of or within the front.

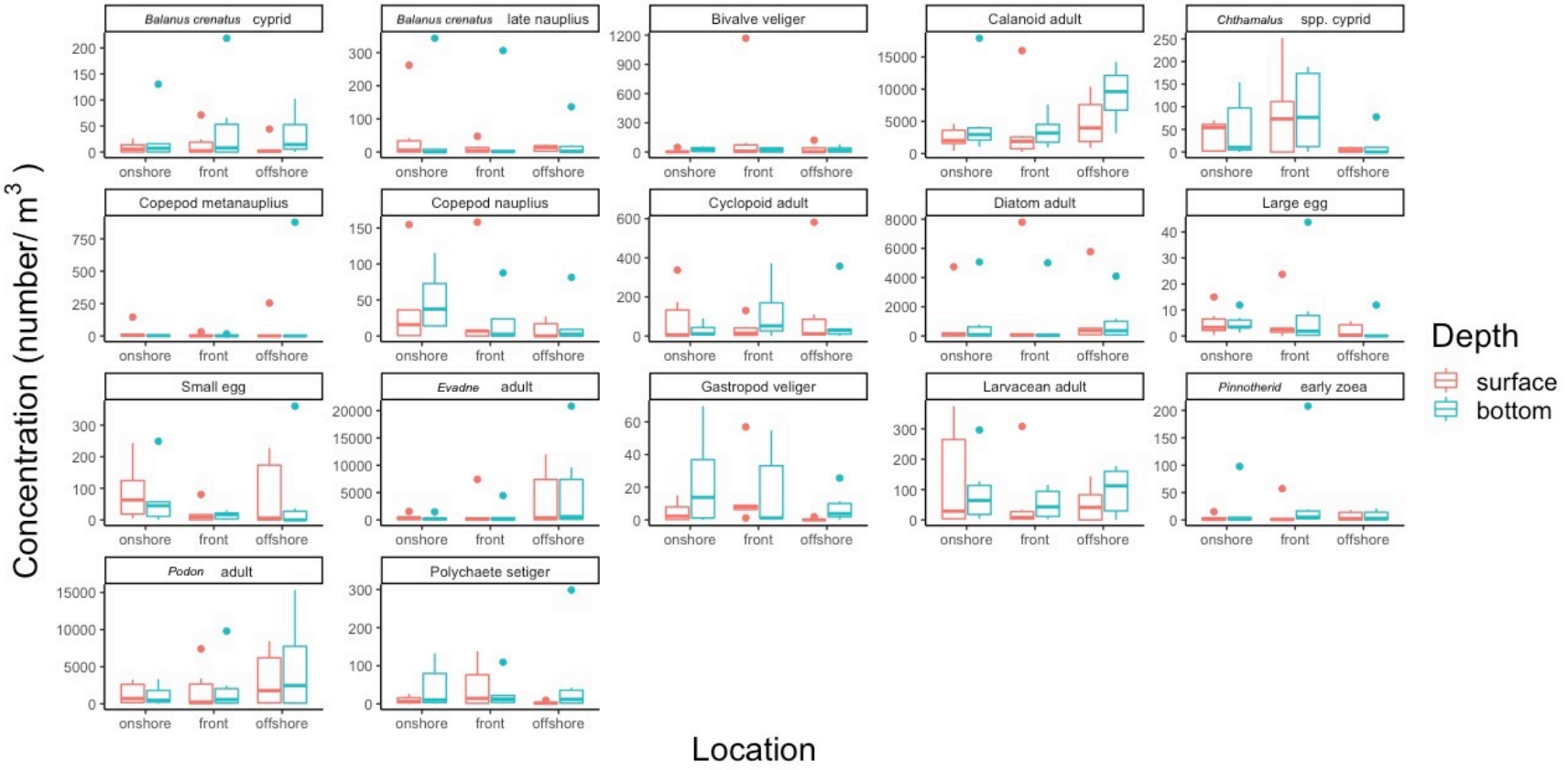

Figure 5. Boxplots of zooplanktonic concentration for the 17 most common types across the front and by depth.

Table 1. Type-specific generalized linear mixed effect model estimates and p-values for fixed effects of location and the interaction between location and depth. Bolded p-values indicate significant effects at $p < 0.05$ Zooplankton types are grouped into coastal meroplankton, holoplankton, and non-swimming plankton.

	Location		Location:Depth	
Type	**Test statistic**	**p-value**	**Test statistic**	**p-value**
Coastal Meroplankton				
Balanus crenatus cyprid	F = 1.78	0.3786	F = 8.19	**0.0084**
Balanus crenatus late nauplius	F = 2.44	0.3786	F = 1.30	0.7787
Bivalve veliger	F = 2.67	0.3786	F = 2.40	0.7787
Chthamalus spp. cyprid	F = 36.3	**0.0016**	F = 4.17	0.1908
Gastropod veliger	F = 4.60	0.1990	F = 12.0	**0.0015**
Pinnotherid zoea	F = 3.78	0.2936	F = 1.23	0.7787
Polychaete larva	F = 6.1	0.0840	F = 16.87	**0.0015**
Pelagic Holoplankton				
Calanoid adult	Chi = 7.92	0.1990	Chi = 8.39	0.4246
Copepod metanauplius	F = 129.88	**0.0016**	F = 32.98	**0.0015**
Copepod nauplius	F = 0.41	0.6705	F = 0.37	0.7787
Cyclopoid adult	F = 2.74	0.3786	F = 4.31	0.1807
Evadne adult	F = 6.62	0.0637	F = 0.68	0.7787
Larvacean adult	F = 4.04	0.2718	F = 0.44	0.7787
Podon adult	F = 7.33	**0.0434**	F = 1.19	0.7787

	Location		Location:Depth	
Type	**Test statistic**	**p-value**	**Test statistic**	**p-value**
Non-swimming				
Diatom	F = 3.34	0.3633	F = 1.83	0.7787
Large eggs	F = 2.10	0.3786	F = 1.19	0.7787
Small eggs	F = 9.83	**0.0105**	F = 0.83	0.7787

Model contrasts among locations relative to the front, for types influenced by location, revealed that when the front influences zooplanktonic distributions, it mostly acts as a barrier to onshore or offshore movement on zooplankton (Table 2). The concentrations of 3 of the 17 most common zooplankton types were higher offshore than in the front or onshore, or they were similar offshore and in the front and least onshore. The reverse was true for polychaete larvae, for which the front appeared to be a barrier to offshore movement with higher abundances onshore. Small eggs were least abundant in the front and *Chthamalus* spp. cyprids were most abundant within the front.

Table 2. Post-hoc pairwise comparisons of cross-front locations. Far right columns summarize relative abundances and the distributional pattern supported by model contrasts. Bolded p-values indicate significant effects at $p < 0.05$. Zooplankton types are grouped into coastal meroplankton, holoplankton, and non-swimming plankton.

	Onshore-Front		Onshore-Offshore		Front-Offshore			
Type	**Estimate**	**p-value**	**Estimate**	**p-value**	**Estimate**	**p-value**	**Summary**	**Hypothesis**
Coastal Meroplankton								
Chthamalus spp. cyprid	-0.75	**0.0162**	1.50	**0.0001**	2.25	**0.0001**	on < f > off	Aggregation
Pelagic Holoplankton								
Copepod metanauplius	-0.08	0.9636	-1.97	**0.0001**	-1.89	**0.0001**	on = f < off	Barrier onshore
Podon adult	0.16	0.8436	-0.89	**0.0135**	-1.05	**0.0029**	on = f < off	Barrier onshore
Non-Swimming								
Small eggs	1.18	**0.0031**	-0.34	0.6757	-1.52	**0.0027**	on > f < off	Dis-aggregation

Community assemblage across the front

We were also interested in how the front might influence spatial structure of zooplankton assemblages, and to integrate data on less common types (i.e., present in 3-18 samples). We calculated the Shannon-Weiner index of each net sample. A 1-way ANOVA of sample diversity indices revealed that there was no statistically significant effect of location on species diversity across the front ($F = 0.852$, $p = 0.436$; Figure 6). ANOSIM showed that community structure differed by survey date (ANOSIM $R = 0.411$, $p = 0.001$), marginally by location (ANOSIM $R = 0.055$, $p = 0.09$), but not by depth (ANOSIM $R = -0.014$, $p = 0.6$). NMDS showed that the zooplankton community sampled varied both within and among survey dates (Figure 7). Samples collected on 2 dates, 15 August 2019 and 6 October 2020, exhibited much less within survey variation. Community differences relative to the front were most pronounced along NMDS axis 1. Samples collected within the front and onshore were more similar to each other (centroid position along NMDS1 = 0.10 and 0.047, respectively) than either was to those collected offshore (NMDS1 = -0.14).

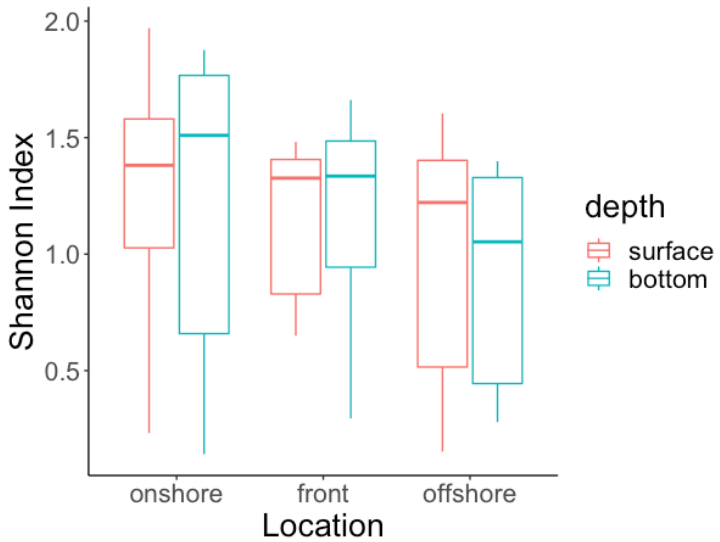

Figure 6. Shannon-Weiner index of zooplankton diversity across the front by depth.

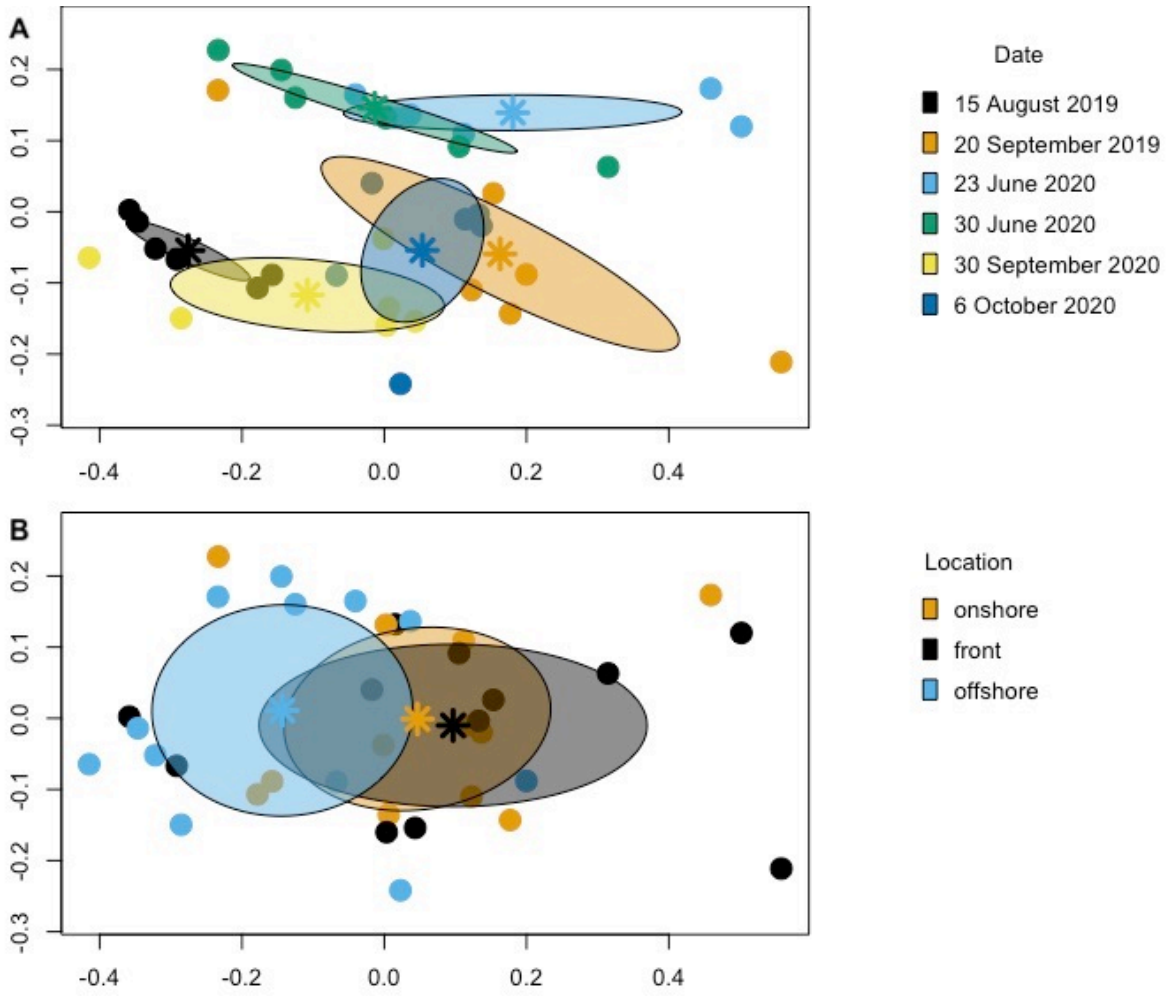

Figure 7. Non-metric multidimensional scaling plots for the zooplankton community. Circles indicate the 2-dimensional projection of each sample in ordination space by (A) survey date (black – 15 August 2019, orange – 20 September 2019, light blue – 23 June 2020, green – 30 June 2020, yellow – 30 September 2020, and dark blue – 6 October 2020) and (B) location across the front (black – front, orange – onshore, light blue - offshore). Stars indicate the centroid of each grouping and ellipses represent the 95% confidence interval of the mean.

DISCUSSION

Physical environment

The front at MP was frequently characterized by a cross-frontal surface (<5 m) thermal gradient, too weak to create a density-driven front but indicative of a flow separation between dissimilar water masses. While we were not able to gather environmental data from both surface

water and vertical profiles (CTD) for most surveys, either of these data sources was enough to determine the presence of a thermal gradient associated with the front for a given survey. Cooler surface waters were observed on the onshore side of the front on 4 of 6 surveys (23 June-6 October 2020). All 4 of these surveys occurred during relaxation conditions following brief periods of upwelling when cool water was observed at the BML seawater monitoring station (Figure 4). All 4 surveys also occurred during or immediately following (30 June 2020) periods of poleward flow near BH (Figure 5). These observations are consistent with our hypothesis that poleward relaxation flows lead to MP flow-separation fronts. As alongshore wind stress weakened, coastal upwelling relaxed allowing warm surface water to return shoreward and progress poleward, as has been observed elsewhere in our region (Wing et al., 1995). As this warm water mass moved past MP, it encountered cooler water on the windward side of the point. Furthermore, the topographically generated front at the interface between these two masses was likely bolstered by recirculation along SCB. We frequently observed foam eddying on the windward side of MP at the most equatorward extent of SCB. The appearance of the eddy in a variety of alongshore flow conditions suggests that this feature may be at least partially due to southeasterly wave-driven beach flow that is deflected upon encountering MP. The eddy likely strengthened the shear front from the onshore side.

Our inferences based on conditions during the 2020 surveys closely align with our hypothesized version of the physical processes driving formation of foam lines and fronts at MP. Observations during both 2019 surveys, however, point to different mechanisms for frontogenesis. The thermal gradient on 15 August 2019 was opposite to that observed during the 2020 surveys with warmer water onshore. While weak poleward flow persisted near MP on 15 August, the survey occurred during an upwelling event when alongshore flow >2 km from the

point was equatorward. Continued upwelling on this date and in the days prior meant that poleward flow past the point was cooler than recirculating water near the beach, reversing the direction of the thermal gradient. The survey on 20 September 2019 was the only one conducted when alongshore flow during and prior to sampling was equatorward. Contrary to our hypothesis for frontogenesis and generation of foam lines, we observed a clear NW foam line extending from MP. As equatorward flow increased offshore of BH throughout the cruise, the foam line bifurcated such that the offshore segment moved counterclockwise relative to MP until it ran parallel to the western edge of BH. One explanation for this could be that wave activity and cross-shore flows helped to establish a foam line in the absence of strong alongshore flow that was then deformed from its typical NW due to equatorward flow past the point.

Our inferences of the physical processes driving frontogenesis at MP were based on regional upwelling conditions, local topography, visual observations, surface currents, and seawater temperature. However, we lacked *in situ* observations of current velocities that have been included in other studies of ephemeral fronts (e.g., Vander Woude et al., 2006; Weidberg et al., 2014; Wijesekera et al., 2020). Collection of current velocities by our acoustic Doppler current profiler was hampered by the sandy substrate and turbulent surf zone of the survey area. Future studies can avoid this issue by using drogues to measure currents *in situ*, albeit only at the surface. However, careful consideration should be given to the time scale of ephemeral features, like the front at MP, when designing surveys. Our observations of the formation of foam lines and changes in their geometry suggest that these features can evolve considerably over hours. Therefore, measurement of environmental conditions should coincide with the collection of zooplankton (or other biotic or abiotic responses).

Influence on zooplankton community

In our surveys, only *Chthamalus* spp. cyprids significantly accumulated at the front (Figure 5), though a second barnacle cyprid, *Pollicipes polymerus*, also apparently accumulated at the front, it was too infrequently observed to analyze with a GLMM. Prior studies have shown that *Chthamalus* spp. cyprids accumulate at surface slicks possibly because cyprids can overcome subduction at frontal boundaries by swimming upward, avoiding transport away from the front and increasing concentration at the front over time (Weidberg et al., 2014). Compensatory vertical flow does occur at the edges of eddies and along flow separations. That so few zooplankton accumulated at the front suggests that such flows may have been substantial at MP, leading to the transport of many zooplankton types away from the front. Indeed, non-swimming small eggs, which would be expected to act as passive tracers of hydrodynamics, were least concentrated at the front. Diatoms exhibited a similar, though non-significant pattern. Three-dimensional ADCP data would be necessary to rigorously test the hypothesis that vertical flows are a likely cause of observed distributions.

For other zooplankton types, the front acted as a barrier to either onshore or offshore movement. Copepod metanauplii and *Podon* spp. were significantly more concentrated offshore of the front. Adult *Evadne* spp., another cladoceran, were also marginally significantly more concentrated offshore of the front. Calanoid copepod adults were also apparently more abundant offshore, but this was made nonsignificant by a single onshore sample in which they were present at very high concentrations. All four types are pelagic holoplankton and are typically associated with offshore waters. A lower onshore concentration of each suggests that their cross-shore distribution is at least partially bounded by the front.

None of the 17 common types were retained close to shore by the front. However, the vertical position of *Balanus crenatus* cyprids, gastropod veligers, and polychaete larvae did appear to be significantly influenced by the front (Figure 5, Table 1). While all three types tended to be more abundant at 5-10 m deep, the effect of the front on their position was inconsistent. Surface (0-5 m) concentrations of gastropod veligers and polychaete larvae increased at the front, indicating that weaker swimming veliger and setiger larvae (Chia et al., 1984), compared to barnacle cyprids, may achieve some limited aggregation at the front by swimming against subducting currents. Concentrations of *Balanus crenatus* cyprids were generally higher offshore and significantly higher at depth but not onshore of the front. At depth, horizontal flows were likely away from the front, advecting most *B crenatus* cyprids away from the interface and reducing vertical layering shoreward of the front. Ultimately, we found that even among the most common zooplankton types, inconsistency in the presence or absence of each across survey dates and severe overdispersion of concentration data, apparent in the abundance of outlying points in Figure 5, made it difficult to estimate a consistent effect of the front on individual types. Nonetheless, taxa exhibiting significant effects for location and location:depth highlight the role of swimming ability and zooplankton provenance in determining the impact of the front on distribution.

We were better able to detect differences in the zooplankton community as a whole across the front. Community distance matrix analyses revealed moderate cross-frontal differences in the zooplankton assemblage (Figure 7) such that NMDS site scores for onshore and front samples were largely similar to each other but were each different from offshore samples, particularly along NMDS1. The zooplankton community sampled within the front was thus more representative of the onshore community than the offshore community. Eighty-one

percent of the top quartile of NMDS1 values for type scores, where front and onshore samples were concentrated within the ordination space, belonged to coastal meroplankton (e.g., ascidian larvae, barnacle cyprids and nauplii, and urchin plutei). Conversely, the bottom quartile, most strongly associated with offshore samples, was composed of 50% pelagic holoplankton (e.g., copepods, chaetognaths, and cladocerans) and the early zoeae of several crab and shrimp species. The prevalence of coastal meroplankton within and onshore of the front, and the segregation of offshore zooplankton types, further suggests that a principal role of headland fronts is to act as a barrier to either seaward or shoreward movement.

Influence on coastal ecology

We showed that fronts forming on the windward side of MP can create spatial structure of nearshore zooplankton communities by inhibiting shoreward movement of offshore zooplankton and aggregating select species. Unlike prior studies of leeward headland flow separations, river plume, and upwelling fronts, which are known to generate spatial heterogeneity in plankton and persist over days, the front at MP is highly ephemeral. We regularly observed the foam line associated with the front to form and break down over the course of hours. Such features are numerous along the West Coast, and while they may not persist long enough to generate very high concentrations of zooplankton, they may offer enough structure to influence larval recruitment dynamics. Segregation of zooplankton communities such that early developmental stages of intertidal, littoral, and benthic species are generally more abundant onshore and within the front may create a larval retention zone during relaxation flows. Relaxation events and associated poleward alongshore flows are common enough (Largier et al., 1993) that this retention zone may facilitate settlement of larvae with short pelagic larval durations (Shanks et al., 2003). Moreover, ephemeral headland fronts may create spatial

variation in benthic communities by facilitating delivery of zooplankton like *Chthamalus* spp., cyprids that accumulated at the front, to nearshore settlement sites. However, we also observed that some precompetent zooplankton (e.g., pinnotherid zoeae) were more affiliated with offshore waters, suggesting that the front is also a barrier to onshore movement of certain species and may be expected to reduce settlement near MP. As the impact of the front appears to be strongly species and stage dependent, it is likely that these features may help explain community structure in rocky intertidal, and sandy subtidal communities.

Another implication of the front's influence on zooplankton communities is the spatial structuring of prey fields for planktivores. Planktivorous fishes (Snyder et al., 2017) and seabirds (Kinder et al., 1982) are known to seek rich foraging sites at fronts. While the MP front was not a strong accumulator of zooplankton, it did appear to create dissimilar prey fields on either side of the front on the windward side of BH. Predators may, therefore, be able to exploit heterogeneity around topographic fronts like the one at MP and increase foraging efficiency by concentrating zooplankton on one side or another of the front. Indeed, the high value for trophic transfer of fronts and retention zones on the leeward (equatorward) side of headlands has been highlighted as a consideration for the design of protected areas. Thus, fronts generated on the windward wide of West Coast headlands, although more ephemeral than leeward features, may also play an important role in trophic dynamics and thus should be considered in spatial conservation planning.

CHAPTER 3 LITERATURE CITED

Axler KE, Sponaugle S, Hernandez F, Jr., Culpepper C, Cowen RK (2020) Consequences of plume encounter on larval fish growth and condition in the Gulf of Mexico. Marine Ecology Progress Series LFC:LFCav14

Barth JA, Pierce SD, Smith RL (2000) A separating coastal upwelling jet at Cape Blanco, Oregon and its connection to the California Current System. Deep Sea Research Part II: Topical Studies in Oceanography 47:783-810

Bates D, Mächler M, Bolker B, Walker S (2015) Fitting linear mixed-effects models using lme4. Journal of Statistical Software; Vol 1, Issue 1 (2015)

Bjorkstedt EP, Rosenfeld LK, Grantham BA, Shkedy Y, Roughgarden J (2002) Distributions of larval rockfishes Sebastes spp. across nearshore fronts in a coastal upwelling region. Marine Ecology Progress Series 242:215-228

Clancy M, Epifanio CE (1989) Distribution of crab larvae in relation to tidal fronts in Delaware Bay, USA. Marine Ecology Progress Series 57:77-82

Dibble C (2020) Larval transport on windy coasts. Ph.D., University of California, Davis, ProQuest

Eggleston DB, Armstrong DA, Elis WE, Patton WS (1998) Estuarine fronts as conduits for larval transport: hydrodynamics and spatial distribution of Dungeness crab postlarvae. Marine Ecology Progress Series 164:73-82

Franks PJS (1992) Sink or swim: accumulation of biomass at fronts. Marine Ecology-Progress Series 82:1-12

Galarza J, Carreras-Carbonell J, Macpherson E, Pascual M, Roques S, Turner G, Rico C (2009) The influence of oceanographic fronts and early-life-history traits on connectivity among littoral fish species. Proceedings of the National Academy of Sciences of the United States of America 106:1473-1478

Grimes CB, Kingsford MJ (1996) How do Riverine Plumes of Different Sizes Influence Fish Larvae: do they Enhance Recruitment? Marine and Freshwater Research 47:191-208

Halpern D (1976) Structure of a coastal upwelling event observed off Oregon during July 1973. Deep Sea Research Oceanographic Research Papers 23:508

Hobday AJ, Hartog JR (2014) Derived Ocean Features for Dynamic Ocean Management. Oceanography 27:134-145

Jacox MG, Edwards CA, Hazen EL, Bograd SJ (2018) Coastal upwelling revisited: Ekman, Bakun, and improved upwelling indices for the U.S. West Coast. Journal of Geophysical Research: Oceans 123:7332-7350

Johnson SY (2015) Chapter 1. Introduction. In: Johnson SY, Cochran SA (eds) California state waters map series - Offshore of Bodega Head, California. U.S. Geological Survey

Karati KK, Vineetha G, Raveendran TV, Muraleedharan KR, Habeebrehman H, Philson KP, Achuthankutty CT (2018) River plume fronts and their implications for the biological production of the Bay of Bengal, Indian Ocean. Marine Ecology Progress Series 597:79-98

Kinder TH, Hunt GL, Schneider D, Schumacher JD (29182) Correlations between seabirds and oceanic fronts around the Pribilof Islands, Alaska. Estuarine, Coastal and Shelf Science 16:309-319

Kvitek RG, Phillips EL, Dartnell P (2012) Colored shaded-relief bathymetry, Hueneme Canyon and vicinity, California. In: Johnson SY (ed) California state waters map series - Hueneme Canyon and vicinity, California. U.S. Geological Survey Scientific Investigations

Largier JL, Magnell BA, Winant CD (1993) Subtidal circulation over the northern California shelf. Journal of Geophysical Research 98:18

Lennert-Cody CE, Franks PJS (1999) Plankton patchiness in high-frequency internal waves. Marine Ecology Progress Series 186:59-66

Mace AJ, Morgan SG (2006) Larval accumulation in the lee of a small headland: implications for the design of marine reserves. Marine Ecology Progress Series 318:19-29

McCabe RM, MacCready P, Pawlak G (2006) Form drag due to flow separation at a headland. Journal of Physical Oceanography 36:2136-2152

McWilliams JC (2021) Oceanic frontogenesis. Annual Review of Marine Science 13:227-253

Morgan SG, Fisher JL (2010) Larval behavior regulates nearshore retention and offshore migration in an upwelling shadow and along the open coast. Marine Ecology Progress Series 404:109-126

Moser HG (ed) (1996) The early stages of fishes in the California Current region. CalCOFI Atlas 33

Oksanen J, Blanchet FG, Friendly M, Kindt R, Legendre P, McGlinn D, Minchin PR, O'Hara RB, Simpson GL, Solymos P, Stevens MHH, Szoecs E, Wagner H (2019) vegan: Community ecology package.

Owen RW (1981) Fronts and eddies in the sea: Mechanisms, interactions, and biological effects. In: Longhurst AR (ed) Analysis of marine ecosystems. Academic Press Inc., London, UK

R Core Team (2019) R: A language and environmental for statistical computing. https://www.R-project.org/

Roughan M, Garfield N, Largier J, Dever E, Dorman C, Peterson D, Dorman J (2006) Transport and retention in an upwelling region: The role of across-shelf structure. Deep Sea Research Part II: Topical Studies in Oceanography 53:2931-2955

Satterthwaite EV, Ryan JP, Harvey JBJ, Morgan SG (2021) Invertebrate larval distributions influenced by adult habitat distribution, larval behavior, and hydrodynamics in the retentive upwelling shadow of Monterey Bay, California, USA. Marine Ecology Progress Series 661

Shanks AL (2001) An identification guide to the larval marine invertebrates of the Pacific Northwest. Oregon State University Press

Shanks AL, McCulloch A, Miller J (2003) Topographically generated fronts, very nearshore oceanography and the distribution of larval invertebrates and holoplankters. Journal of Plankton Research 25:1251-1277

Snyder S, Franks PJS, Talley LD, Xu Y, Kohin S (2017) Crossing the line: Tunas actively exploit submesoscale fronts to enhance foraging success. Limnology and Oceanography Letters 2:187-194

Vander Woude A, Largier J, Kudela R (2006) Nearshore retention of upwelled waters north and south of Point Reyes (northern California)—Patterns of surface temperature and chlorophyll observed in CoOP WEST. Deep Sea Research Part II: Topical Studies in Oceanography 53:2998

Weidberg N, Lobón C, López E, García Flórez L, Fernández Rueda Md P, Largier J, Acuña JL (2014) Effect of nearshore surface slicks on meroplankton distribution: role of larval behaviour. Marine Ecology Progress Series 506:15-30

Whitney JL, Gove JM, McManus MA, Smith KA, Lecky J, Neubauer P, Phipps JE, Contreras EA, Kobayashi DR, Asner GP (2021) Surface slicks are pelagic nurseries for diverse ocean fauna. Scientific Reports 11:3197

Wickham H (2016) ggplot2: Elegant graphics for data analysis. https://ggplot2.tidyverse.org

Wijesekera HW, Wesson JC, Wang DW, Teague WJ, Hallock ZR (2020) Observations of flow separation and mixing around the northern Palau Island/ridge. Journal of Physical Oceanography 50:2529-2559

Wing S, Botsford L, Ralston S, Largier J (1998) Meroplanktonic distribution and circulation in a coastal retention zone of the northern California upwelling system. Limnology and Oceanography 43:1710-1721

Wolanski E, Hamner WM (1988) Topographically controlled fronts in the ocean and their biological significance. Science 241

Woodson CB, Litvin SY (2015) Ocean fronts drive marine fishery production and biogeochemical cycling. Proceedings of the National Academy of Sciences 112:1710-1715

Woodson CB, McManus MA, Tyburczy JA, Barth JA, Washburn L, Caselle JE, Carr MH, Malone DP, Raimondi PT, Menge BA, Palumbi SR (2012) Coastal fronts set recruitment and connectivity patterns across multiple taxa. Limnology and Oceanography 57:582-596

Yi N (2020) NBZIMM: Negative binomial and zero-inflated mixed models.

APPENDIX A

Table 1. Location and bottom depth (in meters) of stations sampled during 2011-2018 NMFS RREAS surveys. Availability of samples varied by year. Samples included in our analysis are marked with an 'X' for each year in the period. We used a subset of stations to construct time series of environmental covariates in Figure 4 (main text). These stations are marked with an 'X' in the last column.

station	latitude	longitude	bottom_depth (m)	2011	2012	2013	2015	2016	2017	2018	figure4
110	36.58330	-122.1750	2304	X	X	X		X		X	X
112	36.65500	-121.9467	73	X	X				X		
114	36.76670	-121.8667	73	X	X	X		X		X	X
116	36.74000	-121.9767	287		X						
117	36.70000	-122.1083	1920	X	X	X		X	X	X	
118	36.76694	-122.1589	1126	X							
124	36.98330	-122.3750	128	X	X	X		X	X	X	X
127	36.98330	-122.7583	1045	X		X		X	X	X	X
131	37.27500	-122.5667	82		X	X		X	X	X	
132	37.27500	-122.6500	95	X	X	X				X	X
134	37.27500	-122.9833	518	X		X		X	X	X	X
138	37.70000	-122.9083	55	X	X	X		X	X		
139	37.79170	-122.8667	55		X	X				X	X
152	37.65830	-123.0417	108	X	X			X			X
156	37.74330	-123.1383	91	X	X				X	X	
165	38.16670	-123.0000	55		X						
166	38.16639	-123.0842	77	X							
167	38.16670	-123.1667	91	X		X		X	X	X	X

station	latitude	longitude	bottom_depth (m)	2011	2012	2013	2015	2016	2017	2018	figure4
170	38.16670	-123.3667	183	X	X	X		X		X	
171	38.16670	-123.4833	400			X			X		X
171	38.16670	-123.4833	1920							X	X
183	38.46670	-123.2333	53	X		X				X	
402	32.71670	-118.4533	222				X	X	X	X	X
411	33.69000	-119.2867	892		X		X	X		X	X
412	33.58670	-119.4483	1874		X				X		
413	33.48670	-119.6050	775		X		X			X	
414	33.38330	-119.7633	103					X			X
421	34.40917	-120.2261	217		X		X				
422	34.31830	-120.3000	380		X		X	X	X	X	X
425	33.91830	-120.7117	1848				X	X	X	X	X
442	35.70330	-121.4300	167	X			X	X	X	X	X
445	35.70330	-121.8667	1050					X	X	X	X
453	38.46670	-123.3867	115	X			X	X	X		X
454	38.46670	-123.7100	910	X		X	X	X		X	X
481	33.01670	-117.7500	798		X		X			X	X
482	32.91670	-117.5833	865		X			X	X	X	
492	35.00000	-120.7933	94		X						
493	35.00000	-120.8833	192		X				X		X
495	35.00000	-121.1167	532				X	X	X	X	X

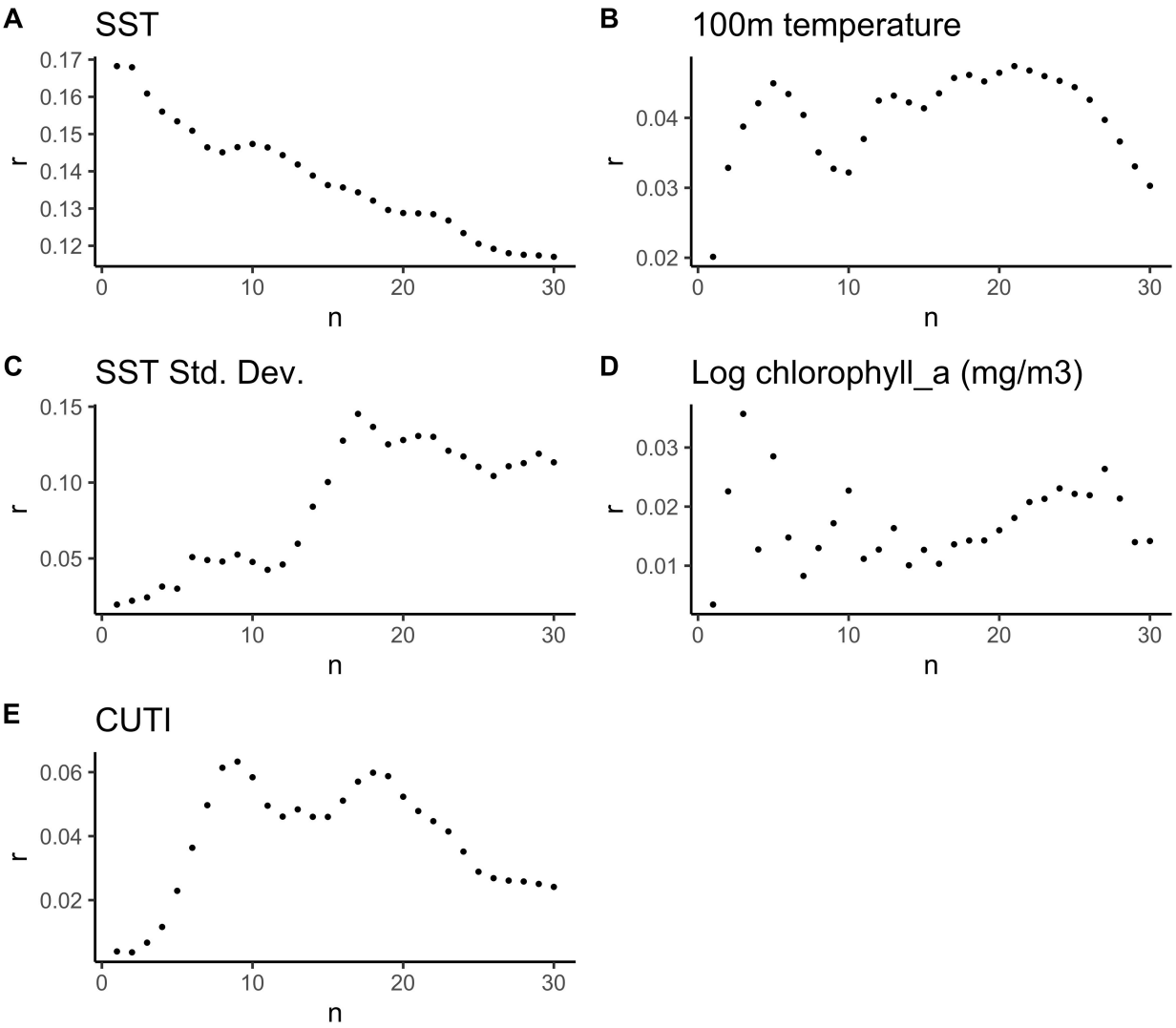

Figure 1. Temporal averaging of environmental predictors included in linear mixed effects models of krill length was determined by plotting coefficient of determination (R^2) against differing averaging periods (n, in days). A-E all show results of this analysis for *Euphausia pacifica* only. Peak values were used as averaging periods in final models except in the case of SST (A) and chlorophyll-*a* (D). For SST, we used an averaging period of 10 days, corresponding with the second peak in R^2, because this period is more in line with what is known of the intermoult period of krill from the CCE, which ranges from 4-13 days (Marinovic & Mangel, 1999; Pinchuk & Hopcraft, 2007; Shaw *et al*., 2010). For chlorophyll-*a*, we used a 27-day period represented by the peak R^2 value after the trend had stabilized.

The following three tables show full model results including estimate confidence intervals for interannual linear mixed effects models of krill length with fixed effect for year and variable station intercepts. All year estimates 2012-2018 are shown relative to the intercept year (2011). These tables correspond to Figure 3A in the text.

Table 2. *E. pacifica*

***E. pacifica* (year only)**

	length	
Predictors	*Estimates*	*CI*
(Intercept)	-0.44	-0.54 – -0.34
year [2012]	0.25	0.18 – 0.32
year [2013]	0.85	0.77 – 0.93
year [2015]	0.37	0.29 – 0.45
year [2016]	0.86	0.79 – 0.93
year [2017]	0.66	0.59 – 0.73
year [2018]	0.64	0.58 – 0.71
Random Effects		
σ^2	0.88	
$\tau_{00\ station}$	0.07	
ICC	0.07	
$N_{\ station}$	33	
Observations	11284	
Marginal R^2 / Conditional R^2	0.091 / 0.157	

Table 3. *T. spinifera*

***T. spinifera* (year only)**

	length	
Predictors	*Estimates*	*CI*
(Intercept)	-0.58	-0.76 – -0.41
year [2012]	1.06	0.97 – 1.14
year [2013]	0.93	0.85 – 1.00
year [2015]	0.08	-0.06 – 0.23
year [2016]	0.78	0.66 – 0.91
year [2017]	0.80	0.72 – 0.88
year [2018]	0.93	0.86 – 1.01
Random Effects		
σ^2	0.65	
$\tau_{00\ station}$	0.23	
ICC	0.26	
$N_{\ station}$	32	
Observations	5865	
Marginal R^2 / Conditional R^2	0.165 / 0.381	

Table 4. *N. difficilis*

***N. difficilis* (year only)**

	length	
Predictors	*Estimates*	*CI*
(Intercept)	0.55	-0.04 – 1.14
year [2012]	-1.47	-1.93 – -1.00
year [2013]	-1.01	-2.70 – 0.69
year [2015]	0.56	0.20 – 0.91
year [2016]	-0.76	-1.18 – -0.35
year [2017]	-1.29	-1.72 – -0.86
year [2018]	-0.70	-1.14 – -0.27
Random Effects		
σ^2	0.82	
$\tau_{00\ station}$	0.65	
ICC	0.44	
$N_{\ station}$	13	
Observations	1636	
Marginal R^2 / Conditional R^2	0.258 / 0.585	

The following three tables show full model results including estimate confidence intervals for interannual linear mixed effects models of krill length with fixed effects for year, sex, and year by sex interaction and variable station intercepts. All year estimates 2012-2018 are shown relative to the intercept year (2011). These tables correspond to Figures 3B and 3C in the text.

Table 5. *E pacifica*

***E. pacifica* (year and sex)**

	length	
Predictors	*Estimates*	*CI*
(Intercept)	-0.30	-0.41 – -0.20
year [2012]	0.22	0.14 – 0.30
year [2013]	0.95	0.85 – 1.04
year [2015]	0.31	0.22 – 0.40
year [2016]	0.93	0.84 – 1.01
year [2017]	0.71	0.63 – 0.79
year [2018]	0.65	0.58 – 0.73
sex [M]	-0.36	-0.44 – -0.28
year [2012] * sex [M]	0.04	-0.07 – 0.16
year [2013] * sex [M]	-0.18	-0.32 – -0.03
year [2015] * sex [M]	0.15	0.01 – 0.29
year [2016] * sex [M]	-0.17	-0.29 – -0.04
year [2017] * sex [M]	-0.10	-0.22 – 0.02
year [2018] * sex [M]	-0.07	-0.19 – 0.05
Random Effects		
σ^2	0.84	
$\tau_{00\ station}$	0.07	
ICC	0.07	
$N_{\ station}$	33	
Observations	11284	
Marginal R^2 / Conditional R^2	0.130 / 0.195	

Table 6. *T. spinifera*

***T. spinifera* (year and sex)**

	length	
Predictors	*Estimates*	*CI*
(Intercept)	-0.35	-0.52 – -0.18
year [2012]	1.18	1.09 – 1.28
year [2013]	1.00	0.90 – 1.09
year [2015]	-0.26	-0.42 – -0.11
year [2016]	0.90	0.75 – 1.06
year [2017]	0.76	0.67 – 0.85
year [2018]	0.96	0.87 – 1.06
sex [M]	-0.49	-0.58 – -0.41
year [2012] * sex [M]	-0.50	-0.63 – -0.37
year [2013] * sex [M]	-0.26	-0.39 – -0.13
year [2015] * sex [M]	0.71	0.51 – 0.91
year [2016] * sex [M]	-0.15	-0.33 – 0.04
year [2017] * sex [M]	-0.32	-0.46 – -0.18
year [2018] * sex [M]	-0.02	-0.15 – 0.12
Random Effects		
σ^2	0.55	
$\tau_{00\ station}$	0.20	
ICC	0.26	
$N_{\ station}$	32	
Observations	5865	
Marginal R^2 / Conditional R^2	0.291 / 0.478	

Table 7. *N. difficilis*

***N. difficilis* (year and sex)**

	length	
Predictors	*Estimates*	*CI*
(Intercept)	1.07	0.61 – 1.54
year [2016]	-1.34	-1.56 – -1.12
year [2017]	-1.70	-1.96 – -1.44
year [2018]	-1.18	-1.43 – -0.92
sex [M]	0.05	-0.20 – 0.30
year [2016] * sex [M]	-0.12	-0.47 – 0.24
year [2017] * sex [M]	-0.34	-0.67 – -0.02
year [2018] * sex [M]	-0.33	-0.83 – 0.16
Random Effects		
σ^2	0.80	
$\tau_{00\ station}$	0.60	
ICC	0.43	
$N_{\ station}$	12	
Observations	1423	
Marginal R^2 / Conditional R^2	0.259 / 0.577	

The following three tables show full model results including estimate confidence intervals for environmental linear mixed effects models of krill length with variable intercepts and slopes. These tables correspond to Figure 5 in the text.

Table 8. *E. pacifica*

	length	
Predictors	*Estimates*	*CI*
(Intercept)	0.43	0.14 – 0.71
chla	-0.22	-0.28 – -0.17
cuti	-0.11	-0.13 – -0.08
moci_spring	0.06	0.02 – 0.09
sex [M]	-0.42	-0.46 – -0.39
sst_sd	0.13	0.10 – 0.16
temp_100	0.02	-0.02 – 0.06
temp_2	0.07	-0.34 – 0.48
sex [M] * temp_100	-0.05	-0.09 – -0.01
sex [M] * temp_2	0.07	0.03 – 0.11
Random Effects		
σ^2	0.81	
$\tau_{00\ station}$	0.41	
$\tau_{11\ station.temp\_2}$	0.92	
$\varrho_{01\ station}$	-0.11	
ICC	0.63	
$N_{\ station}$	24	
Observations	9210	
Marginal R^2 / Conditional R^2	0.073 / 0.653	

Table 9. *T. spinifera*

	length	
Predictors	*Estimates*	*CI*
(Intercept)	0.10	-0.36 – 0.56
chla	-0.52	-0.61 – -0.43
cuti	0.05	0.02 – 0.09
moci_spring	-0.18	-0.22 – -0.14
sex [M]	-0.62	-0.66 – -0.58
sst_sd	0.18	0.14 – 0.22
chla * sex [M]	0.05	0.01 – 0.09
moci_spring * sex [M]	0.16	0.12 – 0.20
Random Effects		
σ^2	0.54	
$\tau_{00\ station}$	1.30	
$\tau_{11\ station.temp\_2}$	1.27	
$\varrho_{01\ station}$	-0.02	
ICC	0.71	
$N_{station}$	31	
Observations	5770	
Marginal R^2 / Conditional R^2	0.154 / 0.751	

Table 10. *N. difficilis*

	length	
Predictors	*Estimates*	*CI*
(Intercept)	0.11	-0.19 – 0.41
chla	0.12	-0.00 – 0.24
cuti	0.26	0.17 – 0.34
moci_spring	0.52	0.42 – 0.61
sex [M]	-0.24	-0.36 – -0.11
chla * sex [M]	0.17	-0.00 – 0.35
cuti * sex [M]	0.11	-0.00 – 0.23
moci_spring * sex [M]	0.23	0.10 – 0.35
Random Effects		
σ^2	0.84	
$\tau_{00\ station}$	0.27	
ICC	0.24	
$N_{station}$	12	
Observations	1558	
Marginal R^2 / Conditional R^2	0.226 / 0.414	

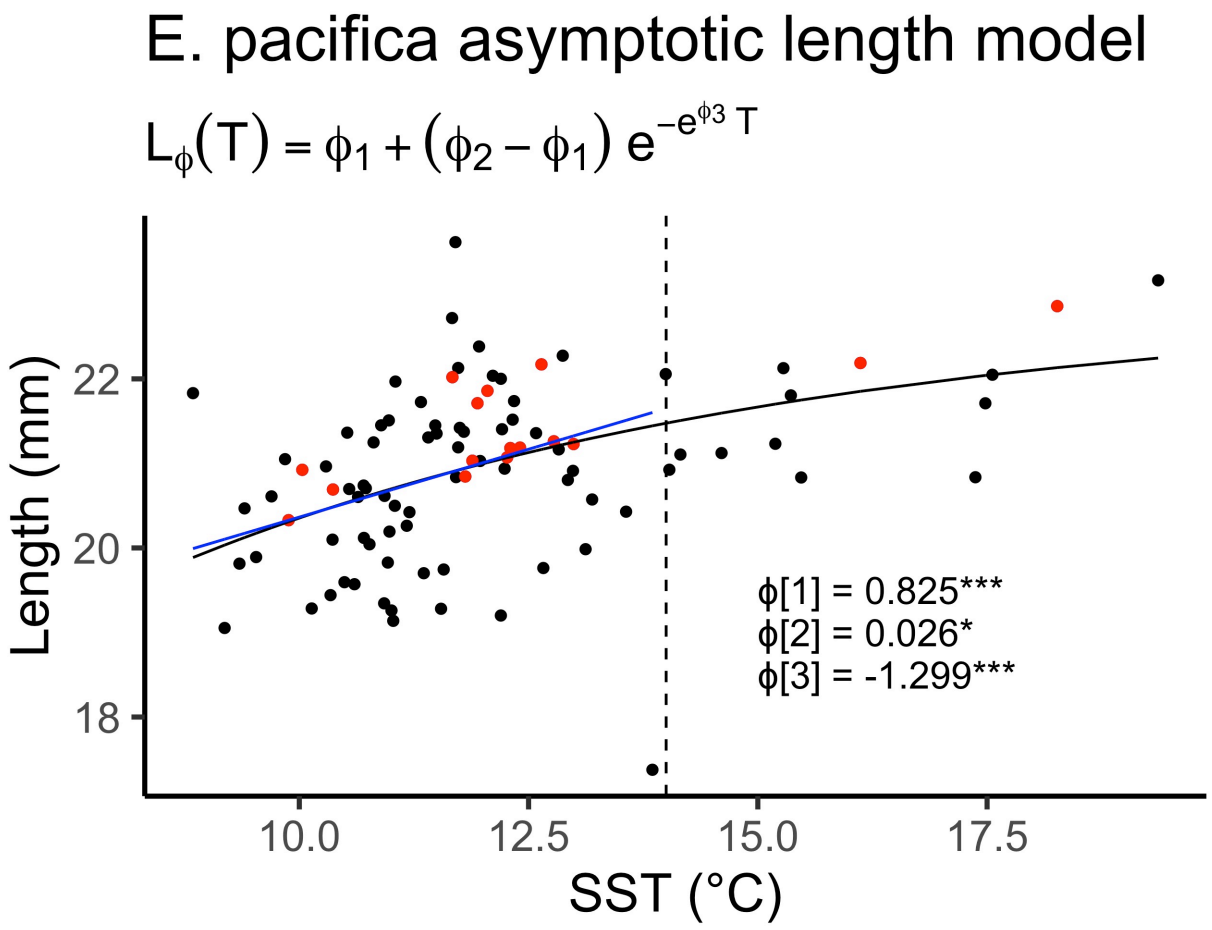

Figure 2. Nonlinear model of the relationship between SST and mean lengths of *E. pacifica* collected off California from 2011-2018 (black line), where ϕ_1 is the asymptote, ϕ_2 is the intercept, and ϕ_3 is the rate constant (stars denote p values). The blue line shows a linear model of length~SST for SST values < 14° C (dotted line). Points show station annual SST values in the 10 days prior to sample collection plotted against mean length, 2017 values are highlighted in red.

Sea Surface Temperature Variability

SST SD was positively associated with adult krill length for both *E. pacifica* and *T. spinifera* when modelled across all years (Figure 6, main text). We included SST SD as a possible indicator of the presence of fronts, which can be cradles of high phyto- and zoo-plankton concentrations, creating high-quality feeding habitat for planktivores (Bjorkstedt *et al*., 2002; Woodson & Litvin, 2015). We also considered the possibility that SST SD may be associated with high-frequency fluctuations in upwelling. Strong upwelling, interrupted by periods of relaxation brings nutrients into the photic zone with little offshore advection, leading to elevated primary production in coastal surface waters (Menge & Menge, 2013). This process may allow phytoplanktivores, including krill, to better access upwelling-derived nutrients (Cury & Roy, 1989; Botsford *et al*., 2006). SST SD was weakly but significantly associated with upwelling intermittence (measured as standard deviation of daily CUTI at each station; R^2 = 13%, $p < 0.001$). This explanation provides a potential mechanism for why adult *E. pacifica* and *T. spinifera* were larger in years with high SST SD and upwelling intermittence, including 2013 and 2017, and why adult krill size did not decrease in 2016, when other measures of ocean condition more closely resembled 2015 (Figure S13). Whether SST SD is a better indicator of fronts, upwelling intermittence, or some other physical process, its positive relationship with krill length (this study) and abundance (*T. spinifera*, Cimino *et al.,* 2020) suggests the measure may be an indicator of elevated krill biomass in the CCE and merits further exploration.

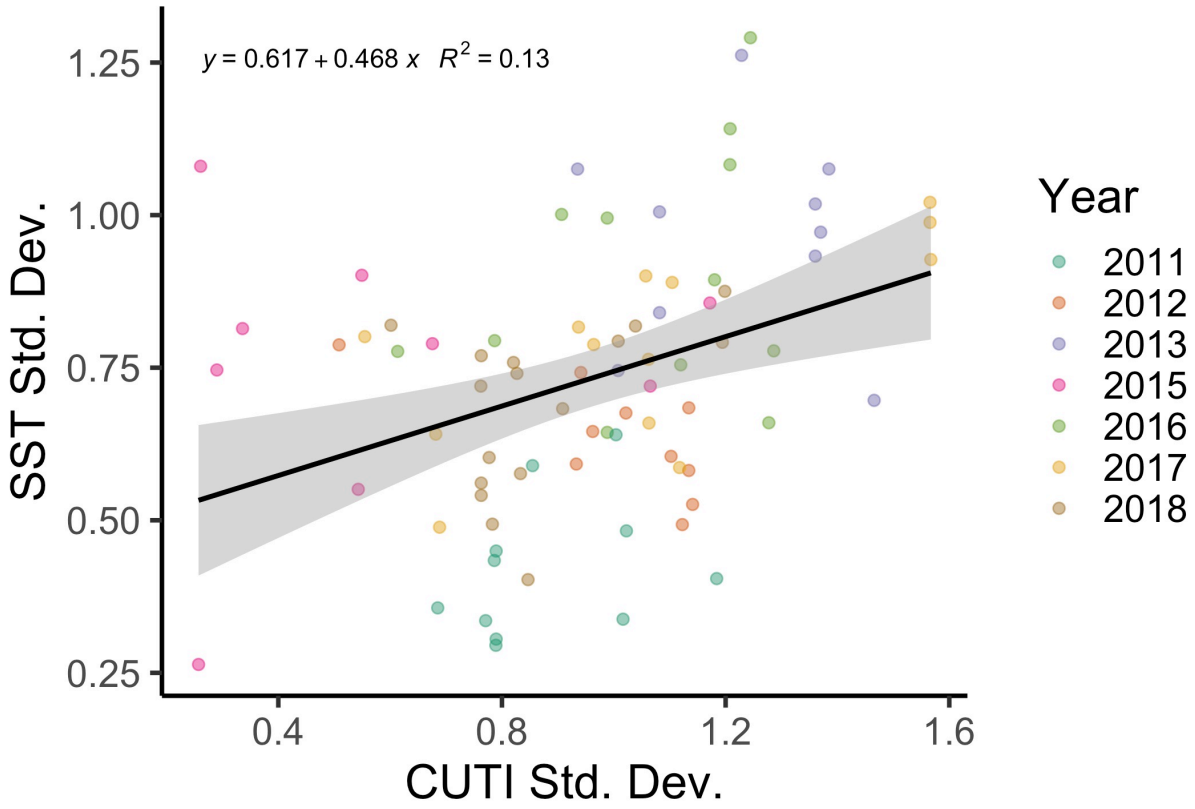

Figure 3. Thirty-day standard deviation of CUTI plotted against 30-day standard deviation of SST for stations indicated in the last column of table S1. Points colored by year to show interannual variability in the relationship between the two measures. Line and equation describe the linear model of the two covariates; gray band shows the 95% confidence interval.

APPENDIX A LITERATURE CITED

Bjorkstedt, E. P., Rosenfeld, L. K., Grantham, B. A., Shkedy, Y., and Roughgarden, J. 2002. Distributions of larval rockfishes *Sebastes spp*. across nearshore fronts in a coastal upwelling region. Marine Ecology Progress Series, 242: 215-228.

Botsford, L. W., Lawrence, C. A., Dever, E. P., Hastings, A., and Largier, J. 2006. Effects of variable winds on biological productivity on continental shelves in coastal upwelling systems. Deep Sea Research Part II: Topical Studies in Oceanography, 53: 3116-3140.

Cury, P., and Roy, C. 1989. Optimal environmental window and pelagic fish recruitment success in upwelling areas. Canadian Journal of Fisheries and Aquatic Sciences, 46.

Marinovic, B., and Mangel, M. 1999. Krill can shrink as an ecological adaptation to temporarily unfavourable environments. Ecology Letters, 2: 338-343.

Menge, B. A., and Menge, D. N. L. 2013. Dynamics of coastal meta-ecosystems: The intermittent upwelling hypothesis and a test in rocky intertidal regions. Ecological Monographs, 83: 283 - 310.

Pinchuk, A. I., and Hopcroft, R. R. 2007. Seasonal variations in the growth rates of euphausiids (*Thysanoessa inermis*, *T. spinifera*, and *Euphausia pacifica*) from the northern Gulf of Alaska. Marine Biology, 151: 257-269.

Shaw, C., Peterson, W., and Feinberg, L. 2010. Growth of *Euphausia pacifica* in the upwelling zone off the Oregon coast. Deep Sea Research Part II: Topical Studies in Oceanography, 57: 584-593.

Woodson, C. B., and Litvin, S. Y. 2015. Ocean fronts drive marine fishery production and biogeochemical cycling. Proceedings of the National Academy of Sciences, 112: 1710-1715.

APPENDIX B

Table 1. Habitats occupied by adults and larvae of fishes collected during the course of our survey and a description of each. Classification indicates how species corresponding with each habitat were grouped for analysis.

Habitats	Description	Classification
rocky intertidal	high to low tide line, affiliated with rocky bottoms	Nearshore
nearshore subtidal	0-50m, often water column dwelling	Nearshore
rocky reef	0-50m, reef affiliated	Nearshore
kelp reef	generally <30m, affiliated with rocky substrate with kelp cover	Nearshore
bay estuary	0-30m, affiliated with bays or estuary environments	Nearshore
coastal pelagic	midwater species, not affiliated with any one substrate	Offshore
nearshore soft bottom	0-50m, affiliated with sandy or muddy substrates	Nearshore
nearshore algae	0-30m, affiliated with either fixed or drift algae	Nearshore
midshelf soft bottom	50-200m, affiliated with soft flat substrates	Midshelf
outer shelf	200-1000m, offshore habitat affiliated	Offshore
deep reef	>200m, rocky reef afiliated	Offshore
mid deep reef	50-200m, affiliated with rocky reef substrates	Midshelf
bathypelagic	>1000m, water column dwelling	Offshore
rocky subtidal	0-50m, affiliated with rocky or cobble benthic substrates	Nearshore
nearshore generalist	benthopelagic in nearshore waters, may affiliate with rivers and estuaries but not as resident	Nearshore
bathydemersal	>1000m, affiliated with benthos	Offshore

Table 2. Adult and early life history habitat affiliations of ichthyoplankton collected during 2017-2019 sampling off Bodega Head and Stewarts Point according to FishBase and California Cooperative Oceanic Fisheries Investigation publications. When no habitat affiliation information was available for early life stages, we assumed spawning and settlement locations to be identical to adult habitat. Classification indicates whether the species was considered to be nearshore, mid-shelf, or offshore for the purposes of our analyses.

Species Name	Common Name	Adult Habitat	Spawning Location	Settlement Location	Classification
Ammodytes hexapterus	Pacific sand lance	nearshore subtidal	nearshore subtidal	nearshore subtidal	nearshore
Artedius corallinus	Coralline sculpin	rocky reef	rocky reef	rocky reef	nearshore
Artedius fenestralis	Padded sculpin	rocky reef	rocky reef	rocky reef	nearshore
Artedius harringtoni	Scalyhead sculpin	rocky reef	rocky reef	rocky reef	nearshore
Artedius lateralis	Smoothhead sculpin	rocky intertidal	rocky intertidal	rocky intertidal	nearshore
Atheresthes stomias	Arrowtooth flounder	outer shelf	outer shelf	outer shelf	offshore
Atherinopsis californiensis	Jack silverside	nearshore subtidal	nearshore subtidal	nearshore subtidal	nearshore
Bathylagus ochotensis	Eared blacksmelt	bathypelagic	bathypelagic	bathypelagic	offshore
Bathylagus pacificus	Slender blacksmelt	bathypelagic	bathypelagic	bathypelagic	offshore
Bothragonus swanii	Rockhead	rocky intertidal	kelp reef	rocky intertidal	nearshore
Brosmophycis marginata	Red brotula	rocky subtidal	rocky subtidal	rocky subtidal	nearshore
Cebidichthys violaceus	Monkeyface prickleback	rocky intertidal	rocky subtidal	rocky intertidal	nearshore

Species Name	Common Name	Adult Habitat	Spawning Location	Settlement Location	Classification
Chauliodus macouni	Pacific viperfish	bathypelagic	bathypelagic	bathypelagic	offshore
Chirolophis decoratus	Decorated warbonnet	midshelf soft bottom	midshelf soft bottom	midshelf soft bottom	midshelf
Chirolophis nugator	Mosshead warbonnet	rocky reef	rocky reef	rocky reef	nearshore
Chitonotus pugetensis	Roughback sculpin	nearshore soft bottom	nearshore soft bottom	nearshore soft bottom	nearshore
Citharichthys sordidus	Pacific sanddab	outer shelf	midshelf soft bottom	midshelf soft bottom	midshelf
Citharichthys stigmaeus	Speckled sanddab	nearshore soft bottom	nearshore soft bottom	nearshore soft bottom	nearshore
Citharichthys xanthostigma	Longfin sanddab	midshelf soft bottom	midshelf soft bottom	midshelf soft bottom	midshelf
Clevelandia ios	Arrow goby	bay estuary	bay estuary	bay estuary	nearshore
Clinocottus acuticeps	Sharpnose sculpin	rocky subtidal	rocky subtidal	rocky subtidal	nearshore
Clinocottus embryum	Calico scupin	rocky intertidal	rocky intertidal	rocky intertidal	nearshore
Clinocottus gobiceps	Mosshead sculpin	rocky intertidal	rocky intertidal	rocky intertidal	nearshore
Clupea pallsii	Pacific herring	bay estuary	bay estuary	bay estuary	nearshore
Cololabis saira	Pacific saury	coastal pelagic	coastal pelagic	coastal pelagic	offshore
Cottus asper	Prickly sculpin	bay estuary	bay estuary	bay estuary	nearshore
Cryptacanthodes aleutensis	Dwarf wrymouth	midshelf soft bottom	midshelf soft bottom	midshelf soft bottom	midshelf
Diaphus theta	California	bathypelagic	bathypelagic	bathypelagic	offshore

Species Name	Common Name	Adult Habitat	Spawning Location	Settlement Location	Classification
	headlightfish				
Embassichthys bathybius	Deep sea sole	outer shelf	outer shelf	outer shelf	offshore
Engraulis mordax	Northern anchovy	coastal pelagic	coastal pelagic	coastal pelagic	offshore
Enophrys bison	Buffalo sculpin	rocky subtidal	rocky subtidal	rocky subtidal	nearshore
Eopsetta jordani	Petrale sole	midshelf soft bottom	midshelf soft bottom	unknown	midshelf
Genyonemus lineatus	White croaker	nearshore soft bottom	nearshore soft bottom	nearshore soft bottom	nearshore
Gibbonsia montereyensis	Crevice kelpfish	nearshore algae	nearshore algae	nearshore algae	nearshore
Glyptocephalus zachirus	Rex sole	midshelf soft bottom	midshelf soft bottom	midshelf soft bottom	midshelf
Hemilepidotus spinosus	Brown Irish lord	rocky reef	rocky reef	rocky reef	nearshore
Heterostichus rostratus	Giant kelpfish	nearshore algae	nearshore algae	nearshore algae	nearshore
Hexagrammos decagrammus	Kelp greenling	rocky subtidal	rocky subtidal	rocky subtidal	nearshore
Hexagrammos lagocephalus	Rock greenling	rocky subtidal	rocky subtidal	rocky subtidal	nearshore
Hexagrammos octogrammus	Masked greenling	rocky subtidal	rocky subtidal	rocky subtidal	nearshore
Hypomesus pretiosus	Surf smelt	neashore generalist	nearshore subtidal	nearshore subtidal	nearshore
Icelinus quadriseriatus	Yellowchin sculpin	nearshore soft bottom	nearshore soft bottom	nearshore soft bottom	nearshore

Species Name	Common Name	Adult Habitat	Spawning Location	Settlement Location	Classification
Isopsetta isolepis	Butter sole	midshelf soft bottom	midshelf soft bottom	nearshore soft bottom	nearshore
Lepidogobius lepidus	Bay goby	nearshore soft bottom	nearshore soft bottom	nearshore soft bottom	nearshore
Lepidopsetta bilineata	Rock sole	midshelf soft bottom	midshelf soft bottom	midshelf soft bottom	midshelf
Leptocottus armatus	Pacific staghorn sculpin	bay estuary	bay estuary	bay estuary	nearshore
Lestidiops pacificum	Pacific barracudina	bathypelagic	bathypelagic	bathypelagic	offshore
Lestidiops ringens	Slender barracudina	bathypelagic	bathypelagic	bathypelagic	offshore
Lethops connectens	Halfblind goby	kelp reef	kelp reef	kelp reef	nearshore
Leuroglossus stilbius	California smoothtongue	bathypelagic	bathypelagic	bathypelagic	offshore
Liparis fucensis	Slipskin snailfish	outer shelf	nearshore subtidal	midshelf soft bottom	midshelf
Liparis mucosus	Slimy snailfish	rocky intertidal	rocky intertidal	rocky intertidal	nearshore
Liparis pulchellus	Showy snailfish	midshelf soft bottom	midshelf soft bottom	midshelf soft bottom	midshelf
Lyopsetta exilis	Slender sole	outer shelf	outer shelf	outer shelf	offshore
Melamphaes lugubris	Highsnout melamphid	bathypelagic	bathypelagic	bathypelagic	offshore
Melamphaes parvus	Little bigscale	bathypelagic	bathypelagic	bathypelagic	offshore
Merluccius productus	North Pacific hake	outer shelf	outer shelf	outer shelf	offshore

Species Name	Common Name	Adult Habitat	Spawning Location	Settlement Location	Classification
Microstomus pacificus	Dover sole	outer shelf	bathydemersal	bathydemersal	offshore
Nansenia candida	Bluethroat argentine	outer shelf	outer shelf	outer shelf	offshore
Odontopyxis trispinosa	Pygmy poacher	midshelf soft bottom	midshelf soft bottom	midshelf soft bottom	midshelf
Ophiodon elongatus	Lingcod	mid deep reef	rocky subtidal	rocky subtidal	nearshore
Orthonopias triacis	Snubnose sculpin	rocky reef	rocky reef	rocky reef	nearshore
Oxylebius pictus	Painted greenling	rocky reef	rocky reef	rocky reef	nearshore
Paralichthys californicus	California halibut	nearshore soft bottom	nearshore soft bottom	bay estuary	nearshore
Paricelinus hopliticus	Thornback sculpin	mid deep reef	mid deep reef	mid deep reef	midshelf
Parophrys vetulus	English sole	midshelf soft bottom	nearshore soft bottom	bay estuary	nearshore
Pholis ornata	Saddleback gunnel	nearshore algae	nearshore algae	nearshore algae	nearshore
Platichthys stellatus	Starry flounder	bay estuary	bay estuary	bay estuary	nearshore
Plectobranchus evides	Bluebarred prickleback	midshelf soft bottom	midshelf soft bottom	midshelf soft bottom	midshelf
Pleuronichthys coenosus	C-o sole	midshelf soft bottom	midshelf soft bottom	midshelf soft bottom	midshelf
Psettichthys melanostictus	Pacific sand sole	nearshore soft bottom	nearshore soft bottom	nearshore soft bottom	nearshore
Pseudobathylagus	Stout	bathypelagic	bathypelagic	bathypelagic	offshore

Species Name	Common Name	Adult Habitat	Spawning Location	Settlement Location	Classification
milleri	blacksmelt				
Radulinus asprellus	Slim sculpin	nearshore soft bottom	nearshore soft bottom	nearshore soft bottom	nearshore
Rathbunella alleni	Stripefin ronquil	rocky reef	rocky reef	rocky reef	nearshore
Ronquilus jordani	Northern ronquil	midshelf soft bottom	mid deep reef	mid deep reef	midshelf
Ruscarius creaseri	Roughcheek sculpin	rocky reef	rocky reef	rocky reef	nearshore
Ruscarius meanyi	Puget sound sculpin	rocky subtidal	rocky subtidal	rocky subtidal	nearshore
Sardinops sagax	Pacific sardine	coastal pelagic	coastal pelagic	coastal pelagic	offshore
Scorpaenichthys marmoratus	Cabezon	rocky subtidal	rocky subtidal	rocky subtidal	nearshore
Spectrunculus grandis	Pudgy cuskeel	bathydemersal	bathydemersal	bathydemersal	offshore
Tarletonbeania crenularis	Blue lanternfish	bathypelagic	bathypelagic	bathypelagic	offshore
Tetragonurus atlanticus	Bigeye squaretail	coastal pelagic	coastal pelagic	coastal pelagic	offshore
Tetragonurus cuvieri	Smalleye squaretail	bathypelagic	bathypelagic	bathypelagic	offshore
Xeneretmus latifrons	Blacktip poacher	outer shelf	outer shelf	outer shelf	offshore
Xeneretmus leiops	Smootheye poacher	outer shelf	outer shelf	outer shelf	offshore
Zaniolepis frenata	Shortspine combfish	deep reef	outer shelf	outer shelf	offshore

APPENDIX B LITERATURE CITED

Froese, R. and D. Pauly. Editors. 2022. FishBase. World Wide Web electronic publication. www.fishbase.org, (06/2022)

Moser, H.G. Editor. 1996. Atlas No. 33: The early stages of fishes in the California Current region, California Cooperative Oceanic Fisheries Investigations